FORMULATION VERSATILITY OF NITRIC OXIDE DONOR MOLECULES FOR THE PREVENTION OF MEDICAL DEVICE-ASSOCIATED COMPLICATIONS

by

MORGAN ASHCRAFT

(Under the Direction of Hitesh Handa)

ABSTRACT

The use of medical devices is often complicated by surface-associated infection and thrombosis. This dissertation explores the versatility of *S*-nitrosothiols (RSNOs) in various formulations to address these issues. RSNOs are commonly used to provide prolonged nitric oxide (NO)-releasing platforms. As NO is an endogenous antimicrobial and antithrombotic agent, NO-releasing materials provide multifunctional interfaces for potential biomedical applications.

This work describes RSNOs in solution, covalently attached to a material for surface coating, and impregnated into medical-grade tubing. Each of these forms provide unique properties for a variety of potential applications. The first investigation employs *S*-nitrosoglutathione (GSNO) in saline as an antibacterial and antithrombotic lock solution for venous catheters. It was established to release NO for the full duration of a potential lock therapy (48 h). The NO-releasing lock solution routinely outperformed clinically used lock solutions in antibacterial and antithrombotic assays. It was also established to be biocompatible.

The second study attached the RSNO *S*-Nitroso-*N*-acetylpenicillamine (SNAP) to graphene oxide (GO) for biomaterial coatings. This novel material was thoroughly characterized via quantitative and qualitative analyses. It was demonstrated to have highly tunable NO release

profiles via changes in preparation and the use of low levels of electrical current. The NO-releasing GO showed superior antibacterial activity compared to unmodified GO in viable adhesion and biofilm dispersal assays. Moreover, it showed improved cytocompatibility.

The third investigation characterized SNAP-impregnated silicon rubber with a hydrophilic, polyethylene glycol (PEG) coating. The NO+PEG substrates showed complementary activities in preventing viable bacteria, plasma proteins, and platelets from adhering *in vitro*. Non-anticoagulated *in vivo* rabbit studies showed excellent resistance to clotting and significantly maintained patency compared to controls.

These various forms and applications of RSNOs demonstrate their versatility and their broad potential to be incorporated into many biomedical applications to help prevent infection and thrombosis.

INDEX WORDS: Antimicrobial, Hemocompatible, Biomaterials, Nitric Oxide, Medical Devices

FORMULATION VERSATILITY OF NITRIC OXIDE DONOR MOLECULES FOR THE PREVENTION OF MEDICAL DEVICE-ASSOCIATED COMPLICATIONS

by

MORGAN ASHCRAFT

B.S., Cleveland State University, 2017

A Dissertation Submitted to the Graduate Faculty of The University of Georgia in Partial Fulfillment of the Requirements for the Degree

DOCTOR OF PHILOSOPHY

ATHENS, GEORGIA

2022

© 2022

Morgan Ashcraft

All Rights Reserved

FORMULATION VERSATILITY OF NITRIC OXIDE DONOR MOLECULES FOR THE PREVENTION OF MEDICAL DEVICE-ASSOCIATED COMPLICATIONS

by

MORGAN ASHCRAFT

Major Professor:	Hitesh Handa
Committee:	Ramana Pidaparti
	Rawad Saleh
	Y. George Zheng

Electronic Version Approved:

Ron Walcott
Vice Provost for Graduate Education and Dean of the Graduate School
The University of Georgia
August 2022

DEDICATION

My first publication (in kindergarten) was dedicated to my sister. Now this one is dedicated to my brother. Thanks for everything, Ryan.

ACKNOWLEDGEMENTS

It has taken a tremendous amount of support from wonderful people to achieve this. Thank you, Dr. Hitesh Handa, for being an amazing mentor and friend and showing me what graduate school could be. I also thank my committee, Dr. George Zheng, Dr. Rawad Saleh, and Dr. Ramana Pidaparti for their support as well as Dr. Elizabeth Brisbois who, while not an official member, has likewise helped shape my research. It cannot be overstated how much I have also learned from and experienced with Dr. Megan Douglass and Mark Garren; long live the M Team/M^3. Invaluable outside support has also come from Dr. Wided Najahi Missaoui, Julie Simmons, Dr. Lillie Barnett, Lauren Golick, and Bethany Hruschak; thank you for the reality checks and vent sessions. This work could not have been done without the Handa and Brisbois labs. In particular, thank you, Dr. Arnab Mondal, Lori Estes, Elaine Wu, Vince Pinon, and Dagney Crowley. Finally, I cannot express enough appreciation to my family. My parents, Paul and Donna (the other Dr. Ashcraft) have been endlessly supportive and compassionate and never as exasperated and they should have been. My brothers, Ryan and Sam, and my aunt, Sandy Musialowski, have likewise been patient, caring, and sympathetic at all the right times. My cats, Minerva and Cleopatra, brought me many stress balls while writing this (without being taught) and always allowed me to talk out my craziest ideas with the appropriate amount of judgement. Thank you, everyone.

TABLE OF CONTENTS

Page

LIST OF TABLES

Page

LIST OF FIGURES

Page

CHAPTER 1

Introduction and Literature Review: Prevention of Medical Device-Associated Infection and Thrombosis[1]

[1]Portions of this chapter were published as: *Combination Strategies for Antithrombotic Biomaterials: An Emerging Trend Towards Hemocompatibility.* Ashcraft, M., Douglass, M., Chen, Y., Handa, H. Biomaterials Science, 2021, 9, 2413-2423. Reprinted here with permission of the publisher.

1.1 Complications of Medical Device Use

Modern healthcare ubiquitously uses medical devices, which vary greatly in form and function. The Food and Drug Administration (FDA) groups medical devices into three classes (Class I, Class II, and Class III) based on the risks that are associated with the particular device. While these risks can be as diverse as medical devices are, two complications for indwelling medical devices stand out – infection and clotting. These are two of the most common complications for devices, such as venous catheters and extracorporeal life support systems, among many others. While they are health complications in and of themselves, infection and thrombosis can also cause additional health concerns (e.g., surface-induced thrombosis is associated with embolism, post-thrombotic syndrome, etc.)[1,2] and/or device failure. Their prevalence contributes greatly to morbidity, mortality, increased length of hospital stays, and healthcare costs. As such, great efforts are made to avoid and treat medical device-associated infection and thrombosis.

1.1.1 Device-Associated Infections

The Center for Disease Control and Prevention (CDC) has estimated that 1.7 million hospital acquired infections (HAIs) occur in the US annually and are associated with 98,000 deaths.[3] There are several kinds of HAIs, over half of which are connected with the use of a medical device.[4] These include central line-associated bloodstream infections (CLABSIs), catheter-associated UTIs, and surgical site infections (SSIs), among others.[3]

These infections generally occur in two ways: 1) via introduction of a non-sterile medical device into the body, including those used in surgery, and 2) via microbes entering the body through an opening created for or provided by a medical device, such as through a catheter.

Regardless of how the pathogens are introduced, indwelling device-associated infections follow a similar progression (**Figure 1.1**). Planktonic, or free floating, microbes adhere to the surface of the medical device using appendages and/or physical forces, such as hydrophobic interactions.[5] Once attached, bacteria in their sessile state express genes that allow for increased excretion of materials out of the bacterial cell, including polysaccharides. This secretion of extracellular polymeric substances (EPS) forms a protective coat around the colonized bacteria called a biofilm.[6] This barrier shields the encased microbes from immune cells,[7] restricts the penetration of antibiotics,[8] and provides an excellent environment for bacterial proliferation and horizontal gene transfer, one of the most common mechanisms for the acquisition of drug-resistant genes.[9-11] Moreover, biofilms are notoriously difficult to disperse and/or eradicate via outside forces. The final stage of the biofilm lifecycle, however, involves partial self-dispersion of the biofilm via various enzymes that loosen and/or breakdown the matrix in order for planktonic bacteria to be released with the aim of colonizing a new area.[12]

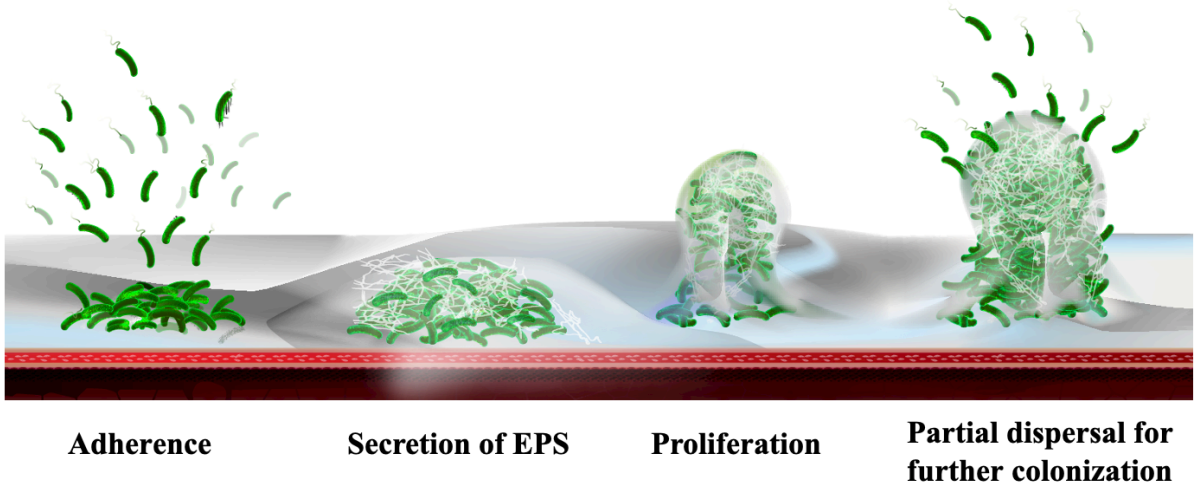

Figure 1.1 Progression of bacterial colonization of a surface.

Biofilms are major issues within healthcare settings because of the current inability to eliminate them, particularly when on indwelling medical devices, and their ability to continuously regenerate when not completely eradicated. Because of the associated risk of reinfection, many medical devices, such as catheters, are removed and/or replaced when biofilm formation is suspected. This causes increased healthcare costs and additional patient discomfort if removal is a viable option. If it is not, biofilm formation can be detrimental to patient morbidity and mortality.

Device-associated infections can be further complicated via the presence of antibiotic resistant bacterial strains. With the alarming rate of emergence of these antibiotic resistant pathogens, particularly in healthcare settings, the prevention of infections has become more important and treatments more difficult.[13-16] The prevention of infection results in less antibiotics used in treatments, which is advantageous to the fight against antibiotic resistance. However, if the method of prevention involves antibiotics (further discussed in **Section 1.2.1**), it may not have this benefit. The presence of biofilms in device-associated infections further exacerbates the situation. As mentioned above, biofilms greatly limit the exposure of the enclosed bacterial cells to antibiotics; it has been shown that biofilms can withstand 100-1000 times the concentration of antibiotics that planktonic bacteria can.[17] This excessive and ineffective use of antibiotics attempting to treat biofilms may have significant contributions to the emergence of further resistant strains.[18]

1.1.2 Device-Associated Thrombosis

Millions of blood-contacting medical devices (BCMD) are used every year in the form of catheters, stents, heart valves, vascular grafts, etc. However, even with the aid of systemic anticoagulation, thrombosis (or clotting) remains one of the most common complications and causes of failure for

these devices.[19] In addition to device failure, surface-induced thrombosis is related to several health concerns. Within a vessel, thrombi may create an occlusion, and, if detached, embolism may occur.[1] Additionally, it is associated with post-thrombotic syndrome, wherein a patient may experience pain, swelling, and redness among other symptoms at the site of clotting.[2] The consumption of blood and immune cells in surface-associated thrombosis can also lead to hypocoagulability post-treatment.[20] Moreover, thrombi can provide a surface that bacteria can easily adhere to, increasing the risk of infection and sepsis.[21]

Contact with foreign surfaces such as BCMD disrupts blood homeostasis and leads to thrombus formation via the contact activation/intrinsic pathway of coagulation. Briefly, the process starts with plasma protein adsorption, leading to platelet adhesion and activation, further cell deposition and fibrin polymerization, and finally results in thrombus formation (**Figure 1.2**). Plasma proteins rapidly adsorb to BCMD surfaces, triggering a number of complex reactions regulating thrombosis. Adsorbed fibrinogen and von Willebrand factor (vWF) mediate platelet adhesion through interaction with GPIIb/IIIa platelet receptors, transforming platelets to a procoagulant state.[19,22] In this state, platelets can bind to factors Va (FVa) and Xa (FXa), forming a prothrombinase complex capable of converting prothrombin to thrombin.[22] Thrombin polymerizes fibrinogen to fibrin, which further stabilizes the blood clot. Circulating leukocytes adhere to adsorbed fibrinogen and release platelet activating factor, interleukins, and tumor necrosis factor, further promoting thrombosis.[19] Contact system components factor XII (FXII) and prekallikrein (PK) initiate the coagulation cascade, ultimately leading to fibrin formation. In addition, activated prekallikrein (PKa) generates kallikrein, triggering complement activation that further propagates platelet activation and tissue factor expression on leukocytes.[23]

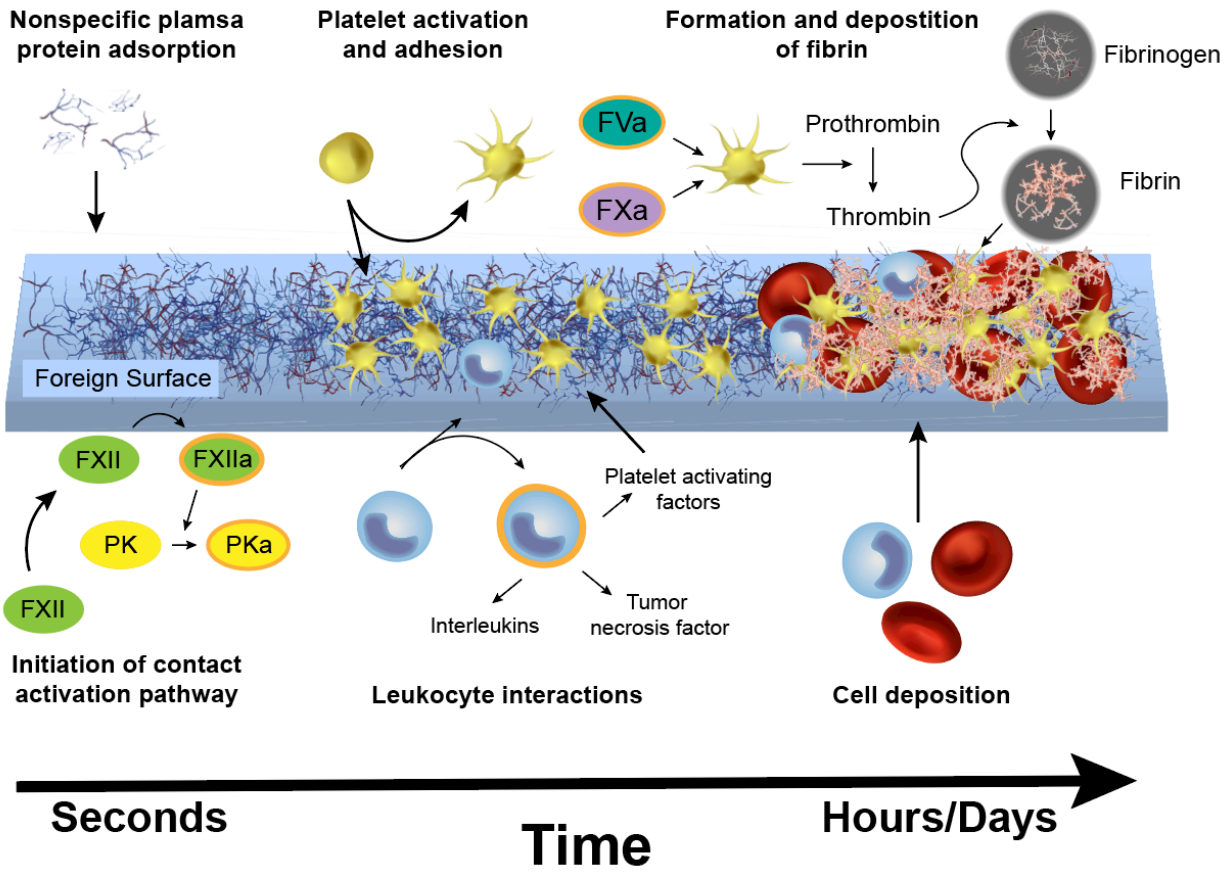

Figure 1.2 Contact activation results in thrombi on foreign surfaces. Factor XII (FXII); Activated factor XII (FXIIa); Prekallikrein (PK); Activated factor V (FVa); Activated factor X (FXa).

Clotting is a ubiquitous issue for BCMD. It demonstrates a lack of compatibility between the body and device, it is associated with the inherent risk of having thrombi that could detach within vessels, and it is a major cause of device failure and other health complications.

1.2 Current Clinical Practices to Minimize Device-Associated Complications

Great care is given clinically to deter device-associated complications and their related contributions to morbidity, mortality, increased length of hospital stays, and healthcare costs. However, practices may vary greatly between healthcare facilities and clinicians. These practices include sterilization techniques, use of prophylactic drugs such as antibiotics and/or

anticoagulants, and use of devices designed to reduce complications. Emphasis is particularly given to the prevention of the onset of any potential complications. Thrombosis and biofilm formation are events that can only be partially undone through medical intervention; thus, prevention is more desirable than treatment.

1.2.1 Clinical Practices to Minimize Device-Associated Infections

1.2.1.1 Aseptic Techniques in Practice

Many, if not all, healthcare settings follow guidelines on aseptic techniques and/or sterility to prevent the spread of infectious agents to and between patients. These practices are recommended by the CDC within their Core Infection Prevention and Control Practices for Safe Healthcare Delivery in All Settings.[24] While generally credited for the reduction of HAIs over the past decades, the still seen prevalence of infection associated with healthcare indicates that current practices are not sufficient by themselves. For example, a systemic review found 7% of parentally prepared injection doses to be contaminated even when using aseptic techniques.[25]

Aseptic techniques have varied success rates in different environments and when performed by different healthcare professionals. For example, a study found greater sterility in doses prepared in a pharmacy compared to those prepared in a clinical setting.[26] Education, training, available supplies, and the cleanliness of setting can all contribute to the success of aseptic practices. This variability and room for human error supports the need for additional antimicrobial interventions within healthcare settings.

1.2.1.2 Prophylactic Use of Antibiotics

In order to prevent the onset of device-associated infections, antibiotics may be administered prior to and/or directly after surgery and/or device implantation. This is done to prevent the onset of a potential infection by eliminating planktonic bacteria before it can gain a foothold. Prophylactic antibiotic use may be localized as well as administered systemically. Localized therapies are most commonly topical antimicrobial agents to prevent skin infections but can be device specific. For example, antimicrobial lock solutions may be used to deter infections in venous catheters. Localized therapies have the advantage of only affecting the desired area, thus not affecting untargeted bacteria such as the natural microbiota. They also reduce the number of microbes exposed to the antibiotics relative to systemic administrations, reducing the potential for the development of resistance.

Prophylactic antibiotic use is controversial in its efficacy and antibiotic stewardship. Some procedures find antibiotic prophylaxis to be effective in reducing infections – infection rates after orthopedic implant surgery drop to 1-3% with preoperative antibiotics compared to 4-8% without.[27] No difference in infection rates with or without preemptive antibiotic use is seen in other situations, however, such as in pacemaker implantation or replacement.[28] With such variation, universal prophylactic antibiotic use is not justified, and its practice may vary between clinics and/or clinicians.[29]

The balance between prophylactic antibiotic therapies and antibiotic stewardship also comes into question when evaluating the potential rate of success and the risks of promoting the development of resistance. As the drug resistance crisis becomes more severe, this dilemma has been both a strategic and ethical issue.[30] While there is still no clear answer, calls have been made

to cease the use of preventative antibiotics in favor of using antiseptic methods and skin hygiene practices that would not promote the emergence of drug resistant strains.[13]

It is also worth noting that in addition to the risk of promoting drug resistance among microbes, antibiotic therapies are not without direct health risks. Allergic reactions to antibiotics are the most common adverse effect seen, as allergies may be undetected.[31] Even when evaluated prior to administration, allergy test results can be misleading, complicating the determination of the correct antibiotic for the patient.[32] Allergic reactions may appear in the form of gastrointestinal issues, rashes, and neurological issues, among others. Gastrointestinal adverse effects may also occur in non-allergic patients as antibiotics commonly disturb the gut microbiota.[31]

1.2.1.3 Antimicrobial Medical Devices

Another strategy to mitigate medical device-associated infections is the use of antimicrobial devices (**Table 1.1**). Applying antibacterial strategies directly to the interface of the potential infection maximizes localization and minimizes interference with the natural microbiota and potential side effects. Many of these medical devices contain antibiotics regularly used as traditional therapies in patients, such as aminoglycosides, minocycline, rifampin, vancomycin, etc.[33-35] While studies have noted their ability to decrease rates of medical device-related infections,[33] there is the same concern of unnecessary antibiotic use that is associated with the prophylactic use of antibiotics.

Other antimicrobial devices avoid this concern by incorporating non-traditional antibiotics, such as carbon, gold, silver, etc.[36-38] Silver is particularly widely used. These compounds are often established antimicrobial agents with insufficient biocompatibility to be used systemically. As with more traditional antibiotic-containing medical devices, having the agents contained within the device itself limits its interaction and potential adverse effects on the patient. These compounds

generally have nonspecific mechanisms of action, hence their adverse effects in patients if administered systemically. For example, silver's attributed antimicrobial actions include cell penetration, interference with signaling pathways, and generation of reactive oxygen species (ROS) and free radicals.[39] With such broad actions, there is little risk of bacteria developing resistance, which is another advantage of their use.

Table 1.1 Representative clinically available, antimicrobial-incorporated variations of common medical devices**.** Central venous catheters (CVCs); Endotracheal tubes (ETTs).

Biocidal Agent	**Medical Device(s)**	**References**
Aminoglycosides	Orthopedic Implants	35,40
Benzalkonium chloride	CVCs	38
Carbon	CVCs	37
Ceragenin	ETTs	41
Chlorohexidine	CVCs	33,34,38
Clindamycin	Orthopedic Implants	40
Colistin	Orthopedic Implants	42
Gold	ETTs	36
Erythromycin	Orthopedic Implants	42
Miconazole	CVCs	38,43
Minocycline	CVCs, Urinary catheters	33,34,38,44
Nitrofurazone	Urinary catheters	45
Palladium	ETTs	36
Platinum	CVCs	37
Rifampin	CVCs, Urinary catheters	33,34,43,44
Silver	CVCs, ETTs, Urinary catheters	33,34,38,45,46
Vancomycin	Orthopedic Implants	35

Besides the incorporation of various antimicrobial agents into medical devices, there have also been advances in material science, providing better options for medical device surfaces. A general trend is increased hydrophilicity to prevent protein and connected bacterial adhesion.[47] However, more complex surfaces have also made it to the market. A textured surface resembling

shark skin has recently been incorporated into clinical medical device design, advertising its antimicrobial properties.[48]

While inherently antimicrobial medical devices may mitigate some infections caused by healthcare environments and imperfect aseptic techniques, the prevalence of HAIs with these available options indicates that they are an imperfect solution. Much investigation research is being done to address the shortcomings of efficacy (discussed in **Section 1.3.1**).

1.2.2 Clinical Practices to Minimize Device-Associated Thrombosis

As blood is preset to clot when exposed to any interface but the endothelium, the risk of inducing thrombosis when using BCMD is high and requires medical interventions to prevent. Prevention, as opposed to treatment, is vital as thrombosis is a non-reversible event. There are some thrombolytic agents, such as alteplase, that can be administered to break up clots that have formed, but the therapies are not indicated for medical device-associated thrombosis (excepting catheter occlusion) and come with risks of serious adverse effects.[49] Thus, prevention is key. Clinical prevention strategies are the use of anticoagulant and/or antiplatelet agents and the use of antithrombotic devices.

1.2.2.1 Use of Anticoagulant and Antiplatelet Agents

Both anticoagulant and antiplatelet agents can be used to mitigate medical device-associated thrombosis. Anticoagulants are considered drugs that inhibit the body's ability to form clots and can have a variety of mechanisms of action (e.g., thrombin inhibitors, factor Xa inhibitors, vitamin K antagonists, etc.).[50] All interfere with components of the common pathway of the coagulation cascade (**Figure 1.3**), although they may also inhibit other parts, such as the

progression of the intrinsic pathway. Antiplatelet agents, as the name suggests, are those that interfere with platelet activation and adherence.

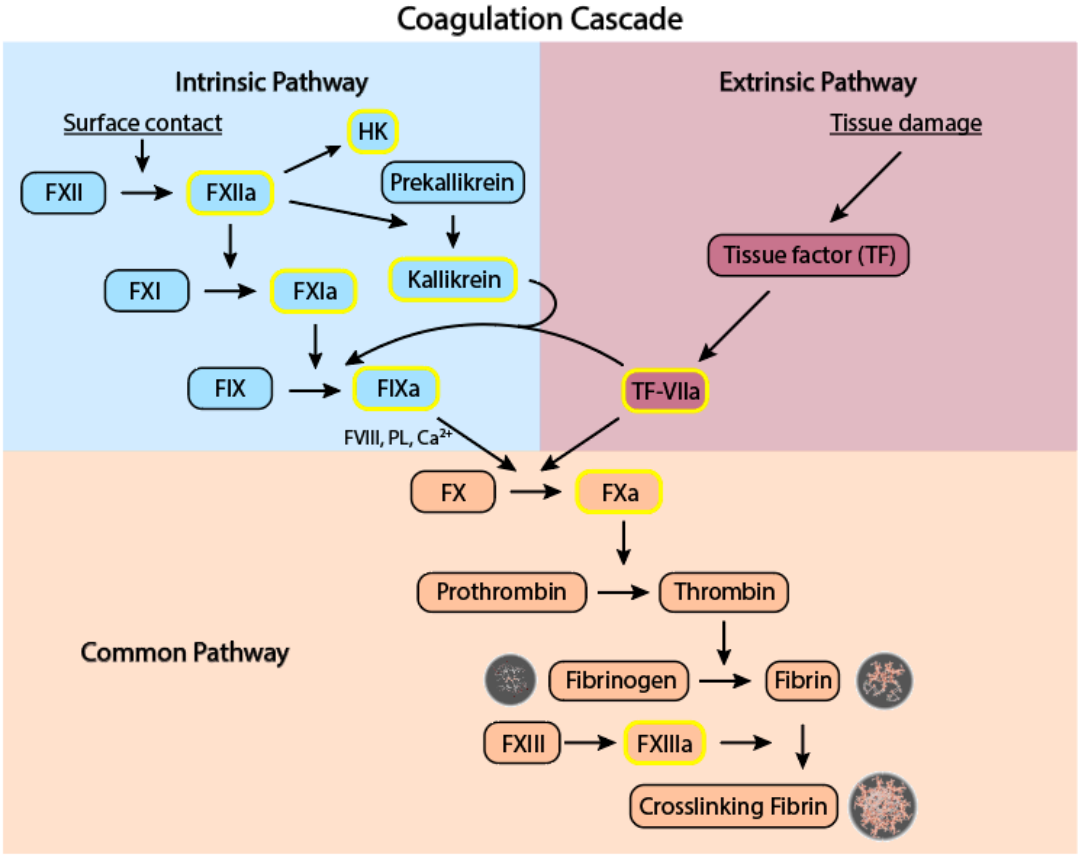

Figure 1.3 Overview of the coagulation cascade. It can be initiated through the intrinsic and extrinsic pathways, both leading to the common pathway and resulting in clot formation.

While generally administered systemically, anticoagulation therapies are also used locally as lock solutions in catheters. Solutions containing anticoagulants (commonly heparin) are inserted into catheter lumen to attempt to prevent clotting at the catheter tip, thus maintaining patency. The localization of this therapy is advantageous in avoiding the risk of adverse effects seen with systemic administration. However, their efficacy in preventing thrombosis is controversial.[51-53]

In addition to inadequate efficacy at prevent device-associated thrombosis, anticoagulation therapies have common, sometimes life-threatening, adverse effects. Namely, there is a high risk

of major bleeding and associated hemorrhagic complications.[54] There may also be therapy specific adverse effects, such as heparin-induced thrombocytopenia.[55] Patients may also experience hypersensitivity reactions; although rare, these reactions may be lifethreatening.[56]

Anticoagulants and antiplatelets do not completely prevent device-induced thrombosis. Device failure rates associated with thrombosis have been reported to be up to 6% even with modern healthcare practices.[19] This can be for several reasons – dosing issues, flow disturbance caused by the device, and incomplete inhibition of the contact activation and/or common pathways. Anticoagulation does not prevent the adsorption of plasma proteins to the surface of medical devices, including the binding and autoactivation of FXII. Thus, there is a need for materials for medical devices that address blood-surface interactions to complement anticoagulation therapies for safer BCMD use.

1.2.2.2 Antithrombotic Medical Devices

Certain marketed medical devices are designed to have decreased thrombogenic effects **(Table 1.2**). The incorporation of heparin is a particularly popular design feature. As with antimicrobial device designs, heparin-bonded or coated devices have the advantage of avoiding potential adverse effects that often accompany systemic administration of the same agent. However, there is a risk of decreased antithrombotic action if the attached heparin is locked into a suboptimal confirmation.[57] This design strategy is considered to be bioactive as it inhibits the coagulation cascade via binding to antithrombin. Other design strategies are considered to be passive as they do not work on the progression of thrombosis; instead, they seek to minimize attachment of blood components to the surface.

Table 1.2 Representative clinically available, antithrombotic variations of common medical devices.

Modification	**Mechanism**	**Device**	**References**
Albumin-coated	Passivating	Extracorporeal circuits, vascular grafts	20,58
Carbon-coated	Negative charge	Peripheral grafts, stents	59,60
Collagen-coated/impregnated	Decreased porosity	Peripheral grafts	61,62
Gelatin-sealed/impregnated	Decreased porosity	Peripheral grafts	62,63
Heparin bonded/coated	Promotes antithrombin inhibition of coagulation factors	Peripheral grafts, ventricular assist devices, membrane oxygenator circuits, catheters	20,57,64,65
Phosphorylcholine-coated	Hydrophilicity and zwitterionic properties	Extracorporeal circuits	20
Polyethylene glycol-coated	Hydrophilicity	Extracorporeal circuits	20

Passivation strategies seen in clinically available medical devices can largely be grouped into polymeric coatings and biomolecule coatings. The exception to this is carbon-coated grafts and stents, whose negative charge is responsible for decrease adhesion of blood components.[59,60] A major aspect of the passivation mechanism of action for both polymeric coatings and biomolecule coatings is increased hydrophilicity. As plasma protein adsorption (the start of the contact activation pathway) is largely driven by hydrophobic interactions, a hydrophilic coating can provide more resistance to this event.[66] Plasma protein adsorption is also driven by electrostatic interactions, which is why zwitterions, such as phosphorylcholine, have been incorporated into coatings that also deter adsorption.[20]

Another consideration related to thrombogenesis is surface texture; generally speaking, smoother surfaces provide less surface area for plasma protein adsorption and, therefore, are associated with less clotting.[67] With this in mind, grafts have been coated with gelatin or collagen to decrease the device's porosity, thus decreasing the potential for surface-induced thrombosis. [61-63]

It should be noted that these devices are to be used with systemic anticoagulation therapies. They are additional prophylactic support against device-associated clotting, not a replacement to the aforementioned risky therapies. However, eliminating the need for anticoagulation via thrombo-resistant materials is a much-pursued goal, discussed further in **Section 1.3.2**.

1.3 Investigative Strategies for Medical Device Complication Prevention

1.3.1 Infection Prevention

1.3.1.1 Nontraditional Antibiotics

In the search for new antibiotics spurred by the rapid emergence of antibiotic resistant bacteria, investigational efforts have strayed from conventional small molecule antibiotics (**Table 1.3**). Unlike traditional antibiotics, some classes of these compounds do not directly aim to kill bacteria. For example, biofilm inhibitors and virulence modulators seek to make bacteria more susceptible to antibiotic therapies and/or host immune cells.[68,69] Vaccines also do not affect bacteria directly, but they can affect the fight against antibiotic resistance via preventing the occurrence of infections, thereby reducing antibiotic usage and exposure.[70]

Table 1.3 Nontraditional Antimicrobial Agent Categories and Descriptions.

Nontraditional Antimicrobials	**Description/Mechanism of Deterring Infection**	**References**
Antibodies	Biological large molecules developed for toxin neutralization, interference with bacterial surface proteins, disruption of defensive structures	71
Antimicrobial peptides	Biological small molecules that act on bacterial membranes or internal targets (nucleic acids, protein synthesis, etc.)	72
Bacteriophages	Viruses that target bacteria, causing lysis	73
Biofilm inhibitors	Small molecules that prevent biofilm formation or disrupt established biofilms	69
Vaccines	Therapies that elicit preventative host immunity	70

Virulence modulators	Small molecules, peptides, and biologic molecules that interfere with biofilms, quorum sensing, inhibition of drug resistant mechanisms, etc.	[68]

The other categories of nontraditional antibiotics are generally biologically derived. Monoclonal antibody therapies could either neutralize toxins produced by the bacteria, relieving symptoms and damage done by the infection, or they could act directly on the bacteria.[71] The field of antimicrobial peptides has gained considerable attention with the growing resistance crisis. A considerable variety have been discovered or developed with a range of mechanisms of action. These include, but are not limited to, disruption of bacterial membranes, inhibition of DNA synthesis, and inhibition of protein synthesis.[72] Bacteriophages, which are viruses that target bacteria, have also been suggested as an alternative to traditional antibiotics.[73] However, the stability of some of all of these biologically derived antibiotics may limit clinical applications.

1.3.1.2 Antimicrobial Materials

Many material designs have been investigated with the goal of developing surfaces resistant to bacterial colonization (**Table 1.4**), thus potentially mitigating medical device-associated infections. As some of these strategies have general antifouling effects, they may also be considered antithrombotic through their resistance to plasma protein adsorption (discussed in **Section 1.3.2.1**). These strategies can be broadly classified into four surface/material categories: 1) Incorporation of antimicrobial agents, 2) Immobilized antimicrobial agents, 3) Surface property modifications, and 4) Release of antimicrobial agents. Within these categories, specific design strategies may be bioactive (playing an active role in biological processes, e.g., killing bacteria before it can adhere itself) or biopassive (minimizing interactions between the material and its biological environment).

Table 1.4 Overview of Antimicrobial Material Design Strategies.

Design Strategy	Activity	Examples	Common Advantages	Common Shortcomings

Incorporated antimicrobial agents	**Bioactive**	• Traditional antibiotics[74,75]
		  • Aminoglycosides
		  • Quinolones
		  • Tetracyclines
			• Stability
			• Biocompatibility
				• Poor antibiotic stewardship
				• Risk of promoting antibiotic resistance

		• Silver[76,77]	• Lack of resistance concerns • Versatile • Broad spectrum	• Safety and efficacy vary with its form • Leaching has toxicity concerns
Immobilized antimicrobial agents	**Bioactive**	• Antimicrobial peptides[78,79]	• Lack of resistance concerns • Can have antibiofilm actions • Can be broad-spectrum	• Potential for hemolysis and unintended biological effects • Lack of preclinical and clinical success
		• Bacteriophages[80-82]	• Specificity of targeted bacteria indicates low risk of adverse effects • May improve general biocompatibility via improved hydrophilicity	• Specificity of targeted bacteria limits uses • Batch-to-batch variability
		• Quaternary ammonium[83,84]	• Wide range of biological effects • Lack of resistance concerns • Broad spectrum	• Biocompatibility concerns
Surface property modifications	**Biopassive**	• Hydrophilicity[85,86]	• Resists protein and bacterial adhesion	• Less effective compared to other antifouling methods
		• Lubrication[87,88]	• Broadly antifouling	• Lubricant can become depleted over time • Sample inconsistency
		• Protein coat[89,90]	• Biocompatible	• Subject to Vroman effect • Less effective compared to other antifouling methods
		• Superhydrophobicity[91]	• Broadly antifouling	• Unstable in biological environments
		• Zwitterions[92]	• Resists protein and bacterial adhesion	• Stability • Uncertain long-term efficacy
	Bioactive	• NO generation[93]	• Broad spectrum	• Lack of demonstrated *in vivo* efficacy

Release of antimicrobial agents	**Bioactive**	• NO-releasing materials[93,94] • Antimicrobial peptides[79]	• Broad spectrum • Low to no risk of promotion of resistance	• Lack of demonstrated clinical efficacy • Finite reservoir • Achieving stable release

The incorporation of antimicrobial agents into a coating or material generally involves either traditional antibiotics or silver. Through their presence on the surface or their diffusion through the coating via water uptake of the material, these antimicrobial agents can kill bacteria before or during attachment. As discussed in **Section 1.2.1.3**, this strategy has been translated into clinical use. However, there are concerns for the promotion of antibiotic resistance (antibiotic coatings) and toxicity (silver coatings) associated with their use.[74-77]

Other antimicrobial agents are immobilized to surfaces. This has the advantage potentially superior biocompatibility compared to materials that diffuse or are released from the surface, but there is also the potential for decreased antimicrobial activity caused by the immobilization method. These agents include antimicrobial peptides,[78,79] bacteriophages,[80-82] and quaternary ammonium.[83,84] Antimicrobial peptides and bacteriophages have effects that are generally limited to bacteria, sometimes even specific bacteria. This minimizes concerns with biocompatibility, but their specificity can also limit their ability to prevent infections. Immobilized quaternary ammonium, conversely, has broad affects, raising concerns of biocompatibility.

Many surface modifications have been investigated to assess the effects of surface properties on deterrence of infection. These properties are largely biopassive and generally antifouling. Hydrophilic coatings can reduce bacterial adhesion by minimizing hydrophobic interactions that may assist in attaching to the surface.[85,86] However, superhydrophobic coatings that prevent wetting can also prevent contact with bacteria.[91] Unfortunately, these coatings have not been demonstrated to be stable in biological environments, especially in dynamic settings.

Similar stability concerns are associated with other surface modifications. Protein coatings can increase hydrophilicity, but their adsorption to the material may be transient as proteins with higher affinities for the surface may displace them via the Vroman effect.[89,90] Zwitterions can also improve hydrophilicity, but they can further prevent bacterial attachment through electrostatic interactions or lack thereof. However, their effects are relatively short lived and have little to no demonstrated long-term success. Compared to other surface modifications, the incorporation of a lubricant may be considered to have prolonged effects. Even still, the lubricant can become depleted over time, especially under flow conditions.[87,88]

The surface modification strategy that is considered to be bioactive involves the generation of nitric oxide (NO) from endogenous NO donor molecules. NO is a broad-spectrum antimicrobial agent utilizes by our immune systems to mitigate infections.[95] While shown to have efficacy *in vitro*, it is still unclear as to if these surfaces can liberate physiologically relevant concentrations of NO from endogenous donors to have biological effects *in vivo*.[93]

NO can also be released from surfaces that are impregnated with NO donor molecules. This strategy has the advantage of producing relevant ranges of NO for antimicrobial effects, although achieving a steady rate is a challenge for the field.[93] Other materials have also been designed to release antimicrobial peptides.[79] A drawback of this strategy, however, is that the materials have a finite reservoir of antimicrobial agent within them.

These investigational materials show great promise for preventing the onset of infections, but many of these strategies are short term solutions. Given, however, that many infections may arise soon after implantation of medical devices, they may have significant clinical impact even with stability or longevity concerns. The combination of these strategies is also being pursued to

assess the advantages of multiple mechanism of infection mitigation, which may also result in the development of more robust materials.

1.3.2 Surface-Induced Thrombosis Prevention

1.3.2.1 Antithrombotic Materials

Investigational antithrombotic materials seek to prevent material-induced clotting through three design strategies – 1) Immobilization of anticoagulants, 2) Modifying surface properties, and/or 3) Releasing antithrombotic compounds (**Table 1.5**). As discussed in **Section 1.2.2.2**, heparin is a commonly incorporated anticoagulant into medical device surfaces, and these deigns have made it into clinical use. A number of other anticoagulants have also been experimentally immobilized, however, including thrombomodulin,[96,97] apyrase,[98] hirudin,[99,100] argatroban,[101] and recombinant tissue factor pathway inhibitor (rTFPI).[102]

Table 1.5 Overview of Antithrombotic Material Design Strategies.

Design Strategy	**Activity classification**	**Examples**	**Common Advantages**	**Common Shortcomings**
Immobilized anticoagulants	**Bioactive (***Inhibition of components of the coagulation cascade)* & **Passive (***Can improve general biocompatibility[103])*	• Heparin[103] • Thrombomdulin[96,97] • Apyrase[98] • Hirudin[99,100] • Argatroban[101] • rTFPI[102]	• Localized effects[101] • Longevity[104] • Improved pharmacokinetics and pharmacodynamics compared to systemic administration[103] • Reduced adverse effects compared to systemic administration[103] • Demonstrated clinical efficacy[57]	• Potential for reduced efficacy caused by immobilization[57] • Efficacy can be reduced with plasma protein adsorption[105] • Specific mechanism of action • Does not prevent the initiation of surface-induced thrombosis

Surface property modifications	**Passive (***Delay of thrombosis via deterring protein adsorption)*	• Hydrophilicity[86] • Superhydrophobicity[106] • Zwitterions[107] • Surface morphology[67,108] • Lubrication[109]	• Reduced/delayed plasma protein adsorption[110] • Antifouling[106]	• Plasma protein adsorption is inevitable[110] • Lack of inhibition of the coagulation cascade
	Bioactive (*Platelet inhibition or clot disintegration)*	• NO generation[111] • Fibrinolysis[112]	• Localized effects[113] • Combats large aspects of thrombosis[114]	• Potential for reduced efficacy once covered by plasma proteins • Does not prevent the initiation of surface-induced thrombosis
Release of antithrombotic compounds	**Bioactive (***Inhibition of components of the coagulation cascade or clot disintegration)*	• NO[93,115] • Heparin[116] • t-PA[117]	• Localized effects[116] • Retained efficacy compared to immobilization methods[104,116]	• Limited load of antithrombotic compound within material • Achieving a steady and/or prolonged release

Changes in surface properties and morphology can deter thrombosis through passive or active means. A large part of the research field is devoted to developing surfaces that decrease plasma protein adsorption (the initiation of the contact activation pathway), a phenomenon driven by hydrophobic and electrostatic interactions with BCMD.[118,119] Generally, hydrophilic surfaces have been shown to be more resistant to protein adsorption than hydrophobic ones;[66] however, the potential of superhydrophobic surfaces for antifouling applications is a growing field.[106] Surface modifications incorporating zwitterions, which form repeating positive and negative regions on the surface resulting in strong hydration forces, have also shown protein adsorption resistance.[107] The effects of surface morphology on protein adsorption have additionally been investigated; some surface nanostructures show potential for controlling aspects of protein adsorption,[108] but, largely, smooth surfaces have less protein adsorption than rough surfaces.[67] Super slippery surfaces have resulted in exceptionally stable omni-repellent liquid layers at surface interfaces and are also being explored for hemocompatible and general antifouling purposes.[109] Through less plasma protein

adsorption, most of these strategies aim to trigger less contact activation response and therefore reduce thrombosis. However, protein adhesion is inevitable on all current materials even if it can be reduced or delayed.[110] Surface designs that reduce protein adsorption passively deters thrombosis, but they do not mimic any of the active antithrombotic mechanisms that the endothelium employs.

Some surface modifications can be considered to be active approaches with mechanisms outside of preventing plasma protein adsorption. As NO is a known platelet inhibitor produced by the endothelium,[120] NO-generating materials have been developed as one such active antithrombotic strategy.[111] These materials liberate NO from endogenous NO donors, localizing its antiplatelet actions.[113] These materials are discussed at length in Section XX. Additionally, there has been investigation into the use of fibrinolytic surfaces. For example, a layer-by-layer substrate containing gold, chitosan, and a copolymer of sodium 4-vinylbenzenesulfonate and 1-adamantan-1-ylmethyl methacrylate with lysine-containing β-cyclodextrin derivatives attached has been shown to deter the formation of nascent clots.[112]

The release of anticoagulants and other antithrombotic compounds from materials is another field of investigation for blood-contacting surfaces. The most commonly released antithrombotic compound is the aforementioned NO. These materials are discussed at length in **Section 1.4**. Other investigated release strategies involve heparin or heparin conjugates. The localized release of heparin and other clinical anticoagulants can minimize the adverse effects seen with systemic administration and not have the decreased bioactivity of immobilized heparin.[116] In an early investigation of this strategy, heparin-prostaglandin E1 complexes were synthesized for release from blood-contacting materials, successfully deterring fibrin formation and platelet aggregations in a rabbit model when released from polyurethane.[121] Heparin itself has been

incorporated into cleavable hydrogels[122] and self-titrating peptide-polysaccaride nanocomplexes[123] to selectively release the anticoagulant in thrombotic conditions. A responsive coating that releases tissue-plasminogen activator (t-PA) has also been designed.[117] Nanocapsules consisting of thrombin-degradable hydrogels containing t-PA were immobilized on various surfaces and demonstrated fibrinolytic actions in the presence of thrombin.

Although these strategies have shown initial promise, improving the hemocompatibility of medical devices *in vivo* for long-term applications has had limited success. Because coagulation is a complex series of reactions, many materials still lack universal properties needed to prevent thrombosis. For example, although some surface modifications have minimized platelet adhesion and activation, foreign surfaces that do not readily prevent protein adsorption will still suffer from thrombotic complications. Similarly, antifouling materials that slow the adsorption and adhesion of proteins and platelets do not actively mediate and prevent thrombogenic factors from being activated. With this in mind, there has been great efforts directed toward combining these three design strategies. It has been demonstrated that combining multiple antithrombotic surface design strategies provides a means to accommodate one strategy's shortcoming or supply an additional means to prevent thrombosis.[124] However, work is still needed to achieve a truly hemocompatible surface that negates the need for anticoagulation therapies, particularly one suitable for clinical applications.

1.3.3 Bioinspired Antifouling Materials

In recent decades, there has been a movement within the field of material sciences to take inspiration from naturally occurring surfaces with antifouling properties. Antifouling refers to the ability to prevent adhesion and/or adsorption of biological components or other matter onto a surface. Thus, antifouling materials may be antimicrobial and/or antithrombotic.

1.3.3.1 Plant-Mimicking Materials

A number of plants have interesting surface features on their leaves and/or petals that have served as inspiration for biomaterials. Perhaps the most well-studied is the lotus leaf. Largely known as a "self-cleaning" plant, the leaves of the lotus plant, *Nelumbo nucifera*, exhibit excellent water-repellency. The observed "lotus effect" involves water particles repelled by the surface of the plant picking up and removing dirt particles as it is propelled off the leaf via low sliding angles.[125] This paragon of superhydrophobicity relies on both nanostructures and wax composition. Wax is a major factor in a plant's wettability. Its composition is often related to its crystal morphology, thus both play a part in the plant's surface properties.[126]

Nanostructures alone can provide varied surface properties, such as tunable adhesive properties. Interestingly, the surface roughness of rose petals produces similar superhydrophobic qualities to lotus leaves, but alternately allows for high adhesion. Much work has gone into elucidating the differences between these two models (chemical composition, nanostructure shape and spacing, etc.) in order to create materials with specific water adhesion properties.[127]

Other plants, such as *Nepenthes*, have inspired the investigation of slippery materials for antifouling applications. *Nepenthes* demonstrates excellent water repellency, which is attributed to a layer of immobilized fluorinated oil. The field of slippery liquid-infused porous surfaces (SLIPS) was thus inspired. These materials have shown good resistance to biofouling, but results vary from species to species as adhesins and appendages such as flagella can afford more adhesive success. There is also concern about the gradual release of the oil over time and under flow conditions and the related effects on the environment that material is in.[128]

Plants have some natural advantages that mimetic materials will struggle to copy. For example, the ability to change its surface properties to suit its needs. Water plants exhibit superhydrophilic properties when submerged in water, but parts of the plant that rise above the water can become superhydrophobic. Additionally, live plants can continue to secrete waxes to maintain their desired surface compositions, while the lifespan of biomimetic surfaces is often limited.[126] Nonetheless, their inspiration advances the field.

1.3.3.2 Animal-Mimicking Materials

The immense biological variety seen in the animal kingdom provides a plethora of subjects for biomaterial inspiration. Some surfaces of animals are inherently antimicrobial through the presence of nanostructures. For example, insects such as dragonflies and cicadas have nanostructures on their wings that have been shown to reduce viable bacterial adhesion, which has been attributed to the nanoarchitecture's mechanical stress applied to bacterial membranes upon attempted adherence.[129-131] A similar effect is produced by bacterial contact on gecko skin.[132] With these as models, a large field of nanostructured surfaces pursuing this contact killing mechanism has arisen.[133]

Superhydrophobicity is seen in animals as well as plants (discussed in **Section 1.3.3.1**). Water striders are able to walk across water because of their unique legs. These legs are covered in hairs with nanostructures covered in wax, producing a superhydrophobic surface.[134] This description is not dissimilar from that of the lotus' superhydrophobicity. Nanostructures associated with superhydrophobicity are also seen on the wings of some butterflies.[135]

Other animal biomimetic materials focus on the general antifouling properties that can be observed in nature. One example is shark skin, which is renowned for its drag reduction and

antifouling properties. This is achieved through a pattern of small scales with riblets. In this surface's case, the anti-biofouling abilities are contributed to the combination of hydrophobicity and the surface pattern. As mentioned in **Section 1.2.1.3**, materials with similar surfaces to shark skin are clinically available.[48]

1.3.3.3 Endothelium-Mimicking Materials

Despite over 50 years of research and development in improving blood-material interactions, the only truly hemocompatible surface remains the endothelium. To achieve and maintain this state, the endothelium employs a number of antithrombotic mechanisms to supplement the specialized physiology of endothelial cells (**Figure 1.4**).[136] Endothelial cells express antithrombotic proteins such as tissue factor pathway inhibitor (TFPI), thrombomodulin, endothelial protein C receptor (EPCR), and heparin-like molecules on their surfaces.[136] TFPI inhibits the formation of two coagulation factors: it prevents the formation of tissue factor-factor VIIa complexes and, therefore, also the activation of factor X to FXa.[137] Thrombomodulin likewise has multiple actions. It binds thrombin, preventing its conversion of fibrinogen into fibrin, and the thrombomodulin-thrombin complex additionally promotes the activation of protein C (another antithrombotic protein) either by itself or more efficiently when it is bound to EPCR.[138] Heparin and heparin-like molecules enhance antithrombin's ability to bind thrombin, again, preventing the polymerization of fibrinogen into fibrin.[139] In addition to the specialized and responsive surface of endothelial cells, the endothelium actively releases antithrombotic agents to mitigate thrombosis. When released, nitric oxide (NO) and prostacyclin (PG12) have antiplatelet activity, temporarily inhibiting their ability to activate and aggregate.[140] Tissue-Plasminogen Activator (t-PA), also produced in and released by endothelial cells, is thrombolytic instead of preventative of thrombosis.[141] It activates plasminogen, which, in turn, activates plasmin. Plasmin is able to

degrade fibrin and dissolve thrombi. Through the production, expression, and release of these many antithrombotic factors, the endothelium can successfully control thrombosis on its surface. The antithrombotic mechanisms of the endothelium have been incorporated into material designs with varying frequency and success. However, a comparison study of these components has yet to be conducted; therefore, a determination of each factor's effectiveness and importance has yet to be made.

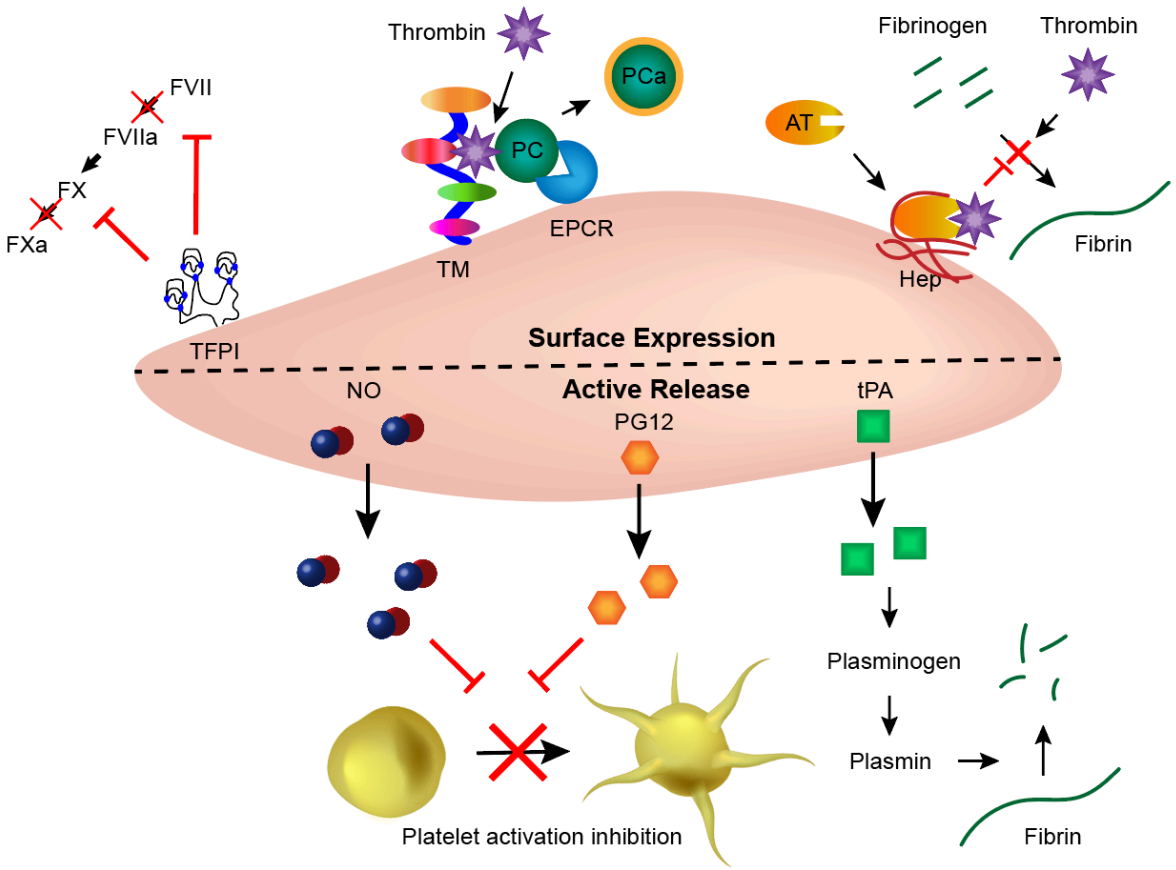

Figure 1.4 Endothelial cells employ many antithrombotic mechanisms. Tissue factor pathway inhibitor (TFPI); Thrombomodulin (TM); Endothelial protein C receptor (EPCR); Protein C (PC); Antithrombin (AT); Heparin-like molecules (Hep); Nitric oxide (NO); Prostacyclin (PG12); tissue-Plasminogen Activator (tPA).

As discussed in **Sections 1.2.2.2** and **1.3.2.1**, several antithrombotic mechanisms that the endothelium employs have been incorporated into biomaterials. Namely, these include NO release, surface TFPI, thrombomodulin, and heparin, and the release of t-PA. There has also been a noted trend in developing materials that have more than one mechanism of thrombotic action, as the endothelium does.[124] Thus, using the endothelium as inspiration, developers aim to create more effective hemocompatible surfaces.

1.4 Nitric Oxide-Releasing Materials

1.4.1 Nitric Oxide Generation vs Release

As briefly introduced in **Sections 1.3.1.2** and **1.3.2.1**, materials that utilize NO's antimicrobial and antithrombotic properties can be NO releasing or NO generating. NO releasing materials have NO stored within them in the form of NO donor molecules (further discussed in **Section 1.4.2**). Upon experiencing certain conditions (heat, light, etc.), NO can be liberated from the molecule, and, as a small, gaseous molecule, can permeate through the material it is contained within. NO generating surfaces, on the other hand, provide the means of liberating NO from endogenous donor molecules. Their catalysis of NO from donors provides similar, localized NO-induced biological effects.

Each of these designs has challenges seeking to be addressed by the NO materials field. NO releasing materials have a finite amount of NO donor stored within it. Consequently, NO release from these materials is bound to be impermanent. While this may be of little concern for short-term medical device applications, this is a limitation for settings where prolonged infection and clotting prevention is needed. Research has shown that the method of NO donor incorporation into a material greatly affects the duration of NO release. Covalently attaching NO donors can provide stabilization and, thus, longer release rates. This has been demonstrated with the

attachment of *S*-nitroso-*N*-acetyl penicillamine (SNAP) to poly(dimethylsiloxane) (PDMS), which resulted in four months of NO release.[142]

Using the natural supply of endogenous NO donors may seem like a natural solution to the longevity drawback of NO releasing materials. However, NO generating materials are not without their weaknesses. In order to achieve NO concentrations that are physiologically relevant, NO donors may have to be added to the system.[143,144] Although, by definition, the catalytic coatings that may generate NO are not consumed in the reactions they facilitate, there are still concerns with their prolonged abilities. The coatings need to be able to come in contact with circulating NO donors. While some studies have shown that coatings can still generate NO with plasma proteins adsorbed,[145,146] there is a lack of evidence that this phenomena does not affect its properties long term.

1.4.2 Nitric Oxide Donor Molecules

NO itself has a very short half-life (~2 seconds).[147] Because of this, NO donor molecules are often employed in order to achieve prolonged NO delivery. There are three classes of NO donor molecules: 1) Nitrate/nitrite/nitroso compounds, 2) *N*-diazeniumdiolates, and 3) *S*-nitrosothiols.[93,148]

1.4.2.1 Nitrate/nitrite/nitroso compounds

This broad class of compounds ranges from organic NO donors such as isoamyl nitrite to inorganic donors such as sodium nitroprusside (**Figure 1.5**). These compounds are largely applied as vasodilators to treat coronary artery disease. Some compounds in this class require exposure to specific enzymes in order to release their NO.[93] Thus, their use in NO releasing systems for medical devices is minimal.

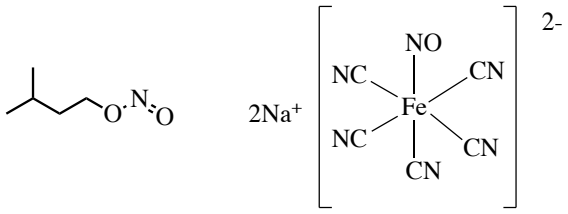

Isoamyl nitrite **Sodium nitroprusside**

Figure 1.5 Structures of isoamyl nitrite and sodium nitroprusside.

1.4.2.2 *N*-diazeniumdiolates

N-diazeniumdiolates (NONOates) are the most widely explored class of NO donor molecules with the start of their synthesis and purification dating back to the 1960s.[149,150] These molecules contain a [N(O-)N=O] group usually attached to an amine. The stability and NO release from these molecules relies greatly on the structure of the nucleophile that the NONO group is attached to (primary amine, secondary amine, etc.).[151] Interestingly, after releasing NO (two moles of NO per one mole of donor molecule), the molecules revert back to their pre-nitrosated form without forming metabolites. NO release from NONOates is generally spontaneous.[152]

The ease of preparation for NONOates is noted and is a cause for their popularity.[93] Generally, NONOates are formed by exposing the base donor molecule to pressurized NO gas in a basic condition.[152] Donor molecules can vary greatly, ranging from small molecules, such as spermine and diethylamine (**Figure 1.6**), to macromolecules, such as dendrimers.[153,154] Despite their variety and investigation in clinical trials, no NONOates are currently available for clinical use.[93]

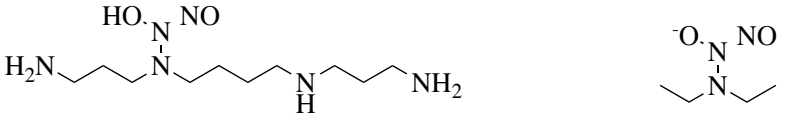

Spermine NONOate **Diethylamine NONOate**

Figure 1.6 Structures of spermine NONOate and diethylamine NONOate.

1.4.2.3 *S*-nitrosothiols

S-nitrosothiols, with the general formula of RSNO, are the third class of widely studies NO donor molecules. The characteristic S-NO bond gives the compounds a green or reddish color (tertiary vs primary or secondary bond) and can be confirmed via UV absorbance at 225-261 and 330-350 nm.[152,155] Unlike NONOates, RSNOs do not spontaneously release their NO. That being said, they are not necessarily more stable than NONOates, both having half-lives ranging from seconds to hours.[151,152]

There are two particularly popular and well-studied RSNOs – *S*-nitrosoglutathione (GSNO) and *S*-nitroso-*N*-acetylpenicillamine (SNAP) (**Figure 1.7**). GSNO is an endogenous NO donor molecule found in red blood cells, plasma, and various tissues.[93,155] It has unusual stability for a primary RSNO; tertiary compounds are generally considered to be more stable. It has been suggested that the γ-glutamyl group of glutathione (GSH) can act as a weak copper chelator.[156] Thus, while not completely known, is has been suggested that this group prevents metal ion catalysis of NO release from GSNO, providing stability. Its excellent solubility in aqueous solutions is another perk of GSNO for biomedical applications. Although not yet clinically available, it has been studied in approximately 20 clinical trials and has been very well tolerated.[155]

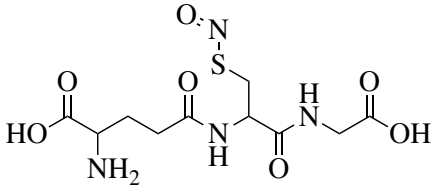

S-nitrosoglutathione (GSNO)

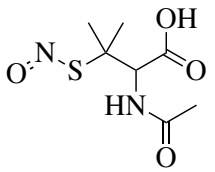

***S*-nitroso-*N*-acetylpenicillamine (SNAP)**

Figure 1.7 Structures of GSNO and SNAP.

SNAP is a tertiary RSNO that is soluble in both aqueous and select organic solvents. This versatility has allowed it to be solvent swelled into varying polymer for biomedical applications.[157,158] This fabrication technique provides an easy method to make existing medical devices NO releasing, as has been demonstrated via urinary catheters and insulin cannulas.[159,160]

SNAP has also been covalently attached to polymers,[142] microparticles,[161] and nanoparticles.[162] This method has led to unprecedentedly long NO release. As stated in Section 1.4.1, covalently attached SNAP-PDMS has demonstrated up to four months of NO release,[142] while typical SNAP-swelled samples may only release NO for 10 days.[163] This extended release is likely due to the stability that covalent attachment affords the SNAP moiety.

1.4.3 Materials with NO Release and Surface Modifications

NO-releasing materials provide inherently multifunctional interfaces as NO has many physiological actions. In addition to the lauded antiplatelet and antimicrobial actions focused on in this dissertation, NO is also an antiviral agent,[148] a neurotransmitter,[164] a mediator of angiogenesis,[165] and a smooth muscle relaxer.[166] However, NO-releasing materials are not infallible. In fact, when exposed to blood, NO-releasing surfaces have been observed to have increased fibrinogen adsorption compared to non NO-releasing surfaces.[167,168]

To accommodate and improve various aspects of biocompatibility, NO-releasing materials are often further modified, providing additional functionalities or defenses against infection and/or thrombosis (**Figure 1.8**). The combination of design strategies, especially those adding supplementary anti-biofouling mechanisms, has repeatedly been shown to be advantageous.[124,160,169-171] These strategies include many discussed in **Sections 1.3.1.2** and **1.3.2.1** – lubrication,[172] zwitterions,[171] improved hydrophilicity,[170,173] anticoagulants,[101,174,175] and

antimicrobials[176,177] among others. This direction of study is very popular because of the abundance of advantages seen in the literature.

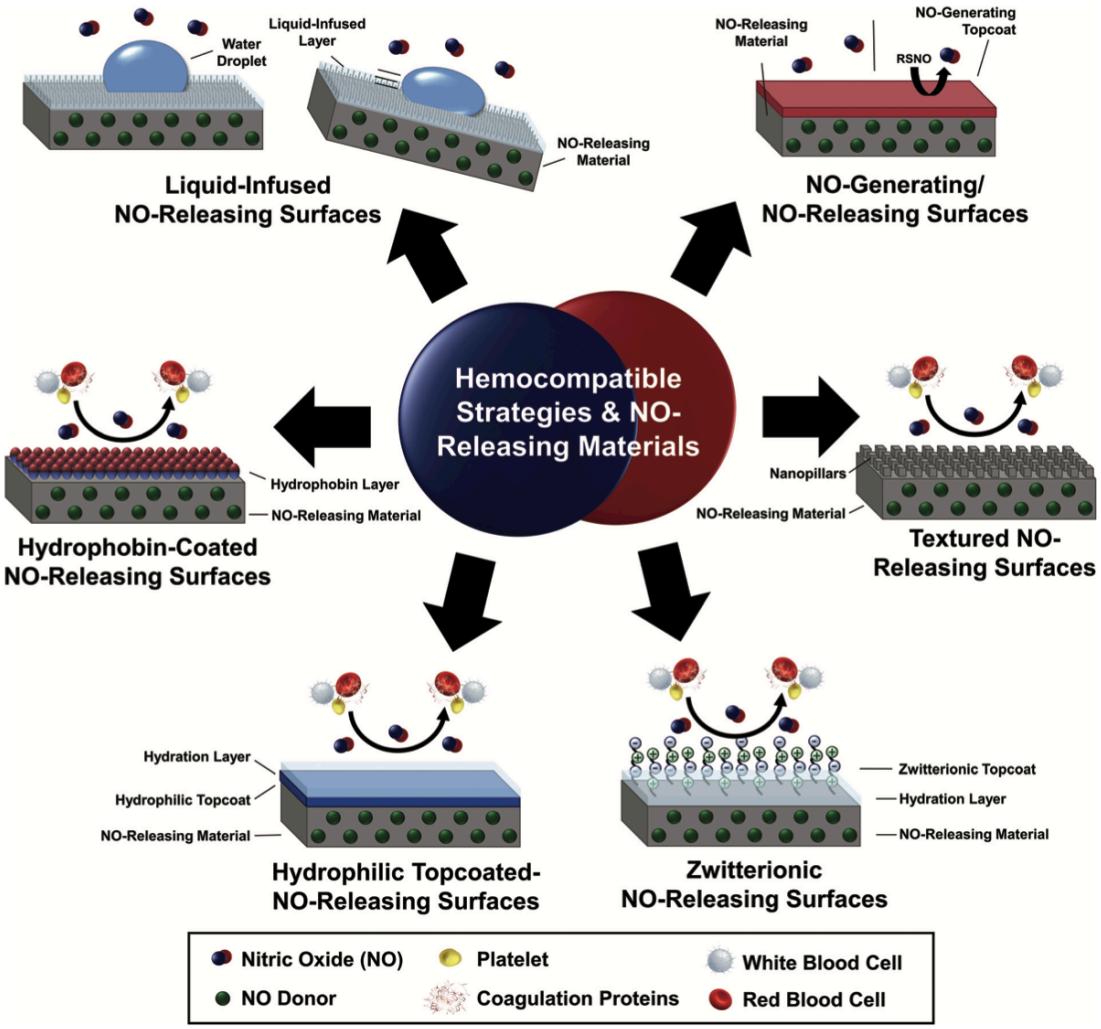

Figure 1.8 Surface modification strategies on NO-releasing materials.

1.5 Statement of Dissertation Research

Healthcare treatments involving medical devices are frequently complicated by infection and thrombosis. Although great progress in both treatments and materials science has been made to minimize these events, their prevalence remains. NO release via NO donor molecules such as RSNOs present a unique, multifaceted approach to mitigating these complications. This

dissertation explores the versatility of RSNOs in various forms as potential solutions for medical device-associate complications. Using a manuscript-style format, this topic is explored. Chapters 1-4 have or will be published in parts or as a whole, and the data within Chapters 2-4 supports current or future grant submissions.

In Chapter 2, an RSNO is dissolved in saline and explored as a lock solution for venous catheters. Its suitability was investigated via in-depth nitric oxide analysis (NOA), which showed that the duration of NO release matched the desired length for a lock solution. Multiple bacterial experiments demonstrated its antibacterial effects, representing the onset of infection and treating infected catheters. The NO-releasing lock solution was also shown to prevent clotting via its antiplatelet actions. Finally, it was shown through hemolysis and cytotoxicity assays that the solution, if leaked, would not have adverse effects.

In Chapter 3, an RSNO is covalently attached to graphene oxide as a potential coating for biomaterials. The novel compound throughout the synthesis was thoroughly characterized using multiple qualitative and quantitative methods. The NO-releasing abilities of the modified graphene oxide was demonstrated to be highly tunable via manner of preparation and also with the use of low-level electrical currents. Moreover, it was demonstrated to have improved antibacterial properties and cytocompatibility compared to unmodified graphene oxide.

In Chapter 4, an RSNO is swelled into medical grade tubing, which is afterwards coated with a hydrophilic, polyethylene glycol (PEG) silane. This novel combination of NO release and PEG showed great potential in *in vitro* bacterial, protein, and platelet adhesion studies. Because of its success, the material was adapted for use in an *in vivo* rabbit model as an extracorporeal circuit. The complementary nature of the material again showed excellence in preventing thrombosis, preserving both platelet and fibrinogen circulation levels significantly better than controls.

Chapter 5 serves as a summary for this dissertation and gives insights into future directions of the field. While this work focused on short-term applications of RSNOs, there is great potential for these explored applications to have longer effects. Through the use of catalysts to promote desired NO release levels and further investigation of covalently attached RSNOs, this work may be further advanced towards prolonged benefits and reduced medical device-associated complications.

1.6 References

1. Labarrere CA, Dabiri AE, Kassab GS. Thrombogenic and Inflammatory Reactions to Biomaterials in Medical Devices. *Frontiers in Bioengineering and Biotechnology.* 2020;8.

2. Polen E, Weintraub M, Stoffer C, Jaffe DH, Burger A, Revel-Vilk S. Post-thrombotic syndrome after central venous catheter removal in childhood cancer survivors: A prospective cohort study. *Pediatr Blood Cancer.* 2015;62(2):285-290.

3. Haque M, Sartelli M, McKimm J, Abu Bakar M. Health care-associated infections - an overview. *Infection and drug resistance.* 2018;11:2321-2333.

4. VanEpps JS, Younger JG. Implantable Device-Related Infection. *Shock.* 2016;46(6):597-608.

5. Khatoon Z, McTiernan CD, Suuronen EJ, Mah T-F, Alarcon EI. Bacterial biofilm formation on implantable devices and approaches to its treatment and prevention. *Heliyon.* 2018;4(12):e01067-e01067.

6. Garrett TR, Bhakoo M, Zhang Z. Bacterial adhesion and biofilms on surfaces. *Progress in Natural Science.* 2008;18(9):1049-1056.

7. Flemming HC, Wingender J, Szewzyk U, Steinberg P, Rice SA, Kjelleberg S. Biofilms: an emergent form of bacterial life. *Nat Rev Microbiol.* 2016;14(9):563-575.

8. Lebeaux D, Ghigo JM, Beloin C. Biofilm-related infections: bridging the gap between clinical management and fundamental aspects of recalcitrance toward antibiotics. *Microbiol Mol Biol Rev.* 2014;78(3):510-543.

9. Madsen JS, Burmolle M, Hansen LH, Sorensen SJ. The interconnection between biofilm formation and horizontal gene transfer. *FEMS Immunol Med Microbiol.* 2012;65(2):183-195.

10. Penesyan A, Nagy SS, Kjelleberg S, Gillings MR, Paulsen IT. Rapid microevolution of biofilm cells in response to antibiotics. *NPJ Biofilms Microbiomes.* 2019;5:34.

11. Steenackers HP, Parijs I, Dubey A, Foster KR, Vanderleyden J. Experimental evolution in biofilm populations. *FEMS Microbiol Rev.* 2016;40(3):373-397.

12. Rumbaugh KP, Sauer K. Biofilm dispersion. *Nature reviews Microbiology.* 2020;18(10):571-586.

13. Mielke M. [The role of infection prevention in the control of antimicrobial resistance : Any avoided infection contributes to the reduction of antibiotic use]. *Bundesgesundheitsblatt Gesundheitsforschung Gesundheitsschutz.* 2018;61(5):553-561.

14. Roca I, Akova M, Baquero F, et al. The global threat of antimicrobial resistance: science for intervention. *New Microbes New Infect.* 2015;6:22-29.

15. Ventola CL. The antibiotic resistance crisis: part 1: causes and threats. *P T.* 2015;40(4):277-283.

16. Whitelaw AC. Role of infection control in combating antibiotic resistance. *S Afr Med J.* 2015;105(5):421.

17. Macia MD, Rojo-Molinero E, Oliver A. Antimicrobial susceptibility testing in biofilm-growing bacteria. *Clinical Microbiology and Infection.* 2014;20(10):981-990.

18. Srinivasan A. Antibiotic stewardship: Why we must, how we can. *Cleve Clin J Med.* 2017;84(9):673-679.

19. Jaffer IH, Fredenburgh JC, Hirsh J, Weitz JI. Medical device-induced thrombosis: what causes it and how can we prevent it? *J Thromb Haemost.* 2015;13 Suppl 1:S72-81.

20. Roberts TR, Garren MRS, Handa H, Batchinsky AI. Toward an artificial endothelium: Development of blood-compatible surfaces for extracorporeal life support. *J Trauma Acute Care Surg.* 2020;89(2S Suppl 2):S59-s68.

21. Rooden CJ, Tesselaar ME, Osanto S, Rosendaal FR, Huisman MV. Deep vein thrombosis associated with central venous catheters - a review. *J Thromb Haemost.* 2005;3(11):2409-2419.

22. Grunkemeier JM, Tsai WB, McFarland CD, Horbett TA. The effect of adsorbed fibrinogen, fibronectin, von Willebrand factor and vitronectin on the procoagulant state of adherent platelets. *Biomaterials.* 2000;21(22):2243-2252.

23. Afshar-Kharghan V. Complement and clot. *Blood.* 2017;129(16):2214-2215.

24. Core Infection Prevention and Control Practices for Safe Healthcare Delivery in All Settings –Recommendations of the HICPAC. https://www.cdc.gov/hicpac/recommendations/core-practices.html. Accessed2022.

25. Suvikas-Peltonen E, Hakoinen S, Celikkayalar E, Laaksonen R, Airaksinen M. Incorrect aseptic techniques in medicine preparation and recommendations for safer practices: a systematic review. *Eur J Hosp Pharm.* 2017;24(3):175-181.

26. Larmené-Beld KHM, Frijlink HW, Taxis K. A systematic review and meta-analysis of microbial contamination of parenteral medication prepared in a clinical versus pharmacy environment. *Eur J Clin Pharmacol.* 2019;75(5):609-617.

27. Uçkay I, Hoffmeyer P, Lew D, Pittet D. Prevention of surgical site infections in orthopaedic surgery and bone trauma: state-of-the-art update. *J Hosp Infect.* 2013;84(1):5-12.

28. Lee W-H, Huang T-C, Lin L-J, et al. Efficacy of postoperative prophylactic antibiotics in reducing permanent pacemaker infections. *Clin Cardiol.* 2017;40(8):559-565.

29. Zanichelli V, Monnier AA, Gyssens IC, et al. Variation in antibiotic use among and within different settings: a systematic review. *J Antimicrob Chemother.* 2018;73(suppl_6):vi17-vi29.

30. Parsonage B, Hagglund PK, Keogh L, Wheelhouse N, Brown RE, Dancer SJ. Control of Antimicrobial Resistance Requires an Ethical Approach. *Frontiers in Microbiology.* 2017;8.

31. Mohsen S, Dickinson JA, Somayaji R. Update on the adverse effects of antimicrobial therapies in community practice. *Can Fam Physician.* 2020;66(9):651-659.

32. Blumenthal KG, Peter JG, Trubiano JA, Phillips EJ. Antibiotic allergy. *Lancet (London, England).* 2019;393(10167):183-198.

33. Casey AL, Mermel LA, Nightingale P, Elliott TS. Antimicrobial central venous catheters in adults: a systematic review and meta-analysis. *Lancet Infect Dis.* 2008;8(12):763-776.

34. Lai NM, Chaiyakunapruk N, Lai NA, O'Riordan E, Pau WS, Saint S. Catheter impregnation, coating or bonding for reducing central venous catheter-related infections in adults. *Cochrane Database Syst Rev.* 2016;3:CD007878.

35. Magnan B, Bondi M, Maluta T, Samaila E, Schirru L, Dall'Oca C. Acrylic bone cement: current concept review. *MUSCULOSKELETAL SURGERY.* 2013;97(2):93-100.

36. Björling G, Johansson D, Bergström L, et al. Tolerability and performance of BIP endotracheal tubes with noble metal alloy coating – a randomized clinical evaluation study. *BMC Anesthesiology.* 2015;15(1):174.

37. Moretti EW, Ofstead CL, Kristy RM, Wetzler HP. Impact of central venous catheter type and methods on catheter-related colonization and bacteraemia. *J Hosp Infect.* 2005;61(2):139-145.

38. Novikov A, Lam MY, Mermel LA, Casey AL, Elliott TS, Nightingale P. Impact of catheter antimicrobial coating on species-specific risk of catheter colonization: a meta-analysis. *Antimicrobial Resistance and Infection Control.* 2012;1(1):40.

39. Dakal TC, Kumar A, Majumdar RS, Yadav V. Mechanistic Basis of Antimicrobial Actions of Silver Nanoparticles. *Frontiers in Microbiology.* 2016;7.

40. Ensing GT, van Horn JR, van der Mei HC, Busscher HJ, Neut D. Copal bone cement is more effective in preventing biofilm formation than Palacos R-G. *Clin Orthop Relat Res.* 2008;466(6):1492-1498.

41. Hashemi MM, Rovig J, Bateman J, et al. Preclinical testing of a broad-spectrum antimicrobial endotracheal tube coated with an innate immune synthetic mimic. *Journal of Antimicrobial Chemotherapy.* 2017;73(1):143-150.

42. Ruzaimi MY, Shahril Y, Masbah O, Salasawati H. Antimicrobial properties of erythromycin and colistin impregnated bone cement. An in vitro analysis. *Med J Malaysia.* 2006;61 Suppl A:21-26.

43. Lorente L, Lecuona M, Ramos MJ, Jiménez A, Mora ML, Sierra A. The use of rifampicin-miconazole-impregnated catheters reduces the incidence of femoral and jugular catheter-related bacteremia. *Clin Infect Dis.* 2008;47(9):1171-1175.

44. Darouiche RO, Smith JA, Jr., Hanna H, et al. Efficacy of antimicrobial-impregnated bladder catheters in reducing catheter-associated bacteriuria: a prospective, randomized, multicenter clinical trial. *Urology.* 1999;54(6):976-981.

45. Johnson JR, Johnston B, Kuskowski MA. In vitro comparison of nitrofurazone- and silver alloy-coated foley catheters for contact-dependent and diffusible inhibition of urinary tract infection-associated microorganisms. *Antimicrobial agents and chemotherapy.* 2012;56(9):4969-4972.

46. Berra L, Kolobow T, Laquerriere P, et al. Internally coated endotracheal tubes with silver sulfadiazine in polyurethane to prevent bacterial colonization: a clinical trial. *Intensive Care Med.* 2008;34(6):1030-1037.

47. Brooks BD, Brooks AE, Grainger DW. Antimicrobial Medical Devices in Preclinical Development and Clinical Use. In: Moriarty TF, Zaat SAJ, Busscher HJ, eds. *Biomaterials Associated Infection: Immunological Aspects and Antimicrobial Strategies.* New York, NY: Springer New York; 2013:307-354.

48. Mann EE, Magin CM, Mettetal MR, et al. Micropatterned Endotracheal Tubes Reduce Secretion-Related Lumen Occlusion. *Ann Biomed Eng.* 2016;44(12):3645-3654.

49. Reed M, Kerndt CC, Nicolas D. Alteplase. In: *StatPearls.* Treasure Island (FL)2022.

50. Harter K, Levine M, Henderson SO. Anticoagulation drug therapy: a review. *West J Emerg Med.* 2015;16(1):11-17.

51. Jaffer IH, Weitz JI. The blood compatibility challenge. Part 1: Blood-contacting medical devices: The scope of the problem. *Acta Biomater.* 2019;94:2-10.

52. Baskin JL, Pui CH, Reiss U, et al. Management of occlusion and thrombosis associated with long-term indwelling central venous catheters. *Lancet.* 2009;374(9684):159-169.

53. Mitchell MD, Anderson BJ, Williams K, Umscheid CA. Heparin flushing and other interventions to maintain patency of central venous catheters: a systematic review. *J Adv Nurs.* 2009;65(10):2007-2021.

54. Shoeb M, Fang MC. Assessing bleeding risk in patients taking anticoagulants. *J Thromb Thrombolysis.* 2013;35(3):312-319.

55. Dhakal B, Kreuziger LB, Rein L, et al. Disease burden, complication rates, and health-care costs of heparin-induced thrombocytopenia in the USA: a population-based study. *Lancet Haematol.* 2018;5(5):e220-e231.

56. Bircher AJ, Harr T, Hohenstein L, Tsakiris DA. Hypersensitivity reactions to anticoagulant drugs: diagnosis and management options. *Allergy.* 2006;61(12):1432-1440.

57. Biran R, Pond D. Heparin coatings for improving blood compatibility of medical devices. *Adv Drug Deliv Rev.* 2017;112:12-23.

58. Marois Y, Chakfé N, Guidoin R, et al. An albumin-coated polyester arterial graft: in vivo assessment of biocompatibility and healing characteristics. *Biomaterials.* 1996;17(1):3-14.

59. Laredo J, Xue L, Husak VA, et al. Silyl-heparin bonding improves the patency and in vivo thromboresistance of carbon-coated polytetrafluoroethylene vascular grafts. *J Vasc Surg.* 2004;39(5):1059-1065.

60. Kornowski R. A critical appraisal of the Janus carbostent. *Catheterization and Cardiovascular Interventions.* 2009;73(2):249-250.

61. Copes F, Pien N, Van Vlierberghe S, Boccafoschi F, Mantovani D. Collagen-Based Tissue Engineering Strategies for Vascular Medicine. *Frontiers in bioengineering and biotechnology.* 2019;7:166-166.

62. Prager MR, Hoblaj T, Nanobashvili J, et al. Collagen- versus gelatine-coated Dacron versus stretch PTFE bifurcation grafts for aortoiliac occlusive disease: Long-term results of a prospective, randomized multicenter trial. *Surgery.* 2003;134(1):80-85.

63. Yasim A, Gul M, Ciralik H, Ergun Y. Gelatin-Sealed Dacron Graft is not more Susceptible to MRSA Infection than PTFE Graft. *European Journal of Vascular and Endovascular Surgery.* 2006;32(4):425-430.

64. Bosiers M, Deloose K, Verbist J, et al. Heparin-bonded expanded polytetrafluoroethylene vascular graft for femoropopliteal and femorocrural bypass grafting: 1-year results. *J Vasc Surg.* 2006;43(2):313-318; discussion 318-319.

65. Lavery KS, Rhodes C, McGraw A, Eppihimer MJ. Anti-thrombotic technologies for medical devices. *Advanced Drug Delivery Reviews.* 2017;112:2-11.

66. Vogler EA, Siedlecki CA. Contact activation of blood-plasma coagulation. *Biomaterials.* 2009;30(10):1857-1869.

67. Xu LC, Bauer JW, Siedlecki CA. Proteins, platelets, and blood coagulation at biomaterial interfaces. *Colloids Surf B Biointerfaces.* 2014;124:49-68.

68. Fleitas Martínez O, Cardoso MH, Ribeiro SM, Franco OL. Recent Advances in Anti-virulence Therapeutic Strategies With a Focus on Dismantling Bacterial Membrane Microdomains, Toxin Neutralization, Quorum-Sensing Interference and Biofilm Inhibition. *Front Cell Infect Microbiol.* 2019;9:74-74.

69. Ghosh A, Jayaraman N, Chatterji D. Small-Molecule Inhibition of Bacterial Biofilm. *ACS Omega.* 2020;5(7):3108-3115.

70. Micoli F, Bagnoli F, Rappuoli R, Serruto D. The role of vaccines in combatting antimicrobial resistance. *Nature Reviews Microbiology.* 2021;19(5):287-302.

71. Motley MP, Banerjee K, Fries BC. Monoclonal antibody-based therapies for bacterial infections. *Curr Opin Infect Dis.* 2019;32(3):210-216.

72. Zhang Q-Y, Yan Z-B, Meng Y-M, et al. Antimicrobial peptides: mechanism of action, activity and clinical potential. *Military Medical Research.* 2021;8(1):48.

73. Taati Moghadam M, Amirmozafari N, Shariati A, et al. How Phages Overcome the Challenges of Drug Resistant Bacteria in Clinical Infections. *Infection and drug resistance.* 2020;13:45-61.

74. Cloutier M, Mantovani D, Rosei F. Antibacterial Coatings: Challenges, Perspectives, and Opportunities. *Trends in Biotechnology.* 2015;33(11):637-652.

75. Olmo JA-D, Ruiz-Rubio L, Pérez-Alvarez L, Sáez-Martínez V, Vilas-Vilela JL. Antibacterial Coatings for Improving the Performance of Biomaterials. *Coatings.* 2020;10(2):139.

76. Möhler JS, Sim W, Blaskovich MAT, Cooper MA, Ziora ZM. Silver bullets: A new lustre on an old antimicrobial agent. *Biotechnology Advances.* 2018;36(5):1391-1411.

77. Rai MK, Deshmukh SD, Ingle AP, Gade AK. Silver nanoparticles: the powerful nanoweapon against multidrug-resistant bacteria. *J Appl Microbiol.* 2012;112(5):841-852.

78. Rai A, Ferrão R, Palma P, et al. Antimicrobial peptide-based materials: opportunities and challenges. *Journal of Materials Chemistry B.* 2022;10(14):2384-2429.

79. Riool M, de Breij A, Drijfhout JW, Nibbering PH, Zaat SAJ. Antimicrobial Peptides in Biomedical Device Manufacturing. *Front Chem.* 2017;5:63-63.

80. Ross A, Ward S, Hyman P. More Is Better: Selecting for Broad Host Range Bacteriophages. *Frontiers in Microbiology.* 2016;7.

81. Wang C, Sauvageau D, Elias A. Immobilization of Active Bacteriophages on Polyhydroxyalkanoate Surfaces. *ACS Applied Materials & Interfaces.* 2016;8(2):1128-1138.

82. O'Connell L, Marcoux PR, Roupioz Y. Strategies for Surface Immobilization of Whole Bacteriophages: A Review. *ACS Biomaterials Science & Engineering.* 2021;7(6):1987-2014.

83. Jiao Y, Niu L-N, Ma S, Li J, Tay FR, Chen J-H. Quaternary ammonium-based biomedical materials: State-of-the-art, toxicological aspects and antimicrobial resistance. *Prog Polym Sci.* 2017;71:53-90.

84. Xue Y, Xiao H, Zhang Y. Antimicrobial Polymeric Materials with Quaternary Ammonium and Phosphonium Salts. *International Journal of Molecular Sciences.* 2015;16(2):3626-3655.

85. Chapman RG, Ostuni E, Liang MN, et al. Polymeric Thin Films That Resist the Adsorption of Proteins and the Adhesion of Bacteria. *Langmuir.* 2001;17(4):1225-1233.

86. Vogler EA. Protein adsorption in three dimensions. *Biomaterials.* 2012;33(5):1201-1237.

87. Peppou-Chapman S, Hong JK, Waterhouse A, Neto C. Life and death of liquid-infused surfaces: a review on the choice, analysis and fate of the infused liquid layer. *Chemical Society Reviews.* 2020;49(11):3688-3715.

88. Sotiri I, Overton JC, Waterhouse A, Howell C. Immobilized liquid layers: A new approach to anti-adhesion surfaces for medical applications. *Experimental Biology and Medicine.* 2016;241(9):909-918.

89. Müller R, Eidt A, Hiller KA, et al. Influences of protein films on antibacterial or bacteria-repellent surface coatings in a model system using silicon wafers. *Biomaterials.* 2009;30(28):4921-4929.

90. Kinnari TJ, Peltonen LI, Kuusela P, Kivilahti J, Könönen M, Jero J. Bacterial adherence to titanium surface coated with human serum albumin. *Otol Neurotol.* 2005;26(3):380-384.

91. Zhan Y, Yu S, Amirfazli A, Rahim Siddiqui A, Li W. Recent Advances in Antibacterial Superhydrophobic Coatings. *Advanced Engineering Materials.* 2022;24(4):2101053.

92. Schlenoff JB. Zwitteration: Coating Surfaces with Zwitterionic Functionality to Reduce Nonspecific Adsorption. *Langmuir.* 2014;30(32):9625-9636.

93. Liang H, Nacharaju P, Friedman A, Friedman JM. Nitric oxide generating/releasing materials. *Future Sci OA.* 2015;1(1).

94. Rong F, Tang Y, Wang T, et al. Nitric Oxide-Releasing Polymeric Materials for Antimicrobial Applications: A Review. *Antioxidants (Basel).* 2019;8(11).

95. Bredt DS. Endogenous nitric oxide synthesis: biological functions and pathophysiology. *Free Radic Res.* 1999;31(6):577-596.

96. de Mel A, Cousins BG, Seifalian AM. Surface Modification of Biomaterials: A Quest for Blood Compatibility. *International Journal of Biomaterials.* 2012;2012:707863.

97. Han HS, Yang SL, Yeh HY, Lin JC, Wu HL, Shi GY. Studies of a novel human thrombomodulin immobilized substrate: surface characterization and anticoagulation activity evaluation. *J Biomater Sci Polym Ed.* 2001;12(10):1075-1089.

98. Nilsson PH, Engberg AE, Back J, et al. The creation of an antithrombotic surface by apyrase immobilization. *Biomaterials.* 2010;31(16):4484-4491.

99. Li F, Wang J, Huang N. In vitro blood compatibility of polyethylene terephthalate with covalently bounded hirudin on surface. *Journal of Wuhan University of Technology-Mater Sci Ed.* 2011;26(5):950-954.

100. Li J, Liu F, Qin Y, et al. A novel natural hirudin facilitated anti-clotting polylactide membrane via hydrogen bonding interaction. *Journal of Membrane Science.* 2017;523:505-514.

101. Yu J, Brisbois E, Handa H, et al. The immobilization of a direct thrombin inhibitor to a polyurethane as a nonthrombogenic surface coating for extracorporeal circulation. *J Mater Chem B.* 2016;4(13):2264-2272.

102. Chandiwal A, Zaman FS, Mast AE, Hall CL. Factor Xa inhibition by immobilized recombinant tissue factor pathway inhibitor. *J Biomater Sci Polym Ed.* 2006;17(9):1025-1037.

103. Murugesan S, Xie J, Linhardt RJ. Immobilization of heparin: approaches and applications. *Curr Top Med Chem.* 2008;8(2):80-100.

104. Zia F, Zia KM, Zuber M, Tabasum S, Rehman S. Heparin based polyurethanes: A state-of-the-art review. *International Journal of Biological Macromolecules.* 2016;84:101-111.

105. van Delden CJ, Engbers GH, Feijen J. The effect of protein adsorption on the anticoagulant activity of surface immobilized heparin. *J Biomater Sci Polym Ed.* 1996;7(8):727-740.

106. Avramescu RE, Ghica MV, Dinu-Pirvu C, Prisada R, Popa L. Superhydrophobic Natural and Artificial Surfaces-A Structural Approach. *Materials (Basel).* 2018;11(5).

107. Liu X, Yuan L, Li D, et al. Blood compatible materials: state of the art. *Journal of Materials Chemistry B.* 2014;2(35):5718-5738.

108. Firkowska-Boden I, Zhang X, Jandt KD. Biocompatibility: Controlling Protein Adsorption through Nanostructured Polymeric Surfaces (Adv. Healthcare Mater. 1/2018). *Advanced Healthcare Materials.* 2018;7(1):1870001.

109. Li J, Ueda E, Paulssen D, Levkin PA. Slippery Lubricant-Infused Surfaces: Properties and Emerging Applications. *Advanced Functional Materials.* 2019;29(4):1802317.

110. Brash JL, Horbett TA, Latour RA, Tengvall P. The blood compatibility challenge. Part 2: Protein adsorption phenomena governing blood reactivity. *Acta Biomater.* 2019;94:11-24.

111. Yang Y, Qi PK, Yang ZL, Huang N. Nitric oxide based strategies for applications of biomedical devices. *Biosurface and Biotribology.* 2015;1(3):177-201.

112. Jin S, Gu H, Chen X, et al. A facile method to prepare a versatile surface coating with fibrinolytic activity, vascular cell selectivity and antibacterial properties. *Colloids and Surfaces B: Biointerfaces.* 2018;167:28-35.

113. Major TC, Brant DO, Burney CP, et al. The hemocompatibility of a nitric oxide generating polymer that catalyzes S-nitrosothiol decomposition in an extracorporeal circulation model. *Biomaterials.* 2011;32(26):5957-5969.

114. Gordge MP, Xiao F. S-nitrosothiols as selective antithrombotic agents - possible mechanisms. *Br J Pharmacol.* 2010;159(8):1572-1580.

115. Wo Y, Brisbois EJ, Bartlett RH, Meyerhoff ME. Recent advances in thromboresistant and antimicrobial polymers for biomedical applications: just say yes to nitric oxide (NO). *Biomater Sci.* 2016;4(8):1161-1183.

116. Wei H, Han L, Ren J, Jia L. Anticoagulant Surface Coating Using Composite Polysaccharides with Embedded Heparin-Releasing Mesoporous Silica. *ACS Applied Materials & Interfaces.* 2013;5(23):12571-12578.

117. Li C, Du H, Yang A, et al. Thrombosis-Responsive Thrombolytic Coating Based on Thrombin-Degradable Tissue Plasminogen Activator (t-PA) Nanocapsules. *Advanced Functional Materials.* 2017;27(45):1703934.

118. Lichtenberg JY, Ling Y, Kim S. Non-Specific Adsorption Reduction Methods in Biosensing. *Sensors (Basel).* 2019;19(11).

119. Wallace A, Albadawi H, Patel N, et al. Anti-fouling strategies for central venous catheters. *Cardiovasc Diagn Ther.* 2017;7(Suppl 3):S246-S257.

120. Jin RC, Loscalzo J. Vascular Nitric Oxide: Formation and Function. *J Blood Med.* 2010;2010(1):147-162.

121. Jacobs H, Okano T, Lin JY, Kim SW. PGE1—Heparin conjugate releasing polymers. *Journal of Controlled Release.* 1985;2:313-319.

122. Maitz MF, Zitzmann J, Hanke J, et al. Adaptive release of heparin from anticoagulant hydrogels triggered by different blood coagulation factors. *Biomaterials.* 2017;135:53-61.

123. Lin KY, Lo JH, Consul N, Kwong GA, Bhatia SN. Self-titrating anticoagulant nanocomplexes that restore homeostatic regulation of the coagulation cascade. *ACS Nano.* 2014;8(9):8776-8785.

124. Ashcraft M, Douglass M, Chen Y, Handa H. Combination strategies for antithrombotic biomaterials: an emerging trend towards hemocompatibility. *Biomaterials Science.* 2021;9(7):2413-2423.

125. Yamamoto M, Nishikawa N, Mayama H, et al. Theoretical Explanation of the Lotus Effect: Superhydrophobic Property Changes by Removal of Nanostructures from the Surface of a Lotus Leaf. *Langmuir.* 2015;31(26):7355-7363.

126. Barthlott W, Mail M, Bhushan B, Koch K. Plant Surfaces: Structures and Functions for Biomimetic Innovations. *Nano-Micro Letters.* 2017;9(2):23.

127. Chen C, Liu M, Zhang L, Hou Y, Yu M, Fu S. Mimicking from Rose Petal to Lotus Leaf: Biomimetic Multiscale Hierarchical Particles with Tunable Water Adhesion. *ACS Applied Materials & Interfaces.* 2019;11(7):7431-7440.

128. Yan H, Wu Q, Yu C, Zhao T, Liu M. Recent Progress of Biomimetic Antifouling Surfaces in Marine. *Advanced Materials Interfaces.* 2020;7(20):2000966.

129. Ivanova EP, Hasan J, Webb HK, et al. Bactericidal activity of black silicon. *Nat Commun.* 2013;4:2838-2838.

130. Kelleher SM, Habimana O, Lawler J, et al. Cicada Wing Surface Topography: An Investigation into the Bactericidal Properties of Nanostructural Features. *ACS Appl Mater Interfaces.* 2016;8(24):14966-14974.

131. Li X. Bactericidal mechanism of nanopatterned surfaces. *Physical Chemistry Chemical Physics.* 2016;18(2):1311-1316.

132. Watson GS, Green DW, Schwarzkopf L, et al. A gecko skin micro/nano structure - A low adhesion, superhydrophobic, anti-wetting, self-cleaning, biocompatible, antibacterial surface. *Acta Biomater.* 2015;21:109-122.

133. Tripathy A, Sen P, Su B, Briscoe WH. Natural and bioinspired nanostructured bactericidal surfaces. *Advances in colloid and interface science.* 2017;248:85-104.

134. Han Z, Mu Z, Yin W, et al. Biomimetic multifunctional surfaces inspired from animals. *Advances in Colloid and Interface Science.* 2016;234:27-50.

135. Fang Y, Sun G, Wang T, Cong Q, Ren L. Hydrophobicity mechanism of non-smooth pattern on surface of butterfly wing. *Chinese Science Bulletin.* 2007;52(5):711-716.

136. van Hinsbergh VW. Endothelium--role in regulation of coagulation and inflammation. *Semin Immunopathol.* 2012;34(1):93-106.

137. Mast AE. Tissue Factor Pathway Inhibitor: Multiple Anticoagulant Activities for a Single Protein. *Arterioscler Thromb Vasc Biol.* 2016;36(1):9-14.

138. Martin FA, Murphy RP, Cummins PM. Thrombomodulin and the vascular endothelium: insights into functional, regulatory, and therapeutic aspects. *Am J Physiol Heart Circ Physiol.* 2013;304(12):H1585-1597.

139. Verhamme P, Hoylaerts MF. The pivotal role of the endothelium in haemostasis and thrombosis. *Acta Clin Belg.* 2006;61(5):213-219.

140. Hamilos M, Petousis S, Parthenakis F. Interaction between platelets and endothelium: from pathophysiology to new therapeutic options. *Cardiovasc Diagn Ther.* 2018;8(5):568-580.

141. Mican J, Toul M, Bednar D, Damborsky J. Structural Biology and Protein Engineering of Thrombolytics. *Comput Struct Biotechnol J.* 2019;17:917-938.

142. Hopkins SP, Pant J, Goudie MJ, Schmiedt C, Handa H. Achieving Long-Term Biocompatible Silicone via Covalently Immobilized S-Nitroso- N-acetylpenicillamine (SNAP) That Exhibits 4 Months of Sustained Nitric Oxide Release. *ACS Appl Mater Interfaces.* 2018;10(32):27316-27325.

143. Garren M, Maffe P, Melvin A, et al. Surface-Catalyzed Nitric Oxide Release via a Metal Organic Framework Enhances Antibacterial Surface Effects. *ACS Applied Materials & Interfaces.* 2021;13(48):56931-56943.

144. Yang Z, Qiu H, Li X, Gao P, Huang N. Plant-inspired gallolamine catalytic surface chemistry for engineering an efficient nitric oxide generating coating. *Acta Biomaterialia.* 2018;76:89-98.

145. Major TC, Brant DO, Burney CP, et al. The hemocompatibility of a nitric oxide generating polymer that catalyzes S-nitrosothiol decomposition in an extracorporeal circulation model. *Biomaterials.* 2011;32(26):5957-5969.

146. Liu K, Meyerhoff ME. Preparation and characterization of an improved Cu(2+)-cyclen polyurethane material that catalyzes generation of nitric oxide from S-nitrosothiols. *Journal of materials chemistry.* 2012;22(36):18784-18787.

147. Thomas DD, Liu X, Kantrow SP, Lancaster JR, Jr. The biological lifetime of nitric oxide: implications for the perivascular dynamics of NO and O2. *Proceedings of the National Academy of Sciences of the United States of America.* 2001;98(1):355-360.

148. Garren MR, Ashcraft M, Qian Y, Douglass M, Brisbois EJ, Handa H. Nitric oxide and viral infection: Recent developments in antiviral therapies and platforms. *Appl Mater Today.* 2021;22:100887-100887.

149. Drago RS, Karstetter BR. The Reaction of Nitrogen(II) Oxide with Various Primary and Secondary Amines. *Journal of the American Chemical Society.* 1961;83(8):1819-1822.

150. Drago RS, Paulik FE. The Reaction of Nitrogen(II) Oxide with Diethylamine. *Journal of the American Chemical Society.* 1960;82(1):96-98.

151. Cheng J, He K, Shen Z, Zhang G, Yu Y, Hu J. Nitric Oxide (NO)-Releasing Macromolecules: Rational Design and Biomedical Applications. *Front Chem.* 2019;7.

152. Sadrearhami Z, Nguyen T-K, Namivandi-Zangeneh R, Jung K, Wong EHH, Boyer C. Recent advances in nitric oxide delivery for antimicrobial applications using polymer-based systems. *Journal of Materials Chemistry B.* 2018;6(19):2945-2959.

153. Worley BV, Schilly KM, Schoenfisch MH. Anti-Biofilm Efficacy of Dual-Action Nitric Oxide-Releasing Alkyl Chain Modified Poly(amidoamine) Dendrimers. *Molecular Pharmaceutics.* 2015;12(5):1573-1583.

154. Majumder S, Sinha S, Siamwala JH, et al. A comparative study of NONOate based NO donors: spermine NONOate is the best suited NO donor for angiogenesis. *Nitric Oxide.* 2014;36:76-86.

155. Broniowska KA, Diers AR, Hogg N. S-nitrosoglutathione. *Biochim Biophys Acta.* 2013;1830(5):3173-3181.

156. R. Noble D, R. Swift H, Lyn H. Williams D. Nitric oxide release from S-nitrosoglutathione (GSNO). *Chemical Communications.* 1999(22):2317-2318.

157. Brisbois EJ, Major TC, Goudie MJ, Bartlett RH, Meyerhoff ME, Handa H. Improved hemocompatibility of silicone rubber extracorporeal tubing via solvent swelling-impregnation of S-nitroso-N-acetylpenicillamine (SNAP) and evaluation in rabbit thrombogenicity model. *Acta Biomater.* 2016;37:111-119.

158. Wang X, Jolliffe A, Carr B, et al. Nitric oxide-releasing semi-crystalline thermoplastic polymers: preparation, characterization and application to devise anti-inflammatory and bactericidal implants. *Biomaterials Science.* 2018;6(12):3189-3201.

159. Douglass M, Ghalei S, Brisbois E, Handa H. Potent, Broad-Spectrum Antimicrobial Effects of S-Nitroso-N-acetylpenicillamine-Impregnated Nitric Oxide-Releasing Latex Urinary Catheters. *ACS Applied Bio Materials.* 2022;5(2):700-710.

160. Douglass M, Hopkins S, Chug MK, et al. Reduction in Foreign Body Response and Improved Antimicrobial Efficacy via Silicone-Oil-Infused Nitric-Oxide-Releasing Medical-Grade Cannulas. *ACS Applied Materials & Interfaces.* 2021;13(44):52425-52434.

161. Grommersch BM, Pant J, Hopkins SP, Goudie MJ, Handa H. Biotemplated Synthesis and Characterization of Mesoporous Nitric Oxide-Releasing Diatomaceous Earth Silica Particles. *ACS Applied Materials & Interfaces.* 2018;10(3):2291-2301.

162. Massoumi H, Kumar R, Chug MK, Qian Y, Brisbois EJ. Nitric Oxide Release and Antibacterial Efficacy Analyses of S-Nitroso-N-Acetyl-Penicillamine Conjugated to Titanium Dioxide Nanoparticles. *ACS Applied Bio Materials.* 2022;5(5):2285-2295.

163. Devine R, Douglass M, Ashcraft M, Tayag N, Handa H. Development of Novel Amphotericin B-Immobilized Nitric Oxide-Releasing Platform for the Prevention of Broad-Spectrum Infections and Thrombosis. *ACS Appl Mater Interfaces.* 2021;13(17):19613-19624.

164. Picón-Pagès P, Garcia-Buendia J, Muñoz FJ. Functions and dysfunctions of nitric oxide in brain. *Biochim Biophys Acta Mol Basis Dis.* 2019;1865(8):1949-1967.

165. Cooke JP, Losordo DW. Nitric Oxide and Angiogenesis. *Circulation.* 2002;105(18):2133-2135.

166. Ignarro LJ. Endothelium-Derived Nitric Oxide: Pharmacology and Relationship to the Actions of Organic Nitrate Esters. *Pharmaceutical Research.* 1989;6(8):651-659.

167. Lantvit SM, Barrett BJ, Reynolds MM. Nitric oxide releasing material adsorbs more fibrinogen. *J Biomed Mater Res A.* 2013;101(11):3201-3210.

168. Zang Y, Popat KC, Reynolds MM. Nitric oxide-mediated fibrinogen deposition prevents platelet adhesion and activation. *Biointerphases.* 2018;13(6):06e403.

169. Douglass ME, Goudie MJ, Pant J, et al. Catalyzed Nitric Oxide Release via Cu Nanoparticles Leads to an Increase in Antimicrobial Effects and Hemocompatibility for Short-Term Extracorporeal Circulation. *ACS Applied Bio Materials.* 2019;2(6):2539-2548.

170. Singha P, Pant J, Goudie MJ, Workman CD, Handa H. Enhanced antibacterial efficacy of nitric oxide releasing thermoplastic polyurethanes with antifouling hydrophilic topcoats. *Biomaterials Science.* 2017;5(7):1246-1255.

171. Singha P, Goudie MJ, Liu Q, et al. Multipronged Approach to Combat Catheter-Associated Infections and Thrombosis by Combining Nitric Oxide and a Polyzwitterion: a 7 Day In Vivo Study in a Rabbit Model. *ACS Applied Materials & Interfaces.* 2020;12(8):9070-9079.

172. Goudie MJ, Pant J, Handa H. Liquid-infused nitric oxide-releasing (LINORel) silicone for decreased fouling, thrombosis, and infection of medical devices. *Sci Rep.* 2017;7(1):13623.

173. Devine R, Singha P, Handa H. Versatile biomimetic medical device surface: hydrophobin coated, nitric oxide-releasing polymer for antimicrobial and hemocompatible applications. *Biomater Sci.* 2019;7(8):3438-3449.

174. Devine R, Goudie M, Singha P, et al. Mimicking the Endothelium: Dual Action Heparinized Nitric Oxide Releasing Surface. *ACS Applied Materials & Interfaces.* 2020.

175. Roberts TR, Garren MRS, Wilson SN, Handa H, Batchinsky AI. Development and In Vitro Whole Blood Hemocompatibility Screening of Endothelium-Mimetic Multifunctional Coatings. *ACS Applied Bio Materials.* 2022;5(5):2212-2223.

176. Pant J, Gao J, Goudie MJ, Hopkins SP, Locklin J, Handa H. A multi-defense strategy: Enhancing bactericidal activity of a medical grade polymer with a nitric oxide donor and surface-immobilized quaternary ammonium compound. *Acta Biomater.* 2017;58:421-431.

177. Chug MK, Massoumi H, Wu Y, Brisbois EJ. Prevention of medical device infections via multi-action nitric oxide and chlorhexidine diacetate releasing medical grade silicone biointerfaces. *Journal of Biomedical Materials Research Part A.* 2022;110(6):1263-1277.

CHAPTER 2

Nitric Oxide-Releasing Lock Solution for the Prevention of Catheter-Related Infection and Thrombosis[2]

[2]*Nitric Oxide-Releasing Lock Solution for the Prevention of Catheter-Related Infection and Thrombosis*. Ashcraft, M., Douglass, M., Garren, M., Mondal, A., Estes, L., Wu, Y., Handa, H. ACS Appl. Bio Mater. 2022, 5, 4, 1519–1527. Reprinted here with permission of the publisher.

2.1 Abstract

Although frequently used, venous catheters are often associated with serious complications such as infection and thrombosis. Lock solution therapies are clinically used to deter these issues but generally address only infection or thrombosis with limited success. Here, we report the development of a dual-functional lock therapy using nitric oxide (NO) donor molecule, S-nitrosoglutathione (GSNO). NO is a potent, broad-spectrum antimicrobial agent that also temporarily inhibits platelet activation, preventing thrombosis. Furthermore, NO has anti-biofilm actions, an ability that traditional antibiotic lock solutions lack, thus limiting their efficacy. In this work, different concentrations of GSNO were characterized via NO analysis to determine a range of NO-releasing lock solution (NOreLS) concentrations to investigate and to demonstrate prolonged potential efficacy. Tested against clinically used vancomycin and gentamicin lock solutions, GSNO based NOreLS repeatedly outperformed in models of different stages of catheter infections. NOreLS also prevented clot formation when exposed to whole blood, showing increased efficacy compared to a heparin lock solution. Moreover, NOreLS was demonstrated to be biocompatible via hemolysis and cytotoxicity assays. NOreLS has excellent potential for safely and effectively preventing infection and thrombosis related to catheter usage.

2.2 Introduction

Over 5 million central venous catheters (CVCs) are used each year for cancer treatments, hemodialysis, parenteral nutrition support, etc., in the United States alone.[1] Despite their frequency of use, complications such as infection and thrombosis are unfortunately common and contribute significantly to increases in morbidity, mortality, length of hospital stay, and healthcare costs. An estimated 250,000 catheter-related bloodstream infections (CRBSIs) occur annually in the US,[2]

costing the healthcare system an estimated 670 million to 2.68 billion dollars per year.[3] CRBSIs are acknowledged to be among the most expensive medical device-associated complications[4] and the most common form of nosocomial bacteremia.[2] Additionally, these infections are associated with considerable mortality rates ranging from 12.24% to 25.96%.[5,6] CRBSIs can be caused by a wide range of pathogens, the most common culprits being coagulase-negative staphylococci, *Pseudomonas aeruginosa*, *Staphylococcus aureus*, and *Candida albicans*.[2,7] With the alarming emergence of antibiotic-resistant pathogens, particularly in healthcare settings, the prevention of infections such as CRSBIs has become more important and treatments more difficult.[8-11]

Antimicrobial lock therapies are often utilized to combat CRSBIs. Current, commonly used antimicrobial lock therapies contain high concentrations of antibiotics such as vancomycin, gentamicin, or cefazolin.[12] However, the use of prophylactic antibiotics is undesirable due to concerns for the emergence of resistant pathogens.[13] Some antiseptic lock solutions are also available, but they are generally considered less effective than antibiotic-based lock solutions[14] or have been associated with adverse effects (e.g., ethanol locks).[12] While antimicrobial lock solutions have been used to prevent catheter infection with moderate success,[15] their efficacy is limited by their inability to penetrate biofilms.[12] Biofilms are self-secreted, jellylike structures that protect the encased microbes from antibiotics, host immune cells, etc.[16,17] They also provide excellent environments for proliferation and horizontal gene transfer, which is one of the most common mechanisms of acquiring antibiotic resistance mechanisms.[18,19] Even highly concentrated antibiotic lock solutions are relatively ineffective against biofilms, as they are unable to penetrate the biofilm matrix.[20] Moreover, attempted and ineffective treatments of biofilms with antibiotics can lead to the rapid development of resistance, exacerbating the situation.[21] As biofilms are notoriously difficult to disperse or eradicate, biofilm formation on catheters necessitates removal

to prevent the onset of CRBSIs and subsequent recurring infections.[20] Thus, there is a need for a broad spectrum, biofilm-dispersing lock solution for improved preventative therapies.

Thrombosis, or blood clotting, is another common complication associated with the use of CVCs and can result in minor to life-threatening issues.[22,23] Catheter-related thrombosis (CRT) has been found to occur in 14-16% of patients, usually within the first 100 days of CVC use,[24] but the frequency increases greatly with long-term CVC use (occurrences of up to 50% in children and 60% in adults).[22] Thrombi can cause vascular and catheter obstruction and provide a surface that bacteria can easily adhere to, increasing the risk of infection and sepsis.[25,26] Additionally, detached thrombi have been seen to cause pulmonary embolism in 10-15% of patients with CRT and can be lethal.[23,27]

The prevention of thrombotic complications is preferred to treatment, but no preventative method is consistently and/or significantly effective.[23,28] Typical prophylactic strategies include the incorporation of anticoagulants (commonly heparin) into lock solutions or systemic administration at low doses. However, there is little evidence for the efficacy of heparin lock solutions compared to normal saline in preventing thrombotic occlusions,[22,29] and similarly, there is no conclusive evidence that systemic warfarin or heparin administration significantly reduces CRT.[23] Moreover, these therapies are associated with serious adverse effects such as major bleeding.[22,28] As such, there is a need for effective anticoagulant prophylaxis strategies to prevent CRT.

To combat the onset of CRBSIs and CRT, herein, we have investigated the use of a nitric oxide-releasing lock solution (NOreLS). Nitric oxide-releasing technologies have been incorporated into numerous promising antimicrobial and antithrombotic materials among others.[30-34] Nitric oxide (NO) can kill a wide range of pathogens, including those most commonly seen in

CRBSIs (coagulase-negative staphylococci, *P. aeruginosa*, *S. aureus*, and *C. albicans*) and multidrug-resistant (MDR) strains.[35,36] As NO has a nonspecific mechanism of action, it does not promote the generation of new resistant strains,[35,37] a growing concern associated with the use of traditional antibiotics. Additionally, NO has been shown to disperse biofilms and prevent their formation,[38,39] an ability most antimicrobial therapies lack. NO release can also help mitigate medical device-associated thrombosis as it temporarily inhibits platelet activation.[40-44]

Previous work has shown the potential that NO-releasing technologies have in lock therapies for effects on microbial viability,[45] but their prevention of CRT has yet to be explored, and their ability to disperse catheter biofilms has yet to be demonstrated. Here, we describe a thorough *in vitro* investigation of NOreLS using *S*-nitrosoglutathione (GSNO). GSNO is an established NO donor molecule,[46,47] but has yet to be applied to mitigation of CRBSIs and CRT in a lock solution. GSNO has far-reaching potential applications and has been investigated in numerous clinical trials.[46] It has demonstrated antimicrobial efficacy when incorporated into various materials (polymers,[42] fibers,[48] creams,[49] etc.), and its solubility in aqueous solutions supports its suitability in a lock solution. Furthermore, GSNO has demonstrated antithrombotic effects via temporary inhibition of platelet activation.[42,48] NOreLS's potential to deter CRBSIs is evaluated at different time points in catheter infection progression, including effects against planktonic bacteria, treatment of an established infection on medical-grade tubing, and biofilm dispersal of a 3-d growth model. CRT prevention is shown through exposure to whole blood and quantification of reduced clot area. Moreover, the biocompatibility of NOreLS is demonstrated via hemolysis and cytotoxicity assays with human umbilical vein endothelial cells (HUVECs).

2.3 Materials and Methods

2.3.1 Materials. Sodium nitrite, Mueller-Hinton broth (MHB) and agar (MHA), Cell Counting Kit-8 (CCK-8), heparin (HEP) and acetic acid were purchased from Sigma-Aldrich (St. Louis, MO 63103). Tygon non-DEHP Surgical and Hospital Tubing (nd-100-65) was purchased from Thomas Scientific (Swedesboro, NJ). Acetone was purchased from VWR (Radnor, PA). Phosphate-buffered saline (PBS), pH 7.4, which was used for all *in vitro* experiments, contained 138 mM NaCl, 2.7 mM KCl, and 10 mM sodium phosphate. The bacterial strains multidrug resistant (MDR) *P. aeruginosa* (ATCC BAA 2110) and methicillin resistant *S. aureus* (ATCC BAA 41) were purchased from American Type Culture Collection (ATCC). Crystal violet was obtained from Fisher Scientific (Waltham, MA). Reduced glutathione, Gentamicin (GEN), and Vancomycin (VAN) was purchased from GoldBio (Saint Louis, MO). Drabkin's reagent was purchased from Ricca Chemical Company (Arlington, TX). Trypsin−EDTA was purchased from Corning (Corning, NY). Fetal bovine serum (FBS) and Penicillin−Streptomycin (Pen-Strep) were purchased from Gibco-Life Technologies (Grand Island, NY). Porcine blood was purchased from Animal Technologies (Tyler, TX).

2.3.2 Preparation of NOreLS. GSNO was synthesized as reported previously.[50] Briefly, reduced glutathione (5 g/16 mmol) was dissolved in 12 M HCl and DI water and cooled in an ice bath. Excess $NaNO_2$ (1.2 g/17 mmol) was added to the mixture, which remained in the ice bath for 40 min. Cold acetone was added to precipitate GSNO, which was collected via vacuum filtration and washed with additional cold acetone and DI water. Once dried overnight under vacuum, GSNO was kept in the dark at -20 °C until used. All NOreLS's tested consisted of GSNO dissolved in PBS buffer, pH 7.4.

2.3.3 Nitric oxide release analysis. NO release measurements were conducted using a Sievers chemiluminescence Nitric Oxide Analyzer (NOA) model 280i (Boulder, CO). A baseline was recorded with 3 mL of PBS buffer with 100 mM EDTA before being replaced with 3 mL of NOreLS to the amber glass vial. The samples were measured at 37 °C to simulate physiological environments. Nitrogen was bubbled into the solution to continuously carry NO into the chemiluminescence detection chamber. The NO release measurements were normalized using the volume of the samples. Unless otherwise indicated, samples were analyzed directly after dissolution. Where applicable, the samples were kept in the dark in an incubator at 37 °C between measurements.

2.3.4 Antibacterial assessment. MRSA strain ATCC BAA 41 and MDR *P. aeruginosa* strain ATCC BAA 2110 with MHB, MHA, and/or PBS were used for all antibacterial experiments. Plating of colony forming units (CFU) was aided by an Eddy Jet W2 spiral plater (IUL, Farmingdale, NY), and the viable colonies on the resulting plates were counted via a SphereFlash automated colony counter (IUL, Farmingdale, NY) after overnight incubation at 37 °C. The limit of detection of the spiral plater is noted to be 2×10^2 CFU/mL.

2.3.4.1 Time kill assay. Time kill assays were conducted with slight modifications to a previously reported procedure.[51] Inoculum cultures were grown until reaching the log phase in MHB before washing with PBS and diluting to a starting OD 600 of 0.05. Growth controls and samples were incubated at 37 °C in a 48-well plate and shaken at 150 RPM. Samples included varying concentrations of GSNO (1, 5, 10, and 20 mg/mL), 5 mg/mL VAN, or 5 mg/mL GEN all dissolved in MHB. VAN and GEN are commonly used antibiotic lock solutions[52,53] and were

included for comparison purposes. Aliquots were taken at specific time points (T = 2, 8, and 24 h) and serially diluted 10-fold in PBS. Only plates with individual colonies able to be detected by the SphereFlash automated colony counter were used. In the event that repeated plating of non-diluted aliquots showed no bacteria growth, the CFU is considered to be 0. These data points are denoted with an asterisk. Data is reported as time-kill curves, plotting the $\log_{10}$ CFU/mL versus time.

2.3.4.2 Treatment of 24 h infected tubing. Sterile, medical-grade tubing was filled with 0.3 OD 600 MRSA or MDR *P. aeruginosa* in MHB after inoculums were grown until log phase and washed with PBS. The infected tubing was incubated at 37 °C for 24 h before being gently rinsed with sterile PBS. The tubing was then locked with PBS, VAN (5 mg/mL in PBS), GEN (5 mg/mL in PBS), or NOreLS (1, 5, 10, or 20 mg/mL) for 2 h at 37 °C and in the dark. After the 2 h treatment period, the tubing was gently flushed with PBS before the attached bacteria were removed via homogenization in PBS. The bacterial solutions were serial diluted 10-fold in PBS before plated. Following overnight incubation at 37 °C, the viable CFU were counted and reported as CFU/cm^2. N = 5 per sample type is reported.

2.3.4.3 72 h Anti-Biofilm assessment. A crystal violet assay was performed to evaluate the biofilm dispersing abilities of the lock solutions, similar to a previously reported procedure.[54] Sterile, medical-grade tubing was filled with 0.1 OD 600 MRSA or MDR *P. aeruginosa* in MHB and shaken at 150 RPM at 37 °C for 72 h. The indwelling solution was removed and replaced with fresh MHB approximately every 12 h. After 72 h of growth, the tubing samples with the resulting biofilms were gently rinsed with PBS to remove unadhered bacteria before being locked with the NOreLS or antibiotic lock therapies for 24 h at 37 °C in the dark. The growth control or treated

tubing samples were gently rinsed with PBS after 72 h of growth or 24 h of treatment, respectively. After washing, the samples were then filled with 0.1% crystal violet for 15 min before being repeatedly flushed with PBS to remove unbound dye. The tubing was cut into 1 cm segments and placed into 300 μL of 30% acetic acid to dissolve the stained biofilm. The absorbance of the resulting solution was read at 550 nm. The amount of remaining biofilm relative to the growth control was calculated using **Equation 2.1**. N = 3 per sample type is reported.

(2.1) $$\text{Remaining biofilm (\%)} = \left(\frac{\text{Average abs of treated 1 cm segment solutions} - \text{abs of blank}}{\text{Average abs of control 1 cm segment soltuions} - \text{abs of blank}}\right) \times 100$$

Viability of bacteria within the biofilms after treatment was also assessed. 72 h biofilms were grown in medical grade tubing as described above. After 72 h (for the growth controls) or the 24 h treatments, the tubings were cut into 1 cm sections and homogenized in PBS. The samples were then serially diluted and plated. Following overnight incubation at 37 °C, the viable CFU were counted and reported as CFU/cm^2. N = 6 per sample type is reported.

2.3.5 Antithrombotic assessment. Locked medical-grade tubing samples containing PBS, HEP (10k units/mL), or NOreLS (1, 5, 10, or 20 mg/mL) were incubated in porcine whole blood to model clotting on the tip of a CVC. Calcium chloride was added to fresh porcine blood with sodium citrate to reverse anticoagulation. Tubing containing lock solution was plugged at one end, leaving the other end open to resemble the tip of a CVC. Each sample was individually placed in 1 mL of whole blood for 20 min before rinsed in CMF-PBS. The surface areas of attached clots were quantified using ImageJ. Data are presented as relative surface area of attached clots compared to those of the PBS control. Final values are reported as the mean ± standard deviation (N = 3).

2.3.6 Biocompatibility assessment.

2.3.6.1 Hemolysis. Hemolysis assessments were conducted according to the NAMSA ASTM F756 protocol. Briefly, fresh porcine whole blood was diluted with calcium and magnesium-free phosphate-buffered saline (CMF-PBS) to a total hemoglobin concentration of 10 ± 1.0 mg/mL. 1 mL of diluted whole blood was incubated with 7 mL CMF-PBS as a negative control, sterile DI water as a positive control, or CMF-PBS containing sample lock solutions. Varying blood/lock solution ratios were tested to simulate full leakage over time and specific leakage events (0.06% - 0.2% lock solution in volume). The samples were incubated at 37 °C for 3 hours with periodic inversions before centrifuging at 800 x g for 15 min. The supernatant containing any freed hemoglobin was combined at a 1:1 ratio with Drabkin's reagent and allowed to stand for 15 min before the absorbance at 540 nm was quantified. In the event that an experimental hemolytic index was found to be less than zero, it is reported here to be 0.0. Percent hemolysis was calculated via **Equation 2.2**.

$$\textit{(2.2)} \qquad \text{Percent Hemolysis (\%)} = \frac{\text{Absorbance of sample} - \text{Absorbance of blank}}{\text{Absorbance of diluted blood} - \text{Absorbance of blank}} \times 100$$

2.3.6.2 Cytocompatibility. Cellular biocompatibility was assessed via 24 h *in vitro* cytotoxicity assays with HUVECs. Cryopreserved stocks of HUVECs were revived and cultured in Clonetics™ EGM™-2 Bulletkit™ containing endothelial cell growth basal medium-2 (EBM-2) supplemented with human Epidermal Growth Factor, Vascular Endothelial Growth Factor, R3-Insulin-like Growth Factor, ascorbic acid, hydrocortisone, human Fibroblast Growth Factor-Beta, heparin, fetal bovine Serum, and Gentamicin/Amphotericin-B per the manufacturer's instructions. HUVECs were subcultured for no more than ten passages between experiments. Cells were grown to ~70% monolayer confluency before being detached with 0.05% trypsin supplemented with 5 mM EDTA. Detached cells were centrifuged down, resuspended in supplemented EBM-2, stained

with trypan blue dye, and counted for the total number of viable cells using an EVE^{TM} cell counting system. In all cytotoxicity tests, 10,000 cells were seeded per well in 96 well plates and grown for 24 h to achieve > 70% confluency before testing. Cells were then treated with 0.06%, 0.09% or 0.2% solutions of vancomycin, gentamicin, heparin, and NOreLS in fresh media to mimic any potential leaking of the lock solution. Cells were incubated for an additional 24 h, afterwards, the media in each well was replaced once more with fresh media supplemented with 10% Cell Counting Kit-8 (CCK-8) reagent. Cells were incubated with CCK-8 for 1 h, during which time dehydrogenase reactions of nicotinamide adenine dinucleotide and nicotinamide adenine dinucleotide phosphate converted the water-soluble tetrazolium dye to its formazan derivative. The presence of the formazan derivative was then quantified via plate reading (OD 450 nm) with baseline reading (OD 650 nm). The final relative cellular viability for each dilution was calculated according to **Equation 2.3**, with respect to the viability of untreated control wells. Final values are reported as the mean ± standard deviation (N = 3 treatment groups from independent passages).

$$\textit{(2.3)} \qquad \text{Percent Cellular Viability (\%)} = \frac{(\text{OD}_{450}\ \text{Read} - \text{OD}_{650}\ \text{Read})_{\text{Lock Solution Dilution}}}{(\text{OD}_{450}\ \text{Read} - \text{OD}_{650}\ \text{Read})_{\text{Untreated Cells}}} \times 100$$

2.3.7 Statistical analysis. Averages and standard deviations were calculated using Graphpad Prism 8. Statistical significance was determined using a one-way analysis of variance (ANOVA) on the same software. A p value < 0.05 was considered statistically significant.

2.4 Results and Discussion

2.4.1 NO release studies. When in the presence of heat, light, or metal ions, NO is released from GSNO, which then forms a dithiol bond with another glutathione molecule to create glutathione disulfide (GSSG)[46] (**Figure 2.1A**). To determine an appropriate range of NO-releasing solutions

to investigate, several concentrations of GSNO in PBS were analyzed via nitric oxide analyzer (NOA) (**Figure 2.1B**). Although the trend is not linear, there is a positive correlation between GSNO concentration and NO flux. NO flux steeply increased with increasing GSNO concentrations until 25 mg/mL. No statistically significant difference was observed in NO release between 20 and 25 mg/mL solutions, though 25 mg/mL took considerably longer to prepare (i.e., ~25 min to dissolve versus 1 min for 20 mg/mL). Since this extended preparation time may limit the potential clinical application of NOreLS, 20 mg/mL GSNO preparations in PBS were chosen as the maximum concentration for further analysis.

The dwell time of lock solutions is recommended to be 8 to 24 hours,[53] but realistically can be 2 minutes to 48 hours.[55] Thus, the NO release of NOreLS over 48 h was measured to demonstrate prolonged potential efficacy (**Figure 2.1C**). Statistical analysis is reported in **Table 2.1**. All GSNO concentrations tested showed release for at least 48 h, which is notably longer than the previous NO-releasing lock solution reported (24 h).[45] This indicates that NOreLS can sustain NO release levels for clinically relevant durations, an issue that has limited the clinical use of other NO-releasing compounds.[56]

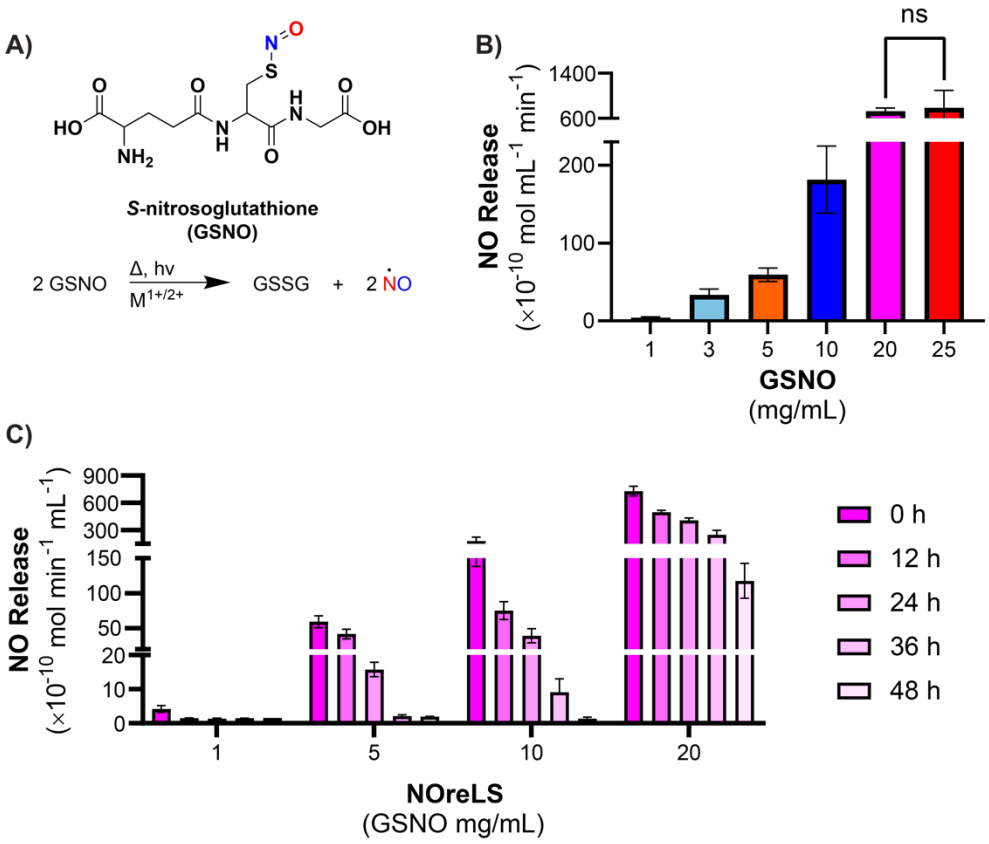

Figure 2.1 A) GSNO releases NO when exposed to heat, light, and/or metal ions. B) NO release of solutions containing varying concentrations of GSNO quantified via NOA at 37 °C. GSNO is dissolved in PBS, pH 7.4. ns indicates no statistically significant difference. C) NO release of NOreLS (20 mg/mL GSNO in PBS) at various time points quantified via NOA at 37 °C. Data are shown as the mean ± standard deviation (N = 3 repeats tested per formulation).

Table 2.1 Calculated *P* Values for NO Release Over Time (Figure 2.1C).

Comparison	NOreLS (1 mg/mL)	NOreLS (5 mg/mL)	NOreLS (10 mg/mL)	NOreLS (20 mg/mL)
0 h vs. 12 h	0.9999	0.8573	<0.0001	<0.0001
0 h vs. 24 h	0.9998	0.1219	<0.0001	<0.0001
0 h vs. 36 h	0.9999	0.02	<0.0001	<0.0001
0 h vs. 48 h	>0.9999	0.0197	<0.0001	<0.0001
12 h vs. 24 h	>0.9999	0.5919	0.2755	0.0001
12 h vs. 36 h	>0.9999	0.1884	0.0052	<0.0001
12 h vs. 48 h	>0.9999	0.1862	0.0015	<0.0001
24 h vs. 36 h	>0.9999	0.9375	0.4432	<0.0001
24 h vs. 48 h	>0.9999	0.9357	0.223	<0.0001
36 h vs. 48 h	>0.9999	>0.9999	0.9921	<0.0001

2.4.2 Antibacterial evaluations. To demonstrate the antibacterial effects of NOreLS, it was tested against MRSA and MDR *P. aeruginosa* to represent Gram-positive and Gram-negative bacteria, respectively, and drug-resistant strains. *S. aureus* and *P. aeruginosa* are also two of the most common causes of CRBSIs.[7] PBS was used as a control, and two antibiotics commonly used in clinical lock solutions, gentamicin (GEN) and vancomycin (VAN) were included for comparison. The antibiotics were used at concentrations of 5 mg/mL as this is one of the highest concentrations used clinically considering solubility and precipitation concerns.[53]

Time kill assays were used to simulate the start of a potential CRBSI, i.e., the effects of lock solutions on planktonic bacteria. Decreases in viable MRSA CFUs were seen over time for the antibiotics and 5, 10, and 20 mg/mL NOreLS (**Figure 2.2A**). 1 mg/mL NOreLS did not affect the viability of MRSA. No viable CFUs were observed after 2 h treatments with 20 mg/mL NOreLS and GEN, 8 h treatment with 10 mg/mL NOreLS, and 24 h treatment with VAN. Similar trends were seen in MDR *P. aeruginosa* treatment (**Figure 2.2B**). No viable CFUs were seen after 2 h with GEN, 10, and 20 mg/mL NOreLS, 8 h with 5 mg/mL NOreLS, and 24 h with VAN. Statistical analyses are reported in **Tables 2.2** and **2.3.** These results indicate that GEN and 20 mg/mL NOreLS are most effective at quickly preventing both Gram-positive and -negative bacterial colonization.

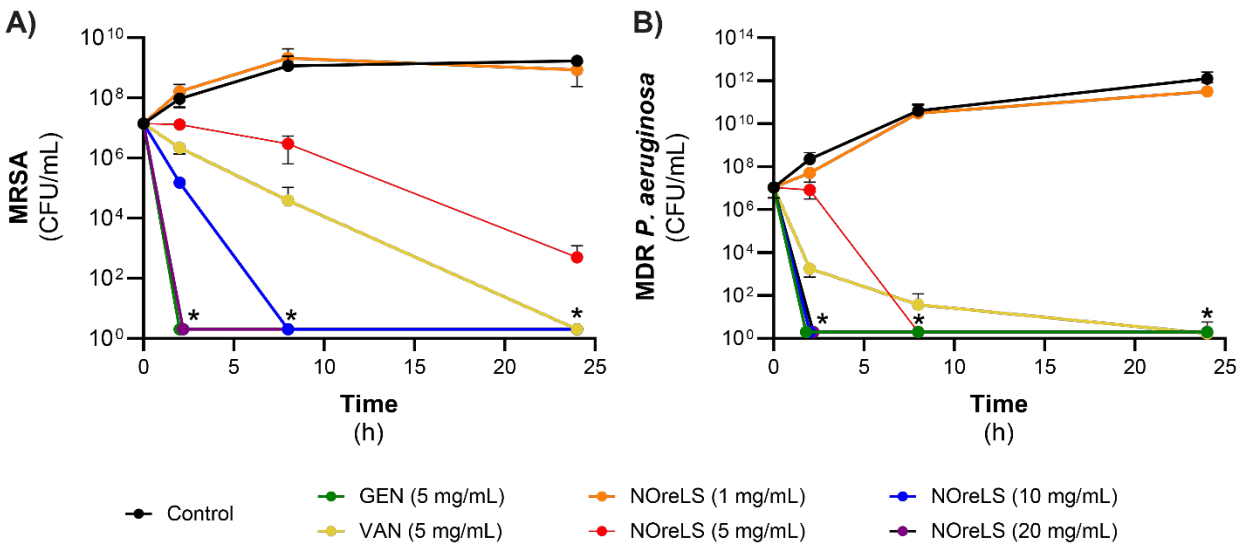

Figure 2.2 Time kill curves of MRSA (A) and MDR P. aeruginosa (B). *No viable CFU detected. Data are shown as the mean ± standard deviation (N = 3 repeats tested per formulation).

Table 2.2 Calculated *P* Values for MRSA Time Kill (Figure 2.2A).

Comparison	2 h	8 h	24 h
Control vs. VAN	0.0062	<0.0001	<0.0001
Control vs. GEN	<0.0001	<0.0001	<0.0001
Control vs. NOreLS (1 mg/mL)	0.9954	0.9963	0.8742
Control vs. NOreLS (5 mg/mL)	0.3155	<0.0001	<0.0001
Control vs. NOreLS (10 mg/mL)	<0.0001	<0.0001	<0.0001
Control vs. NOreLS (20 mg/mL)	<0.0001	<0.0001	<0.0001

Table 2.3 Calculated *P* Values for MDR *P. aeruginosa* Time Kill (Figure 2.2B).

Comparison	2 h	8 h	24 h
Control vs. VAN	<0.0001	<0.0001	<0.0001
Control vs. GEN	<0.0001	<0.0001	<0.0001
Control vs. NOreLS (1 mg/mL)	0.7219	0.9999	0.8326
Control vs. NOreLS (5 mg/mL)	0.0392	<0.0001	<0.0001
Control vs. NOreLS (10 mg/mL)	<0.0001	<0.0001	<0.0001
Control vs. NOreLS (20 mg/mL)	<0.0001	<0.0001	<0.0001

Once infected, current inabilities to eradicate adhered bacteria necessitate the catheter's removal to prevent CRBSIs.[3] However, removal and replacement are not always options for critical patients who may have multiple catheters or pediatric patients with limited access sites.[12]

Therefore, it is highly desirable to have more effective antimicrobial lock therapies to prevent infected catheters leading to CRBSIs. To model an infected catheter, medical-grade tubing was filled with bacterial solutions and incubated for 24 h prior to 2-h lock therapies. Statistically significant decreases in viable MRSA CFUs on tubing were seen after treatment with GEN, 10, and 20 mg/mL NOreLS with 2.5-, 3.2-. and 4.4-fold reductions, respectively (**Figure 2.3A**). Moreover, 20 mg/mL NOreLS significantly decreased viable CFUs ($p < 0.05$) compared to GEN and VAN, as well as 1 and 5 mg/mL NOreLS, which did not have significant effects on the established MRSA infections. Similar to the time kill assays, MDR *P. aeruginosa* was more susceptible to NOreLS compared to MRSA when treating colonies adhered to tubing (**Figure 2.3B**). GEN as well as 5, 10, and 20 mg/mL NOreLS showed significant reductions ($p < 0.05$) in viable MDR *P. aeruginosa*. However, treatment with GEN, which only had a decrease slightly above 1-fold, was significantly ($p < 0.01$) outperformed by 5, 10, and 20 mg/mL NOreLS, which had 4.1-, 4.9-, and 5.2-fold reductions, respectively.

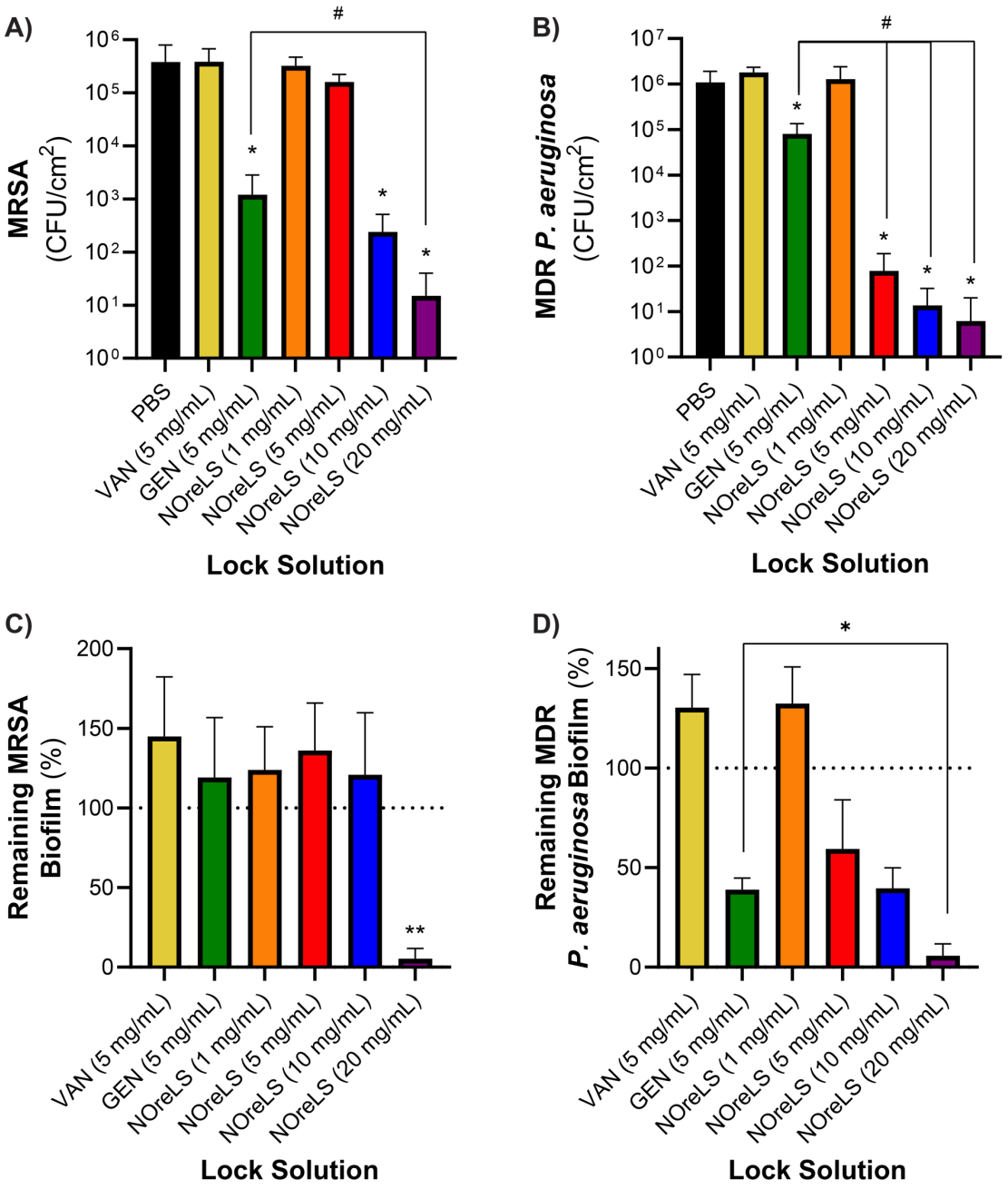

Figure 2.3 MRSA (A) and MDR *P. aeruginosa* (B) adherence to medical grade tubing after 24 h bacterial exposure and 2 h lock therapy. *$p < 0.05$ compared to control; # $p < 0.01$ compared to GEN. Remaining MRSA (C) and MDR *P. aeruginosa* (D) biofilm on medical grade tubing after 24 h lock treatments compared to a growth control. Data are shown as the mean ± standard deviation.

Biofilms are a formidable adversary in combatting device-associated infections, including CRBSI. Biofilm penetration and/or dispersion are two major challenges for antimicrobial therapies.[57] 72-h biofilms were grown within medical grade tubing as a model of severely infected

CVCs. 24-h lock therapies within these samples demonstrated the greatly improved biofilm-mitigating capabilities of NOreLS compared to clinically used antibiotic lock solutions. Compared to 72-h growth controls, 24-h biofilm treatments with VAN, GEN, as well as 1, 5, and 10 mg/mL NOreLS did not decrease the amount of MRSA biofilm present on the tubing (**Figure 2.3C**). This is consistent with previous studies with treatments of VAN, GEN, and low levels of NO with *S. aureus* biofilms.[58-60] However, VAN, GEN, and 5 and 10 mg/mL NOreLS did decrease the number of viable bacteria within the biofilms even if they were unable to disperse it (**Figure 2.4A**). Treatment with 20 mg/mL NOreLS, however, reduced the adhered biofilms by 94.73 ± 6.51%, which is statistically significant ($p < 0.01$) compared to all other treatments. As with all other antibacterial assessments, MDR *P. aeruginosa* biofilms were more susceptible to treatment with NOreLS compared to MRSA (**Figure 2.3D**). Compared to the 72-h growth controls, 5, 10, and 20 mg/mL NOreLS decreased adhered biofilms by 40.55 ± 24.66%, 60.41 ±10.29%, and 94.21 ± 5.90%, respectively. GEN also reduced the amount of biofilm adhered to the tubing by 61.09 ± 5.92%, but it was significantly ($p < 0.05$) outperformed by 20 mg/mL NOreLS. VAN and 1 mg/mL NOreLS treatments did not deter the MDR *P. aeruginosa* biofilm, but VAN (and all other lock solutions excepting 1 mg/mL NOreLS) was able to reduce the viable bacteria within it (**Figure 2.4B**).

These combined results indicate that 20 mg/mL NOreLS is a fast-acting, broad-spectrum antimicrobial therapy that has the potential as a lock therapy to prevent the onset of CRBSIs at many stages of bacteria colonization of CVCs. Compared to the commonly used clinical antibiotic lock therapies (VAN and GEN), only GEN matched 20 mg/mL NOreLS for efficiency in the time-kill assay, and 20 mg/mL NOreLS continually outperformed both antibiotics in all assessments involving established infections.

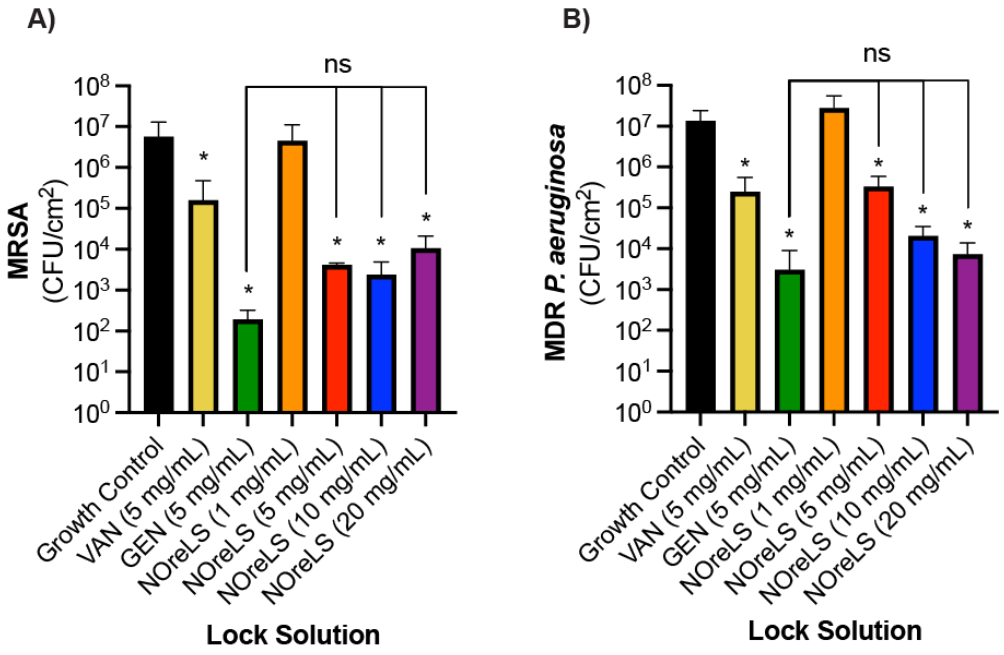

Figure 2.4 MRSA (A) and MDR *P. aeruginosa* (B) adherence to medical grade tubing after 24 h bacterial exposure and 2 h lock therapy. *$p < 0.05$ compared to control; ns is not statistically significant. Data are shown as the mean ± standard deviation. N = 6.

2.4.3 Antithrombotic evaluation. Antithrombotic lock solutions aim to prevent thrombosis at the tip of the catheter, where clots commonly form.[61] Locked medical-grade tubing that contained PBS, HEP, or NOreLS (1, 5, 10, or 20 mg/mL) and was open at one end was incubated in whole blood to observe prevention of thrombi formation on the samples (**Figure 2.5**). Compared to the PBS controls, all HEP and NOreLS samples reduced clot formation on the surface of the tubing. HEP only reduced the clot area by 44.0 ± 11.7%. There is a trend of further area reduction with increasing NOreLS concentrations with both 10 and 20 mg/mL being statistically significant compared to HEP, reducing the clot areas by 73.5 ± 5.0% and 81.2 ± 7.8%, respectively. This supports that NOreLS has excellent potential to address efficacy issues currently seen in clinically used antithrombotic lock solutions.

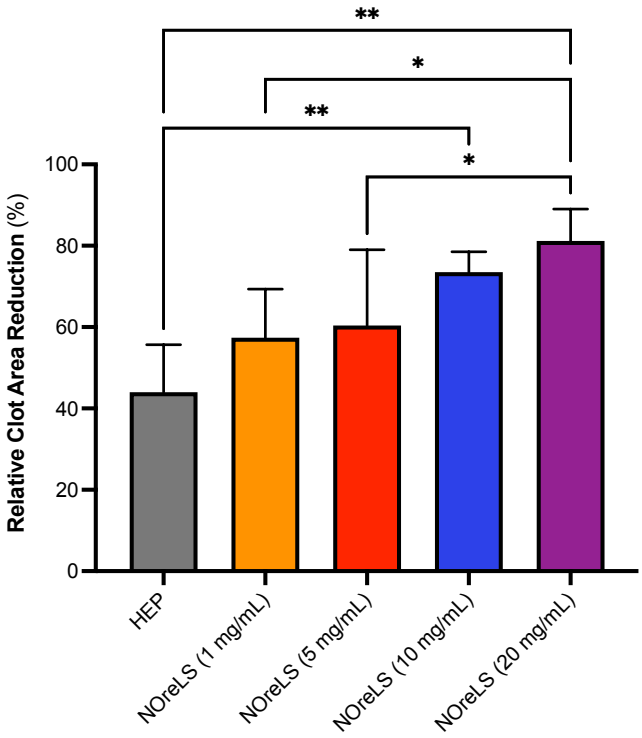

Figure 2.5 Percent reduction in clot area on medical grade tubing with lock therapy after 20 minutes exposure in porcine whole blood. Data are shown as mean ± standard deviation (N = 4). *$p < 0.05$ between compared groups.

2.4.4 Biocompatibility evaluations. The small volumes of lock solution that may leak from a CVC are generally not considered to be a major toxicity concern,[53] particularly because catheter tips are commonly positioned within the superior vena cava,[62] a place of rapid, high-volume blood flow. However, as 10-15% of the lock solution may leak into circulation within the first 10 min of administration,[63] the effects of concentrated lock solutions should be considered. The volume per lumen and number of lumens vary between devices. Even for larger devices, ≤ 3 mL of lock solution will sufficiently fill the lumen, but it has been reported that 5-10 mL of lock solution may be used clinically.[61] A range of leaked lock solution volumes was thus tested. 3 mL, 4.5 mL, and 10 mL of leaked lock solution into 5 L of blood correspond to the 0.06%, 0.09%, and 0.2% lock solution (calculated using **Equation 2.4**) used in biocompatible evaluations.

$$\textit{(2.4)} \quad Percent\ lock\ solution = \frac{Volume\ of\ lock\ solution\ used}{Volume\ of\ blood} \times 100$$

As they are primarily in contact with blood, the potential hemolytic effects of clinically used lock solutions (PBS, VAN, GEN, and HEP) and NOreLS were evaluated (**Table 2.4**). According to the NAMSA ASTM F756 protocol, samples that have a 2 - 5% hemolytic activities are considered slightly hemolytic and > 5% are hemolytic.[64] All NOreLS, antibiotic lock solutions, and heparin lock solution at all lock-solution-to-blood ratios were therefore found to be non-hemolytic.

Table 2.4 Hemolytic activities of clinically used lock solutions and NOreLS. Data are shown as the mean ± standard deviation (N = 3 repeats tested per formulation).

Lock Solution	0.06% LS	0.09% LS	0.2% LS
VAN (5 mg/mL)	0.0	0.0	0.0
GEN (5 mg/mL)	0.0	0.0	0.001 ± 0.023
HEP (10k unit/mL)	0.005 ± 0.023	0.0	0.0
NOreLS (1 mg/mL)	0.005 ± 0.023	0.0	0.0
NOreLS (5 mg/mL)	0.0	0.0	0.0
NOreLS (10 mg/mL)	0.0	0.0	0.0
NOreLS (20 mg/mL)	0.0	0.0	0.0

Further cytocompatibility evaluation was conducted with HUVECs to explore any potential cytotoxic effects of the clinically used lock solutions and NOreLS based on potential percent by volume leaking of the lock solutions into the physiological environment. In parallel to blood studies, confluent monolayers of HUVECs were treated with 0.06%, 0.09%, and 0.20% solutions of VAN, GEN, HEP, and NOreLS prepared in culture media to evaluate any cytotoxic effects from lock solution leaking. As shown in **Figure 2.6**, leaking of the lock solution biocidal/anticoagulant agents did not induce any cytotoxic response in HUVECs, with each treatment resulting in > 80% cellular viability with respect to untreated controls.

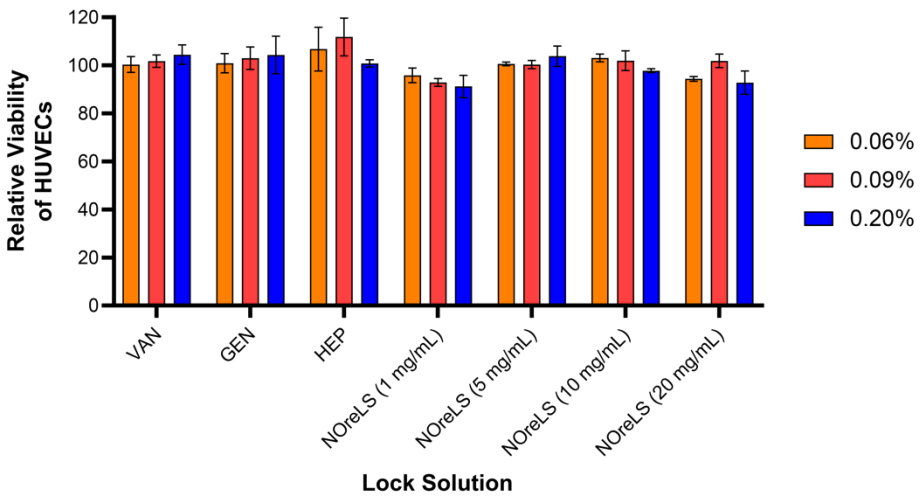

Figure 2.6 Cellular cytocompatibility evaluation of lock solutions with HUVECs over 24 h studies with 0.06%, 0.09%, and 0.20% solutions of the antimicrobial/anti-clotting agents. Lock solution dilutions reflect possible concentrations of antibiotic/anti-clotting agents that may leak into the physiological environment. Data are shown as mean ± standard deviation (N = 3).

2.5 Conclusion. CVC use is often complicated by CRBSIs and CRT, leading to exacerbated healthcare issues. In this work, NOreLSs containing the NO donor molecule GSNO are shown to have the potential to combat these complications. Varying concentrations of NOreLS characterized via NOA all showed NO release for at least 48 h, the maximum dwell time for a lock solution. NOreLS consistently outperformed clinically used antibiotic lock solutions (VAN and GEN) at different stages of bacterial colonization of medical-grade tubing. Notably, 20 mg/mL NOreLS was able to reduce adhered MRSA and MDR *P. aeruginosa* biofilms by 94.73 ± 6.51% and 94.21 ± 5.90%, respectively. 20 mg/mL NOreLS was also able to reduce the area of clot formation on medical-grade tubing by 81.2 ± 7.8%, surpassing the effects of a clinically relevant HEP lock solution. All concentrations of NOreLS were established to be non-hemolytic and non-cytotoxic to HUVECs. In conclusion, this work demonstrates the potential of NOreLS in deterring CRBSIs and CRT and, thus, improving the medical outcome and quality of life of patients with CVCs.

2.6 References.

1. Kornbau C, Lee KC, Hughes GD, Firstenberg MS. Central line complications. *Int J Crit Illn Inj Sci.* 2015;5(3):170-178.

2. Gahlot R, Nigam C, Kumar V, Yadav G, Anupurba S. Catheter-related bloodstream infections. *Int J Crit Illn Inj Sci.* 2014;4(2):162-167.

3. Shah H, Bosch W, Thompson KM, Hellinger WC. Intravascular catheter-related bloodstream infection. *Neurohospitalist.* 2013;3(3):144-151.

4. Anand P, Kranker K, Chen AY. Estimating the hospital costs of inpatient harms. *Health Serv Res.* 2019;54(1):86-96.

5. Zhong Y, Zhou L, Liu X, et al. Incidence, Risk Factors, and Attributable Mortality of Catheter-Related Bloodstream Infections in the Intensive Care Unit After Suspected Catheters Infection: A Retrospective 10-year Cohort Study. *Infect Dis Ther.* 2021;10(2):985-999.

6. Ziegler MJ, Pellegrini DC, Safdar N. Attributable mortality of central line associated bloodstream infection: systematic review and meta-analysis. *Infection.* 2015;43(1):29-36.

7. Goede MR, Coopersmith CM. Catheter-related bloodstream infection. *Surg Clin North Am.* 2009;89(2):463-474, ix.

8. Mielke M. [The role of infection prevention in the control of antimicrobial resistance : Any avoided infection contributes to the reduction of antibiotic use]. *Bundesgesundheitsblatt Gesundheitsforschung Gesundheitsschutz.* 2018;61(5):553-561.

9. Roca I, Akova M, Baquero F, et al. The global threat of antimicrobial resistance: science for intervention. *New Microbes New Infect.* 2015;6:22-29.

10. Ventola CL. The antibiotic resistance crisis: part 1: causes and threats. *P T.* 2015;40(4):277-283.

11. Whitelaw AC. Role of infection control in combating antibiotic resistance. *S Afr Med J.* 2015;105(5):421.

12. Kim EY, Saunders P, Yousefzadeh N. Usefulness of anti-infective lock solutions for catheter-related bloodstream infections. *Mt Sinai J Med.* 2010;77(5):549-558.

13. Srinivasan A. Antibiotic stewardship: Why we must, how we can. *Cleve Clin J Med.* 2017;84(9):673-679.

14. Arechabala MC, Catoni MI, Claro JC, et al. Antimicrobial lock solutions for preventing catheter-related infections in haemodialysis. *Cochrane Database Syst Rev.* 2018;4:CD010597.

15. Zhang J, Li RK, Chen KH, Ge L, Tian JH. Antimicrobial lock solutions for the prevention of catheter-related infection in patients undergoing haemodialysis: study protocol for network meta-analysis of randomised controlled trials. *BMJ Open.* 2016;6(1):e010264.

16. Flemming HC, Wingender J, Szewzyk U, Steinberg P, Rice SA, Kjelleberg S. Biofilms: an emergent form of bacterial life. *Nat Rev Microbiol.* 2016;14(9):563-575.

17. Lebeaux D, Ghigo JM, Beloin C. Biofilm-related infections: bridging the gap between clinical management and fundamental aspects of recalcitrance toward antibiotics. *Microbiol Mol Biol Rev.* 2014;78(3):510-543.

18. Madsen JS, Burmolle M, Hansen LH, Sorensen SJ. The interconnection between biofilm formation and horizontal gene transfer. *FEMS Immunol Med Microbiol.* 2012;65(2):183-195.

19. Steenackers HP, Parijs I, Dubey A, Foster KR, Vanderleyden J. Experimental evolution in biofilm populations. *FEMS Microbiol Rev.* 2016;40(3):373-397.

20. Gominet M, Compain F, Beloin C, Lebeaux D. Central venous catheters and biofilms: where do we stand in 2017? *APMIS.* 2017;125(4):365-375.

21. Penesyan A, Nagy SS, Kjelleberg S, Gillings MR, Paulsen IT. Rapid microevolution of biofilm cells in response to antibiotics. *NPJ Biofilms Microbiomes.* 2019;5:34.

22. Baskin JL, Pui CH, Reiss U, et al. Management of occlusion and thrombosis associated with long-term indwelling central venous catheters. *Lancet.* 2009;374(9684):159-169.

23. Wall C, Moore J, Thachil J. Catheter-related thrombosis: A practical approach. *J Intensive Care Soc.* 2016;17(2):160-167.

24. Kamphuisen PW, Lee AY. Catheter-related thrombosis: lifeline or a pain in the neck? *Hematology Am Soc Hematol Educ Program.* 2012;2012:638-644.

25. Nakazawa N. Infectious and thrombotic complications of central venous catheters. *Semin Oncol Nurs.* 2010;26(2):121-131.

26. Rooden CJ, Tesselaar ME, Osanto S, Rosendaal FR, Huisman MV. Deep vein thrombosis associated with central venous catheters - a review. *J Thromb Haemost.* 2005;3(11):2409-2419.

27. Burns KE, McLaren A. Catheter-related right atrial thrombus and pulmonary embolism: a case report and systematic review of the literature. *Can Respir J.* 2009;16(5):163-165.

28. Lee AY, Kamphuisen PW. Epidemiology and prevention of catheter-related thrombosis in patients with cancer. *J Thromb Haemost.* 2012;10(8):1491-1499.

29. Mitchell MD, Anderson BJ, Williams K, Umscheid CA. Heparin flushing and other interventions to maintain patency of central venous catheters: a systematic review. *J Adv Nurs.* 2009;65(10):2007-2021.

30. Liang H, Nacharaju P, Friedman A, Friedman JM. Nitric oxide generating/releasing materials. *Future Sci OA.* 2015;1(1).

31. Rong F, Tang Y, Wang T, et al. Nitric Oxide-Releasing Polymeric Materials for Antimicrobial Applications: A Review. *Antioxidants (Basel).* 2019;8(11).

32. Ashcraft M, Douglass M, Chen Y, Handa H. Combination strategies for antithrombotic biomaterials: an emerging trend towards hemocompatibility. *Biomaterials Science.* 2021.

33. Shen Z, Zheng S, Xiao S, Shen R, Liu S, Hu J. Red-Light-Mediated Photoredox Catalysis Enables Self-Reporting Nitric Oxide Release for Efficient Antibacterial Treatment. *Angewandte Chemie International Edition.* 2021;60(37):20452-20460.

34. Tao S, Cheng J, Su G, et al. Breathing Micelles for Combinatorial Treatment of Rheumatoid Arthritis. *Angewandte Chemie International Edition.* 2020;59(49):21864-21869.

35. Schairer DO, Chouake JS, Nosanchuk JD, Friedman AJ. The potential of nitric oxide releasing therapies as antimicrobial agents. *Virulence.* 2012;3(3):271-279.

36. Jones ML, Ganopolsky JG, Labbe A, Wahl C, Prakash S. Antimicrobial properties of nitric oxide and its application in antimicrobial formulations and medical devices. *Appl Microbiol Biotechnol.* 2010;88(2):401-407.

37. Privett BJ, Broadnax AD, Bauman SJ, Riccio DA, Schoenfisch MH. Examination of bacterial resistance to exogenous nitric oxide. *Nitric Oxide.* 2012;26(3):169-173.

38. Barraud N, Kelso MJ, Rice SA, Kjelleberg S. Nitric oxide: a key mediator of biofilm dispersal with applications in infectious diseases. *Curr Pharm Des.* 2015;21(1):31-42.

39. Xiong Y, Liu Y. Biological control of microbial attachment: a promising alternative for mitigating membrane biofouling. *Appl Microbiol Biotechnol.* 2010;86(3):825-837.

40. Devine R, Singha P, Handa H. Versatile biomimetic medical device surface: hydrophobin coated, nitric oxide-releasing polymer for antimicrobial and hemocompatible applications. *Biomater Sci.* 2019;7(8):3438-3449.

41. Mondal A, Douglass M, Hopkins SP, et al. Multifunctional S-Nitroso-N-acetylpenicillamine-Incorporated Medical-Grade Polymer with Selenium Interface for Biomedical Applications. *ACS Applied Materials & Interfaces.* 2019;11(38):34652-34662.

42. Douglass ME, Goudie MJ, Pant J, et al. Catalyzed Nitric Oxide Release via Cu Nanoparticles Leads to an Increase in Antimicrobial Effects and Hemocompatibility for Short-Term Extracorporeal Circulation. *ACS Applied Bio Materials.* 2019;2(6):2539-2548.

43. Goudie MJ, Singha P, Hopkins SP, Brisbois EJ, Handa H. Active Release of an Antimicrobial and Antiplatelet Agent from a Nonfouling Surface Modification. *ACS Applied Materials & Interfaces.* 2019;11(4):4523-4530.

44. Hopkins SP, Pant J, Goudie MJ, Schmiedt C, Handa H. Achieving Long-Term Biocompatible Silicone via Covalently Immobilized S-Nitroso- N-acetylpenicillamine (SNAP) That Exhibits 4 Months of Sustained Nitric Oxide Release. *ACS Appl Mater Interfaces.* 2018;10(32):27316-27325.

45. Kumar R, Massoumi H, Chug MK, Brisbois EJ. S-Nitroso-N-acetyl-l-cysteine Ethyl Ester (SNACET) Catheter Lock Solution to Reduce Catheter-Associated Infections. *ACS Applied Materials & Interfaces.* 2021;13(22):25813-25824.

46. Broniowska KA, Diers AR, Hogg N. S-nitrosoglutathione. *Biochim Biophys Acta.* 2013;1830(5):3173-3181.

47. Corpas F, Alché J, Barroso J. Current overview of S-nitrosoglutathione (GSNO) in higher plants. *Frontiers in Plant Science.* 2013;4(126).

48. Douglass M, Hopkins S, Pandey R, Singha P, Norman M, Handa H. S-Nitrosoglutathione-Based Nitric Oxide-Releasing Nanofibers Exhibit Dual Antimicrobial and Antithrombotic Activity for Biomedical Applications. *Macromolecular Bioscience.* 2021;n/a(n/a):2000248.

49. Doverspike JC, Zhou Y, Wu J, Tan X, Xi C, Meyerhoff ME. Nitric oxide releasing two-part creams containing S-nitrosoglutathione and zinc oxide for potential topical antimicrobial applications. *Nitric Oxide.* 2019;90:1-9.

50. Douglass M, Hopkins S, Pandey R, Singha P, Norman M, Handa H. S-Nitrosoglutathione-Based Nitric Oxide-Releasing Nanofibers Exhibit Dual Antimicrobial and Antithrombotic Activity for Biomedical Applications. *Macromolecular Bioscience.*n/a(n/a):2000248.

51. Sim J-H, Jamaludin NS, Khoo C-H, et al. In vitro antibacterial and time-kill evaluation of phosphanegold(I) dithiocarbamates, R3PAu[S2CN(iPr)CH2CH2OH] for R = Ph, Cy and

Et, against a broad range of Gram-positive and Gram-negative bacteria. *Gold Bulletin.* 2014;47(4):225-236.

52. Bleyer AJ. Use of Antimicrobial Catheter Lock Solutions to Prevent Catheter-Related Bacteremia. *Clinical Journal of the American Society of Nephrology.* 2007;2(5):1073.

53. Justo JA, Bookstaver PB. Antibiotic lock therapy: review of technique and logistical challenges. *Infect Drug Resist.* 2014;7:343-363.

54. O'Toole GA. Microtiter dish biofilm formation assay. *J Vis Exp.* 2011(47).

55. Zhang J, Wang B, Wang J, Yang Q. Ethanol locks for the prevention of catheter-related infection in patients with central venous catheter: A systematic review and meta-analysis of randomized controlled trials. *PLoS One.* 2019;14(9):e0222408.

56. Yang T, Zelikin AN, Chandrawati R. Progress and Promise of Nitric Oxide-Releasing Platforms. *Advanced Science.* 2018;5(6):1701043.

57. Fux CA, Stoodley P, Hall-Stoodley L, Costerton JW. Bacterial biofilms: a diagnostic and therapeutic challenge. *Expert Rev Anti Infect Ther.* 2003;1(4):667-683.

58. He X, Yuan F, Lu F, Yin Y, Cao J. Vancomycin-induced biofilm formation by methicillin-resistant Staphylococcus aureus is associated with the secretion of membrane vesicles. *Microb Pathog.* 2017;110:225-231.

59. Hess DJ, Henry-Stanley MJ, Wells CL. Gentamicin promotes Staphylococcus aureus biofilms on silk suture. *J Surg Res.* 2011;170(2):302-308.

60. Jardeleza C, Foreman A, Baker L, et al. The effects of nitric oxide on Staphylococcus aureus biofilm growth and its implications in chronic rhinosinusitis. *Int Forum Allergy Rhinol.* 2011;1(6):438-444.

61. Goossens GA. Flushing and Locking of Venous Catheters: Available Evidence and Evidence Deficit. *Nurs Res Pract.* 2015;2015:985686.

62. Silverstein DM, Trerotola SO, Clark T, et al. Clinical and Regulatory Considerations for Central Venous Catheters for Hemodialysis. *Clin J Am Soc Nephrol.* 2018;13(12):1924-1932.

63. McGah PM, Gow KW, Aliseda A. Leakage of Central Venous Catheter Locking Fluid by Hemodynamic Transport. *ASAIO Journal.* 2014;60(4).

64. Brisbois EJ, Major TC, Goudie MJ, Meyerhoff ME, Bartlett RH, Handa H. Attenuation of thrombosis and bacterial infection using dual function nitric oxide releasing central venous catheters in a 9day rabbit model. *Acta Biomaterialia.* 2016;44:304-312.

CHAPTER 3

Derivatization of Graphene Oxide Nanosheets with Tunable Nitric Oxide Release for Antibacterial Biomaterials[3]

[3]This chapter is prepared for submission as: Ashcraft, M.*, Garren, M.*, Crowley, D., Handa, H. Derivatization of Graphene Oxide Nanosheets with Tunable Nitric Oxide Release for Antibacterial Biomaterials. To be submitted to ACS Applied Bio Materials. (* Indicates that these authors contributed equally).

3.1 Abstract

To prevent infections, multifunctional antibacterial materials have been of increasing interest in recent years. Having inherent antimicrobial properties as well as interesting conductive and mechanical properties, graphene oxide (GO) is one such material. This work describes the first combination of GO and an S-Nitrosothiol (RSNO), a nitric oxide (NO) donor molecule. Adding NO release to GO's plethora of materials characteristics provides an additional, active antibacterial mechanism. Through a multistep process, S-nitroso-N-acetylpenicillamine (SNAP) is covalently attached to functionalized GO. This novel compound and its precursors are thoroughly characterized by both quantitative and qualitative methods, including FTIR, XPS, and NO release analysis. It is demonstrated that the NO release profile of this GO derivative is highly tunable via synthesis parameters and the use of low-level electrical currents. NO-releasing GO is shown to have increased antibacterial activity compared to unmodified GO in adhesion and biofilm dispersal assessments. Moreover, equivalent or improved cytocompatibility was observed upon the indirect exposure of human fibroblast cells to NO-releasing GO compared to GO at a range of concentrations. Overall, this work presents a novel and highly tunable material for antibacterial applications.

3.2 Introduction

Recently, particular emphasis has been given to the development of multifunctional materials systems for their efficiency and broad range of potential applications, including those in the biomedical fields.[1] Graphene materials, such as graphene oxide (GO), are often employed in these systems due to its versatility.[2,3] In terms of materials properties, GO is known for its thermal,

conductive, and mechanical characteristics as well as its ability to be functionalized. Potential functionalization, as well as its inherent antimicrobial[4] and antiviral[5] properties, makes GO a scaffold of interest for many biomedical applications such as tissue engineering, biosensing, drug/gene delivery, and, broadly, biomaterials for medical devices.[6]

The specific formulation of GO substrates (shape, size, number of layers, oxygen content, etc.) effects its antimicrobial properties. Generally speaking, however, multiple mechanisms of action are proposed including disruption of the bacterial cell membrane via interactions with proteins and lipids and production of reactive oxygen species (ROS).[7] With this nonspecific mechanism of action, GO has been shown to be effective against a broad spectrum of bacteria including multi-drug resistant bacteria.[8] Moreover, it has been demonstrated to have anti-biofilm actions, inhibiting formation and affecting mature biofilms.[9] It has been noted that GO conjugated with other antimicrobial agents can increase its antibacterial effects.[7]

Nitric oxide (NO)-releasing materials have similarly been of increasing interest for their multifunctionality. NO is an endogenous antimicrobial[10,11] and antiviral[12] agent that also participates in cell signaling, including mediation of platelet activation[13] and angiogenesis.[14] As NO itself has a very short half-life,[15] NO-releasing materials containing NO donor molecules, such as S-Nitrosothiols (RSNOs), are used to provide sustained, localized NO delivery.[16] In particular, covalently bound NO donors have demonstrated excellent stability and longevity.[17] Moreover, NO-releasing materials have been shown to have complimentary, sometimes synergistic, properties when combined with other surface/material modification strategies that further the design's multifunctionality.[18,19]

For the first time, the combination of an RSNO and GO is investigated. In this study, a precursor to the NO donor molecule, S-nitroso-N-acetylpenicillamine (SNAP), is covalently

attached to silanated, amine-functionalized GO. SNAP is an established donor molecule, and its incorporation into various materials has demonstrated antimicrobial, antithrombotic, and anti-inflammatory effects.[20-22] Various ratios of functionalization are explored to assess the tunability of the compound. The final product, which is achieved through nitrosation, and all intermediates are thoroughly characterized via quantification assays, Fourier Transform Infrared Spectroscopy (FTIR), and X-ray Photoelectron Spectroscopy (XPS). The ability to tune the amount of functionalization and subsequent NO loading is thus confirmed. The suspension stability of the compounds in solution is also determined via zeta potential measurements.

The described NO-releasing graphene oxide (GO-$(NH)_x$-SNO) has prolonged NO release that is roughly proportional to the amount of NO loaded in each sample type. With GO's conductive properties in mind, the effective of low-leveled electrical currents on the release of NO from GO-$(NH)_x$-SNO is investigated. The resulting differences in burst release and cumulative release when exposed to current indicate that GO-$(NH)_x$-SNO can be a highly tunable NO-releasing material. While other systems have used light and catalysts to achieved desired NO release levels,[23,24] this is the first example of current-induced NO release.

While it has been demonstrated that the combination of NO release and GO is cytocompatible,[25] the combination's antibacterial potential has never been explored. In this study, we endeavor to thoroughly explore this benefit of GO-$(NH)_x$-SNO through proof-of-concept bacterial adhesion and biofilm dispersion studies. It is thus exhibited that GO-$(NH)_x$-SNO has broad-spectrum antibacterial and anti-biofilm actions. GO-$(NH)_x$-SNO repeatedly outperformed control GO in reducing viable attachment of methicillin-resistant *Staphylococcus aureus* (MRSA) and *Escherichia coli* and dispersing their established biofilms. This implies that GO-$(NH)_x$-SNO

has excellent potential for applications where GO and other graphene compounds are already being incorporated.

Overall, this study provides an in-depth assessment of the combination of NO and GO and its potential as a highly tunable material. We present an extremely novel system of controlling NO release through both degrees of functionalization and low levels of electrical current. Furthermore, we demonstrate the biological advantages of this material through bacterial adhesion and biofilm dispersion assays. GO-$(NH)_x$-SNO is also established to have improved cytocompatibility compared to unmodified GO.

3.3 Materials and Methods

3.3.1 Materials. Monolayer graphene oxide (SKU# PO0705) and reduced monolayer graphene oxide (SKU# PO0712) nanosheets were purchased from MSE Supplies LLC (Tucson, AZ USA). Acetic anhydride, 5,5'-dithiobis(2-nitrobenzoic acid) (DNTB, Ellman's reagent), chloroform, hydrochloric acid, methanol, *N*-acetyl-D-penicillamine (NAP), 2-morpholinoethanesulfonic acid monohydrate (MES), ninhydrin reagent, potassium bromide, phosphate buffered saline (PBS 1x), pyridine, (3-aminopropyl)triethoxysilane (APTES), Mueller–Hinton agar (MHA), Mueller–Hinton broth (MHB), crystal violet, acetic acid, and sodium nitrite were purchased from Sigma Aldrich (St. Louis, MO USA). All organic solvents were purchased reagent grade and anhydrous. All other reagents were purchased from VWR (Radnor, PA USA).

3.3.2 Synthesis of N-(2,2-dimethyl-4-oxothietan-3-yl)acetamide (NAPTH). The synthesis of NAPTH followed previous reports with some minor deviation in the synthetic strategy.[26,27] In

brief, 5 g of NAP was dissolved in 10 mL of acetic anhydride and 20 mL of pyridine in a round bottom flask, sealed, and purged with argon gas. The pot was allowed to react for 12 h with protection from light. Subsequently, the solvent was removed via rotary evaporation and the crude precipitate was resuspended in chloroform (30 mL). The dissolved mixture was washed 3x with an equal volume of 1 M HCl, and the organic phase was dried over anhydrous magnesium sulfate. The final mixture was condensed to a small volume and triturated in chilled hexanes at -20 ºC overnight. The precipitated NAPTH crystals were collected via vacuum filtration and washed with chilled hexanes. The crystals were then dried under vacuum at room temperature for 12 h. The NAPTH was stored at -20 ºC between uses.

3.3.3 Synthesis of Graphene Oxide Derivatives. Aminated graphene oxide (GO-$(NH_2)_x$) was synthesized following previous reports with minor deviation.[28] In brief, 1 g of GO suspended in 160 mL of anhydrous toluene was brought to reflux under nitrogen atmosphere. Afterwards, a molar amount of APTES was dissolved in 9 mL of anhydrous chloroform and injected into the reaction pot. The pot was allowed to react for 72 h under reflux. The resulting crude was vacuum filtered, washed with excess anhydrous chloroform, and dried under vacuum at 80 ºC for 48 h. GO-$(NH_2)_x$ was stored as a dried powder at -20 °C between uses.

Thiolated graphene oxide (GO-$(NH)_x$-SH) was subsequently prepared via the reaction of aminated GO derivatives with NAPTH following a modified protocol for thiolactone aminolysis reactions previously reported.[29,30] In a representative setup, 500 mg of GO-$(NH_2)_x$ is suspended in 50 mL of MES Buffer (0.5 M, pH 6) with 10x stoichiometric excess of NAPTH provided relative to the quantitatively determined amine content. The vessel was purged under argon gas and stirred for 48 h protected from light. Afterwards, the crude mixture was vacuum filtered, washed 3x times

with 100 mL of deionized water to remove unreacted NAPTH and byproducts, and dried under vacuum at room temperature for 12 h. GO-$(NH)_x$-SH was stored as a dried powder at -20 ºC between uses.

NO-releasing graphene oxide (GO-$(NH)_x$-SNO) was achieved via nitrosation of the GO-$(NH)_x$-SH analogs using acidified nitrite conditions. In brief, 100 mg of the GO-$(NH)_x$-SH was dissolved in 25 mL of 2 M HCl, chilled in an ice bath, and protected from light. DPTA was added to achieve a final concentration of 500 μM to act as a metal ion chelator. Finally, sodium nitrite was added in greater than 10x stoichiometric excess relative to the quantitatively determined thiol content. The resulting mixture was allowed to react for 2 h before worked up via decantation of the solvent via centrifugation (4000 RPM, 4 ºC, 10 min) and treatment with chilled methanol. This washing step was repeating three times, with the NO-releasing conjugate finally dried under vacuum at room temperature for 2 h. GO-$(NH)_x$-SNO was stored as a dried powder at -20 °C between uses.

3.3.4 Fourier Transform Infrared Spectroscopy (FTIR). FTIR analysis of the GO analogues was carried out using a KBr loading method collecting absorbance readings across the infrared spectra from 4000 – 650 cm^{-1} with a Spectrum Two spectrometer from Perkin Elmer (Greenville, SC USA). A total of 32 scans were collected for each loaded sample with a resolution of 4 cm^{-1}. Independently prepared batches of the derivatized GO nanosheets were evaluated for each modification (N = 3 per modification).

3.3.5 Amine Quantification. A ninhydrin assay was used to quantify the amines of GO-$(NH_2)_x$ using previously reported methods.[31] Briefly, GO-$(NH_2)_x$ samples in 0.1% acetic acid with excess

ninhydrin reagent were placed in boiling water for 10 min. The GO-$(NH_2)_x$ was filtered out of solution before reading at 570 nm. The amine contents of the samples were calculated via comparison to a standard curve of glycine. Final data are reported as the mean mol of amine per mass of GO analyte ± SD, averaged across five technical repeats (N = 5) across three independently prepared batches of material.

3.3.6 Sulfhydryl Quantification. Conjugated thiols were quantified via Ellman's assay as previously reported.[31] GO-$(NH)_x$-SH samples were incubated with DTNB for 15 min before filtered out the GO-$(NH)_x$-SH and reading at 412 nm. The thiol contents of the samples were calculated via comparison to a standard curve of NAP. Final data reported as the mean mol of thiol per mass of GO analyte ± SD, averaged across five technical repeats (N = 5) across three independently prepared batches of material.

3.3.7 Nitric Oxide Analysis. Quantification of NO release from derivatized GO was achieved using a Zysense chemiluminescence-based Nitric Oxide Analyzer (NOA) model 280i (Boulder, CO). In each experiment, NO is evolved from an analyte in solution phase within a sample chamber continuously purged with dried N_2 gas. This purge stream is fed into a reaction chamber within the NOA, which simultaneously passes O_2 gas through an ozone generator and into the reaction chamber. Concomitantly, NO and O_3 gas react to produce excited state NO_2^* gas, which subsequently relaxes to emit a photon (**Equations 1** and **2**).

$$\textit{(1)} \qquad NO + O_3 \rightarrow NO_2^* + O_2$$

$$\textit{(2)} \qquad NO_2^* \rightarrow NO_2 + h\nu$$

The photon is then detected through a cooled photomultiplier tube, generating a voltage signal that is correlated to PPB NO. A NO gas standard (45 PPM) is used to develop an internal calibration constant (mol-NO/PPB×s), enabling calculation of the instantaneous release profile of NO normalized to mass of analyte (mol-NO/(mg-analyte×min)).

3.3.8 S-Nitrosothiol Quantification. GO-$(NH)_x$-SNO samples were placed in 3 mL of PBS within the NOA sample chamber. Cysteine (10 mM) and $CuCl_2$ (50 mM) were added to catalyze the release of NO from GO-$(NH)_x$-SNO as in previous reports.[32] The catalysis was allowed to run until the entire NO payload was exhausted. The subsequent instantaneous release rate profile was then numerically integrated and normalized to the mass of the GO analyte (mol-NO/mg-analyte). This normalized quantity was then compared to the number of moles of thiol calculated for the precursor GO-$(NH)_x$-SH, enabling calculation of nitrosation efficiency (**Equation 3**).

$$\textit{(3)} \qquad \text{Nitrosation Efficiency (\%)} = \frac{\frac{\text{mol NO produced}}{\text{mg analyte}}}{\frac{\text{mol SH on precursor}}{\text{mg precursor}}} \times 100\%$$

Final data are reported as the mean percent nitrosation efficiency ± SD, averaged across three technical repeats (N = 3) across three independently prepared batches of analyte.

3.3.9 NO-Release Profiles. NOA analysis was performed to determine the real-time instantaneous release rate of NO from GO-$(NH)_x$-SNO samples suspended in 1x PBS (1 mg/mL analyte). One mg/mL Solutions were examined for release at 25 °C in amber glass sample chambers with supplemented EDTA in solution to avoid secondary emission of NO from the presence of light and metal ions. Each GO-$(NH)_x$-SNO derivatization was assessed across three independently prepared batches (N = 3), with final data reported as the mean release rate of NO normalized to mass of analyte (mol NO/(mg-analyte × s)) at given time points.

3.3.10 Current-Induced NO Release. Low levels of current (4, 8, or 16 mA) were applied to 6 mL of GO-$(NH)_{2x}$-SNO solutions (1 mg/mL) during NO analysis by a LB78 Signal Generator. Carbon fiber rods (1.5 mm in diameter) were used as current conductors to avoid inadvertent RSNO catalysis via traditional metal conductors. The amount of current output was confirmed via Klein Tools multimeter. Measurements were conducted at 25 °C and with stirring to ensure a homogenized solution throughout the hour of data collection. Data are presented as the mean five-minute release rate averages of NO normalized to mass of analyte (mol NO/(mg-analyte × s)) at given time points (N = 3).

3.3.11 Zeta Potential Measurements. A Zetasizer Nano ZS Analyzer (Malvern Panalytical Ltd) was used for all zeta potential measurements. 1 mg/mL solutions of all GO derivatives were made in varying pH solutions of DI H_2O adjusted with HCl or NaOH. Each sample type was run five times (N = 5). Data are presented as the mean zeta potential (mV) ± SD.

3.3.12 X-ray Photoelectron Spectroscopy. Controls and experimental samples including all synthesis steps were analyzed via x-ray photoelectron spectroscopy (XPS) to confirm elemental changes and characterize bonds. All XPS was conducted on a Kratos Axis Ultra XPS ((MC)2, University of Michigan). Monochromatic Al kα X-ray radiation at 1.486keV of photon energy and an angle of incidence of 54.7º was used to excite the samples. The resulting photoelectrons were collected from a 300 μm × 700 μm area of interest. Background subtraction and peak fitting was enabled by CASAXPS software.

3.3.13 Viable Bacterial Adhesion Assessment. The effect of GO and GO-$(NH)_x$-SNO on viable bacterial adhesion were assessed via a previously published protocol with slight adaptations.[33] The samples were vacuum filtered onto a cellulose filter and allowed to air dry before being exposed to bacteria. MRSA and *E. coli* were used as representatives of Gram positive and negative bacteria, respectively. The bacterial solutions were grown to 0.8-1 OD 600 in MHB, centrifuged and washed with sterile PBS, and finally diluted to 0.1 OD 600 in PBS. Each sample (2 cm^2) was exposed to 1 mL of this bacterial solution for four hours. After incubation, the samples were rinsed in sterile PBS to remove unadhered bacteria and homogenized to remove adhered bacteria. The homogenization solutions were diluted 10-fold and plated on MHA with the aid of an Eddy Jet W2 spiral plater (IUL, Farmingdale, NY). Overnight incubation at 37 °C allowed viable colonies to grow and be counted via a SphereFlash automated colony counter (IUL, Farmingdale, NY). Data are presented as the mean viable CFU/cm^2 ± SD (N = 8).

3.3.14 Biofilm Dispersion Assessment. The biofilm-dispersing properties of GO and GO-$(NH)_x$-SNO were tested with 24 h biofilms. MRSA or *E. coli* in MHB were grown in a 96-well plate with shaking at 37 °C. After 24 h, the bacterial solutions were removed and replaces with 0.5 mg/mL GO or GO-$(NH)_x$-SNO solutions in sterile PBS. PBS was used as a control. Following 24 h of treatment at 37 °C, the wells were washed with PBS and the remaining biofilms were dyed with 0.1% crystal violet for 15 min. After repeated washing with PBS to removed unbound dye, the stained biofilms were dissolved in 30% acetic acid, and the plate was read at 550 nm. Data are presented as the mean absorbances at 550 nm ± SD (n = 16). Percent reduction is calculated using **Equation 4**:

$$\textit{(4)} \qquad \text{Percent Bacterial Reduction} = \frac{\text{Control abs} - \text{sample abs}}{\text{Control abs}} \times 100\%$$

3.3.15 Cytocompatibility Assessment.

3.3.15.1 Mammalian Cell Culture. BJ cells were revived from cryopreserved stocks stored under vapor phase of liquid nitrogen. Cells were subcultured in MEM media supplemented with 10% FBS and 1% penicillin-streptomycin in a 5% CO_2-humidified atmosphere at 37 °C. Cells were subcultured for up to ten passages. Monolayers showing > 70% sub-confluency were split by treating with 0.25% trypsin supplemented with 5 mM EDTA, centrifuging down the cell pellet (200 rcf, 5 min), and resuspending in clean media. For cytotoxicity screening, cells were seeded onto 12 mm hydrophilic polytetrafluoroethylene inserts (Millicell® PICM01250) pretreated with type I rat-tail collagen (300 μg insert^{-1}) at a density of 40,000 cells cm^{-2} within 24-well plates. Extraluminal space was supplemented with 600 μL of clean media while the intraluminal space contained 400 μL of media with the cell suspension. Cells were grown for an initial 24 h before treatment.

3.3.15.2 Indirect Contact Cytotoxicity Screening (24 h). The cytocompatibility of the GO analogues was determined in accordance with the International Organization for Standardization (ISO) 10993-5 standards and our previously reported methods.[34,35] Following 24 h incubation of seeded inserts, the intraluminal media was replaced with fresh media. In the extraluminal space, media was aspirated and replaced with fresh media supplemented with GO analogues to achieve a desired concentration (accounting for total volume on both sides of the insert). Untreated cells (hereafter referred to as Control) were also prepared with clean media on both sides of the insert. Following 24 h incubation, media was aspirated from both sides of the inserts and replaced with fresh media supplemented with 3-(4,5-dimethylthiazol-2-yl)-2,5-diphenyltetrazolium bromide (MTT) to a final concentration of 0.5 mg mL^{-1}. Cells were incubated

for an additional 3 h to permit formation of the formazan precipitate. Afterwards, the supernatant was aspirated, and the formazan precipitate dissolved in dimethyl sulfoxide (350 μL insert^{-1}). Absorbance of the formazan solutions was quantified at 570 nm with reference at 630 nm. Relative cell viability was then calculation according to **Equation 5**.

$$\textit{(5)} \qquad \text{Relative Cell Viability (\%)} = \frac{\text{Mean OD}_{\text{Treatment}}}{\text{Mean OD}_{\text{Control}}} \times 100$$

3.3.16 Statistical Analyses. All statistical comparisons were calculated using GraphPad Prism 9 (GraphPad Software, San Diego, GA). Comparisons between the different GO analytes at a given timepoint were made using ordinary one-way analysis of variance (ANOVA) with Tukey's method for correction of multiple comparisons. Values of $p < 0.05$ were deemed significant.

3.4 Results and Discussion

3.4.1 Synthesis and Chemical Characterization. Derivatized GO with amine, thiol, and *S*-nitrosothiol (RSNO) functional handles (**Figure 3.1**) were synthesized building off previous reports of aminosilylated GO nanosheets[28,36] and other reports of RSNO-modified silica nanoparticles.[31,37,38] In developing the NO-releasing GO nanosheets, it was essential to characterize each reaction step for covalent binding of functional groups to the nanosheets in order to ensure that any NO-release was from the scaffold as opposed to unbound reagent. Therefore, FTIR and XPS were used to assess products.

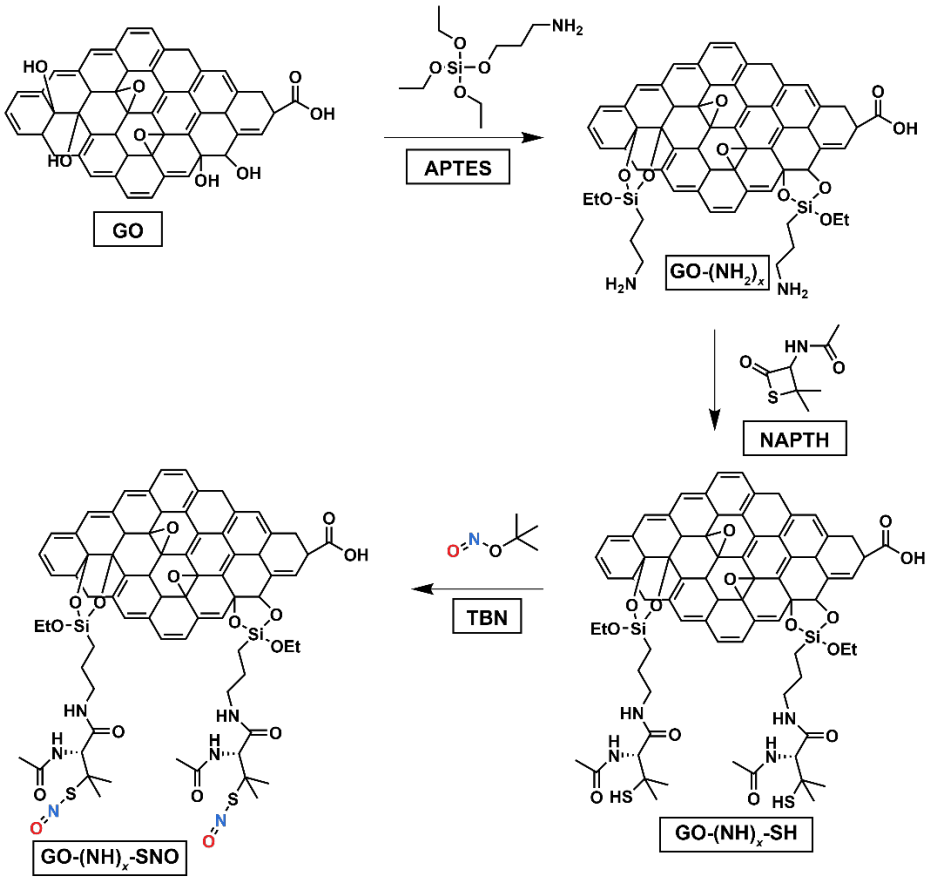

Figure 3.1 Overview of graphene oxide modification for NO release using aminosilane surface conjugation of GO nanosheets followed by aminolysis of a thiolactone derivative of penicillamine (NAPTH) to afford NO-releasing GO nanosheets (GO-$(NH)_x$-SNO) with *x* stoichiometric ratios of aminosilane.

3.4.1.1 FTIR Analysis. FTIR analysis supported the development of distinctive functional groups in each of the GO analogues (**Figure 3.2A**). Pristine GO shows a broad band at 3290 cm^{-1}, confirming the presence of -OH groups, similar to prior reports.[36] Aminosilylation of the nanosheets is supported by the appearance of methyl peaks at 2930 and 2800 cm^{-1}, amine peaks at 1575 cm^{-1}, and Si-O bonds at 1120 cm^{-1}. Subsequent aminolysis with NAPTH resulted in a shift at 1640 and 1530 cm^{-1}, consistent with secondary amide formation.[38] These findings support the successful conjugation of NAP to the nanosheet surface via the aminosilane linker. Following

nitrosation, further chemical shifts are observed in this region, with the emergence of a strong peak at 1570 cm^{-1}, correspond to N-O bond stretching.

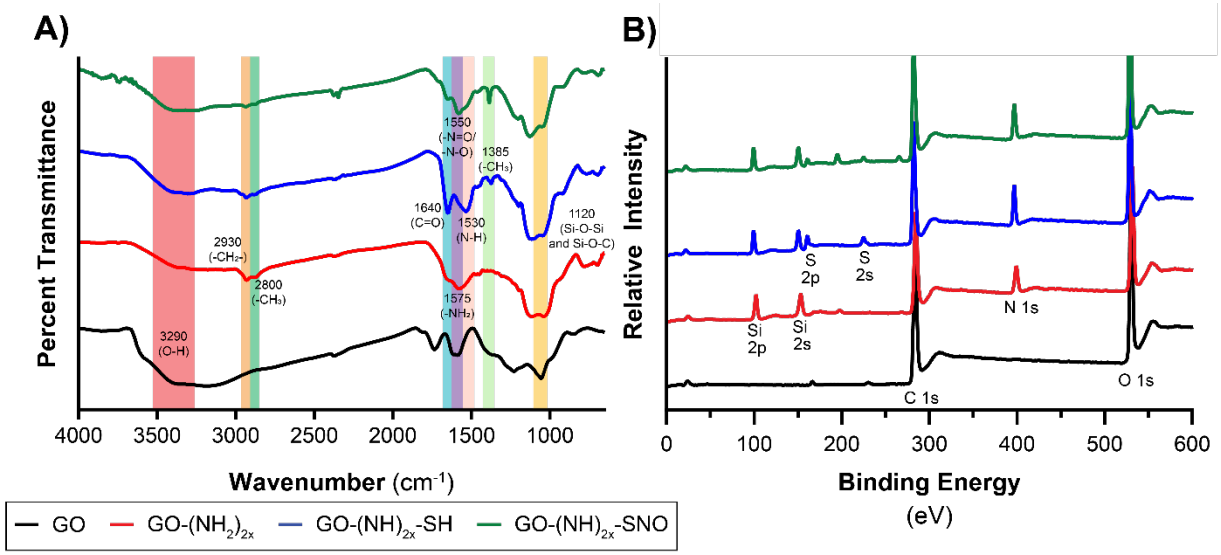

Figure 3.2 Fourier-transform infrared spectroscopy (FTIR) measurement (A) of GO nanosheets and derivatized aminated, thiolated, and nitrosated materials. Sequential reaction order demonstrates the emergence of key bond peaks. X-ray photoelectron spectroscopy (XPS) measurements demonstrating the emergence of regions characteristic of amination and thiolation of the derivatized GO nanosheets.

3.4.1.2 XPS Analysis. GO analogues were further characterized by XPS to obtain more detail about the surface chemistry. Survey spectra of the GO analogues (**Figure 3.2B**) first demonstrated the emergence of several distinct peaks during the fabrication process corresponding to the bonding of functional groups to the nanosheet surfaces. The emergence of Si 2p (102.00 eV) and 2s (153.00 eV) peaks in addition to an N 1s peak (399.00) with GO-$(NH_2)_{2x}$, corresponding to Si-O-C bond formation and amine content. This is supported by analysis of the peak deconvolutions (**Figure 3.3**), which show bound -NH_2 groups. Further analysis of the thiolated analogue showed emergence of strong S 2p (161.00 eV) and 2s (225.00) peaks, for which deconvolutions showed strong (3/2) and (1/2) bands associated with S-H environments (**Figure 3.4**). Deconvolution of the N 1s band further supported the addition of NAP with a loss in the

relative area% of C-NH_2 (398.38 eV) and increased relative area% of NH-C=O compared to the aminated precursor, supporting the formation of amide bonding (**Figure 3.4**). Finally, surveying of the nitrosated GO-$(NH)_2$-SNO product showed retention of peaks from prior steps. Deconvolution of the nitrosated compound showed loss of some sulfate (SO_4) impurities (**Figure 3.5**) present in the samples as an artifact of preparation of the GO nanosheets by Hummers Method with sulfuric acid.[39] In addition, deconvolution of the O 1s peak showed increased relative %area of the O-N band compared to the thiolated precursor, supporting the development of nitrosated product.

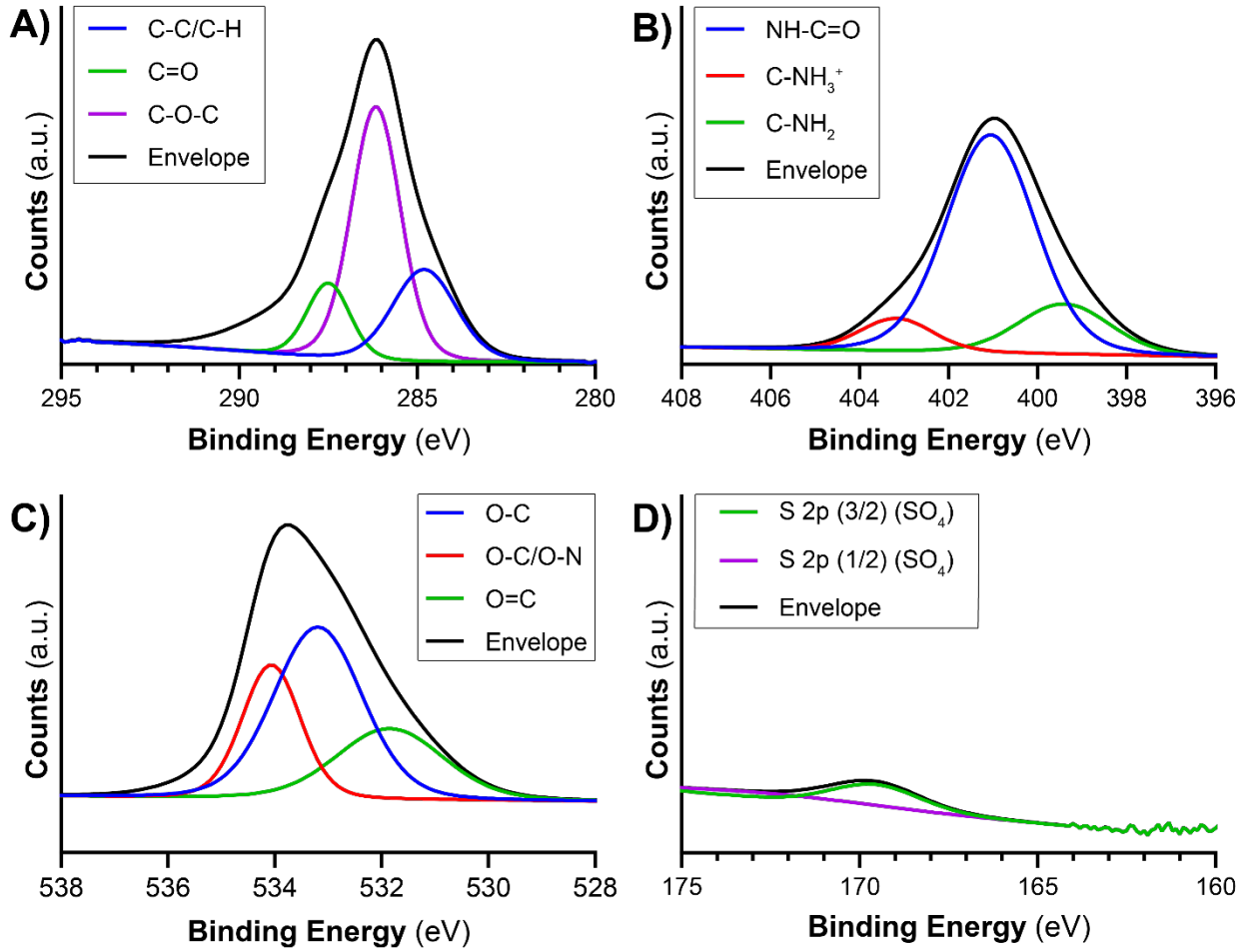

Figure 3.3 XPS peak deconvolutions of GO-$(NH_2)_{2x}$ for (A) C 1s, (B) N 1s, (C) O 1s, and (D) S 2p. Emergence of peak at 399.40 eV in N 1s is indicative of aminosilylation of nanosheet surface and free amine (C-NH_2) availability, as well as C-NH_3^+ (401.51 eV) and NH-C=O (400.04 eV) groups from possible direct acid-base interactions with the carboxylic and hydroxyl groups on GO.

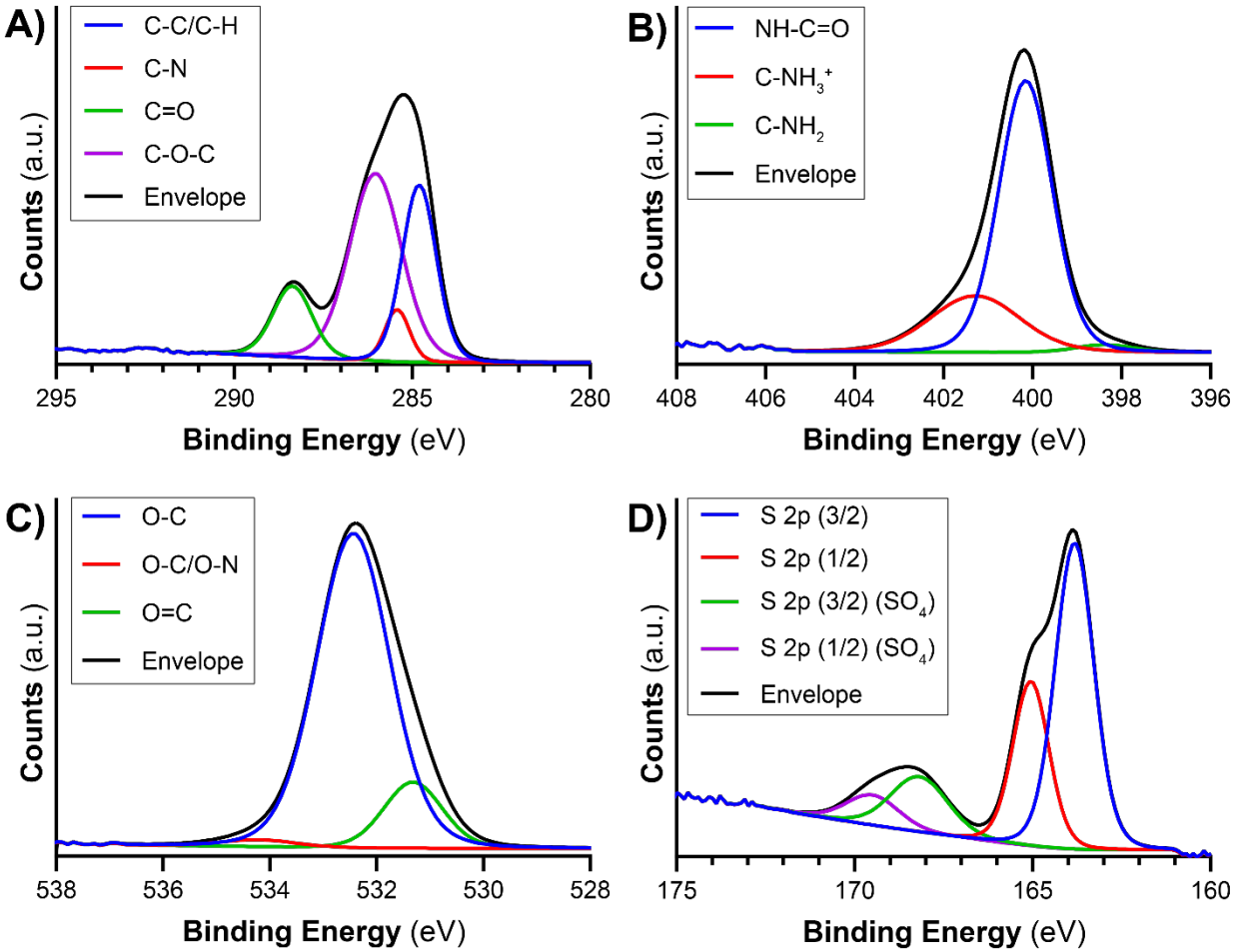

Figure 3.4 XPS peak deconvolutions for GO-$(NH)_{2x}$-SH for (A) C 1s, (B) N 1s, (C) O 1s, and (D) S 2p. Loss of primary amine peak (C-NH_2) intensity in the N 1s deconvolution (398.38 eV) from 18 relative area% to < 2 area% is achieved due to aminolysis reaction with NAPTH. Emergence of thiol-related peaks in S 2p deconvolution at 2p (3/2) (163.81 eV) and 2p (1/2) (165.04 eV) associated with S-H, S-C, and S-S environments supports that the derivitized GO-$(NH)_{2x}$-SH contains bound thiol groups after purification.

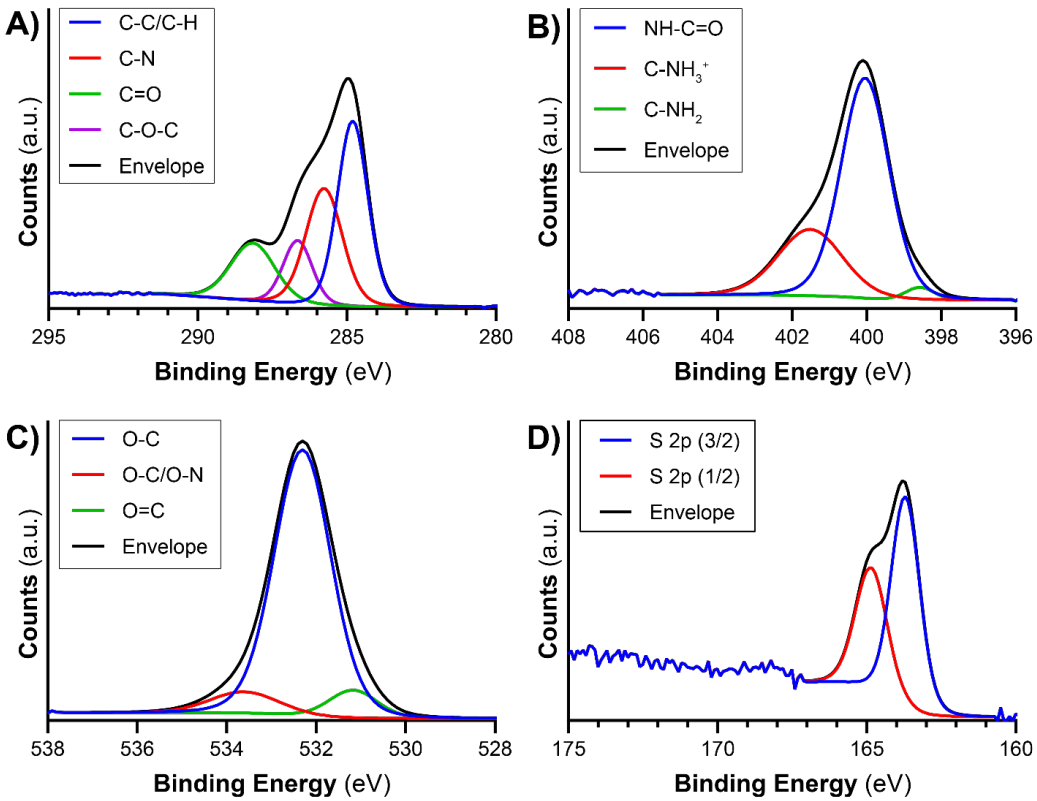

Figure 3.5 XPS peak deconvolutions for GO-$(NH)_{2x}$-SNO for (A) C 1s, (B) N 1s, (C) O 1s, and (D) S 2p. Increase in the O-C/O-N peak (533.61 eV) intensity in the O 1s deconvolution (from 1.91 relative area% for the thiolated precursor to 8.14 area% with the nitrosated product) provides evidence of bound *S*-nitrosothiol groups.

3.4.1.3 Quantification of Functional Handles To explore the tunability of modified GO substrates, the aminosilylation step (**Figure 3.1**) was performed with different ratios of moles of APTES/mg of GO nanosheets. Previously, GO nanosheets have been functionalized with APTES at a ratio of 0.01 mmol-APTES/mg-GO (denoted herein as 1x). To maximize possible NO release from the GO conjugates, several ratios of APTES were investigated, including [0.005, 0.01, 0.02, and 0.04] mmol-APTES/mg-GO, corresponding to 0.5x, 1x, 2x, and 4x analogues of the GO-(NH_2). As summarized in **Table 3.1**, increasing this ratio led to nearly proportionate increases in immobilized amine groups, with GO-$(NH_2)_{4x}$ yielding no statistically significant difference in amine groups over GO-$(NH_2)_{2x}$ (**Figure 3.6**), indicating saturation. Therefore, GO-$(NH_2)_{2x}$ was

chosen to be the maximum amine functionalized GO analogue for further investigation. NAPTH was attached to GO-$(NH_2)_x$ with conversion efficiencies similar to prior reports[27,31,38] and corresponding to the ratio of amines available for binding.

Table 3.1 Quantification of Chemical Functionalization of Derivatized Graphene Oxide

Formulation	Amine Groups (μmol/mg)	Sulfhydryl Groups (μmol/mg)	Thiolactone Conversion Efficiency (%)	*S*-Nitrosothiol Groups (μmol/mg)	Nitrosation Efficiency (%)
GO-$(NH)_{0.5x}$-SNO	0.200 ± 0.055	0.024 ± 0.006	12.2	0.024 ± 0.006	100
GO-$(NH)_{1x}$-SNO	0.392 ± 0.019	0.052 ± 0.011	13.4	0.048 ± 0.011	93.1
GO-$(NH)_{2x}$-SNO	0.977 ± 0.062	0.134 ± 0.023	13.8	0.098 ± 0.017	73.3

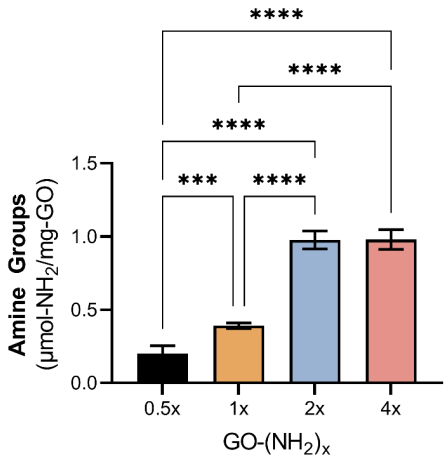

Figure 3.6 Average amine immobilization to GO nanosheets with varied ratio of aminosilane linker (APTES) with respect to the mass of GO nanosheets. Data are shown as mean ± SD (N = 5). Statistical significance is expressed as *** ($p < 0.001$) and **** ($p < 0.0001$).

Further nitrosation of the thiolated analogue showed proportional increases in the amount of RSNO groups on each surface, though interestingly the nitrosation efficiency was negatively correlated with increased thiol content (**Table 3.1**). We hypothesize this trend is a result of increased interactions between thiols, supporting oxidation and subsequent dimerization. Regardless, thiol conjugation showed significant improvement over several comparable silica-based materials, with comparable RSNO loading ability.[31,38]

3.4.2 NO Release Studies. NO release measurements were conducted with a chemiluminescent NO analyzer (NOA), the current gold standard for the field. The varying amounts of NO loaded onto GO-$(NH)_{0.5x}$-SNO, GO-$(NH)_{1x}$-SNO, and GO-$(NH)_{2x}$-SNO are evident in all NO release profiles. The average release profiles over the first hour in PBS w/ EDTA show burst releases typically seen upon NO-releasing materials' introduction into NOA sample chambers, followed by sustained release (**Figure 3.7A**). The rates of both the burst releases (**Figure 3.7B**) and sustained releases (**Figure 3.7C**) over this time period show greater NO release from the GO derivatives with greater NO loading. The statistically significant differences of NO release between GO-$(NH)_x$-SNO samples is further demonstrated when quantifying the total NO released from samples (including both the burst release and sustained release) (**Figure 3.7D**). The trend is continued for at least 24 h with all GO-$(NH)_x$-SNO samples continuing to release NO at statistically significant rates after incubation in PBS with EDTA at 25 °C (**Figure 3.7E**). It should be noted that although the amine contents approximately double between GO-$(NH)_x$ samples, this does not translate into an exact doubling of NO release rates. This may be due to the differing NAPTH conjugation and nitrosation efficiencies as well as the non-linear correlation between availability of NO donor molecules and NO release previously noted in the literature.[11]

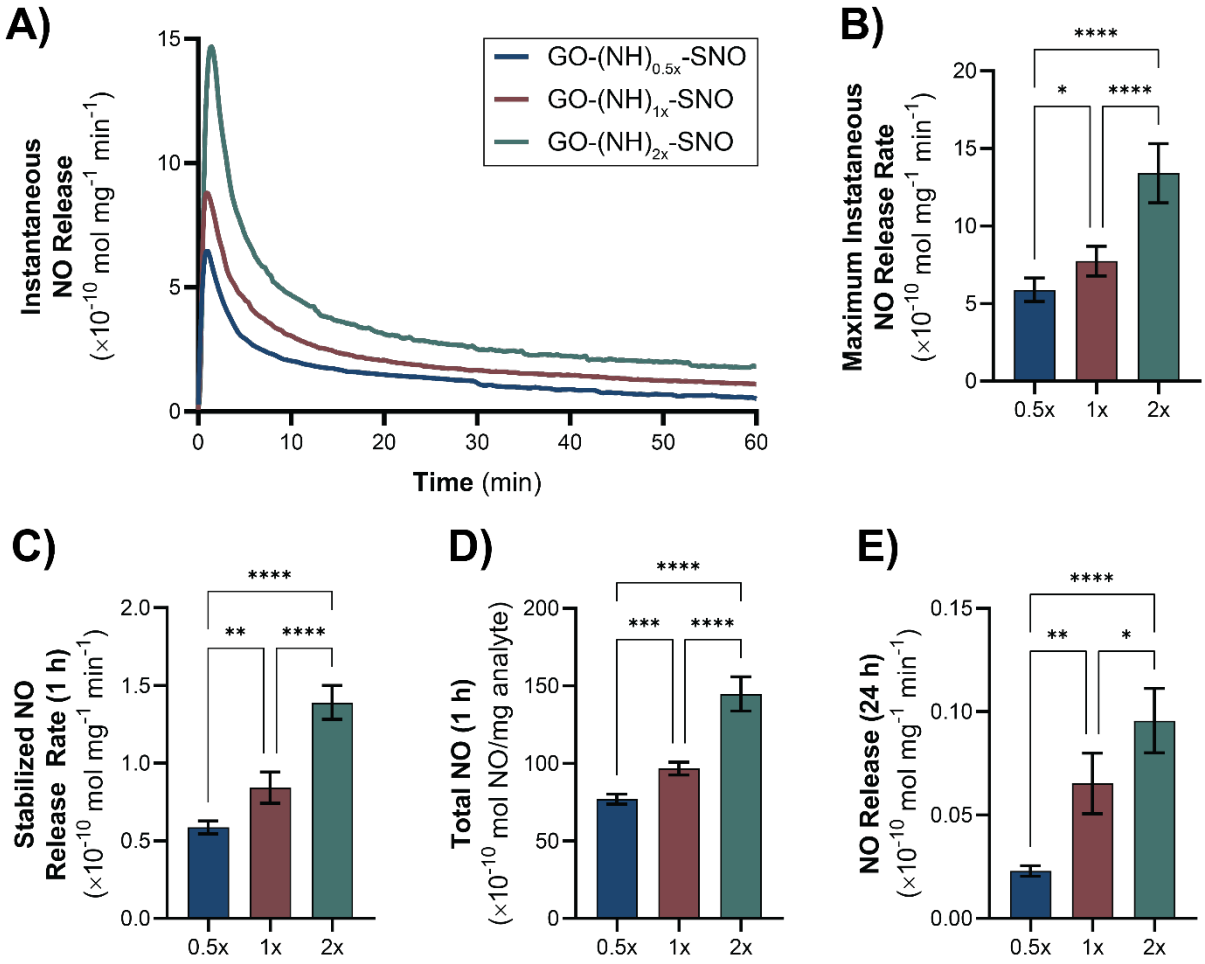

Figure 3.7 NO release studies of derivatized GO nanosheets with varied stoichiometric ratios in aminosilylation. (A) Representative instantaneous NO release profiles of GO-$(NH)_x$-SNO nanosheets during first hour of incubation under physiological conditions (1x PBS w/ EDTA, 37 °C). B) Average maximum instantaneous release rate during first hour of incubation. (C) Average stabilized NO release rates after 1 h incubation. (D) Average total NO released normalized to mass of derivatized nanosheets in first hour of incubation. ((E) Average release rates of derivatized nanosheets following 24 h incubation. Data shown as mean ± SD (N = 5). Statistical significance is expressed as * ($p < 0.05$), ** ($p < 0.01$), *** ($p < 0.001$), and **** ($p < 0.0001$).

3.4.2.1 Current-Induced NO Release In a proof-of-concept study, low levels of electrical current were applied to GO-$(NH)_{2x}$-SNO during NOA analysis (**Figure 3.8**). The differing amounts of applied current produce distinct changes in NO release profiles. Compared to the controls (0 mA), 4, 8, and 16 mA have consecutively higher burst releases of NO at the onset.

Conversely, the higher the applied current, the sooner the NO release rates resemble those of the controls. As the C/O ratio of GO derivatives largely affects their conductive properties,[40] and carboxylic acid groups are often used for GO modification and attachment, the exact NO release profiles of GO-$(NH)_x$-SNO in application settings is difficult to predict. However, these results support that the incorporation of GO-$(NH)_x$-SNO into various material systems can have highly tunable NO releasing properties.

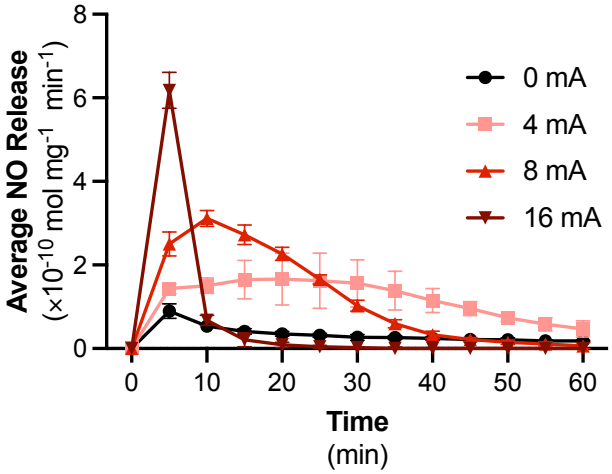

Figure 3.8 Current-induced NO release. NO release profiles of 1 mg/mL GO-$(NH)_{2x}$-SNO while electrical current is being applied (25 °C). Data are presented as the average release rate of the 30 sec before and after the 5-min intervals ± SD (N = 3).

3.4.3 Zeta Potential The zeta potential of GO derivatives and controls was evaluated at varying pHs. As the literature states, particle suspensions are considered stable above +30 mV or below -30 mV.[41] GO forms stable dispersions at all pHs tested, similar to previously published reports (**Figure 3.9**).[41,42] rGO, with less carboxylic acid groups than GO, expectedly has a higher zeta potential at lower pHs. GO-$(NH_2)_x$ at all ratios increased the observed surface charge. While stable at low pHs, the zeta potential of GO-$(NH_2)_x$ gradually decreased as the pH increased. Notably, more amine content decreased the range seen throughout the varying pH environments. Similar trends have been noted in the literature.[43] The addition of NAPTH to GO-$(NH_2)_x$, specifically to

the amines, lessens their ability to carry a positive charge in acidic conditions. Thus, a steeper decline in zeta potential is seen with increasing pHs compared to the trend seen with GO-$(NH_2)_x$. All ratios of GO-$(NH)_x$-SNO, however, exhibited zeta potentials above 30 mV for all pH conditions, indicating stability within the suspension. Moreover, a positive surface charge is desirable for potential antibacterial effects.

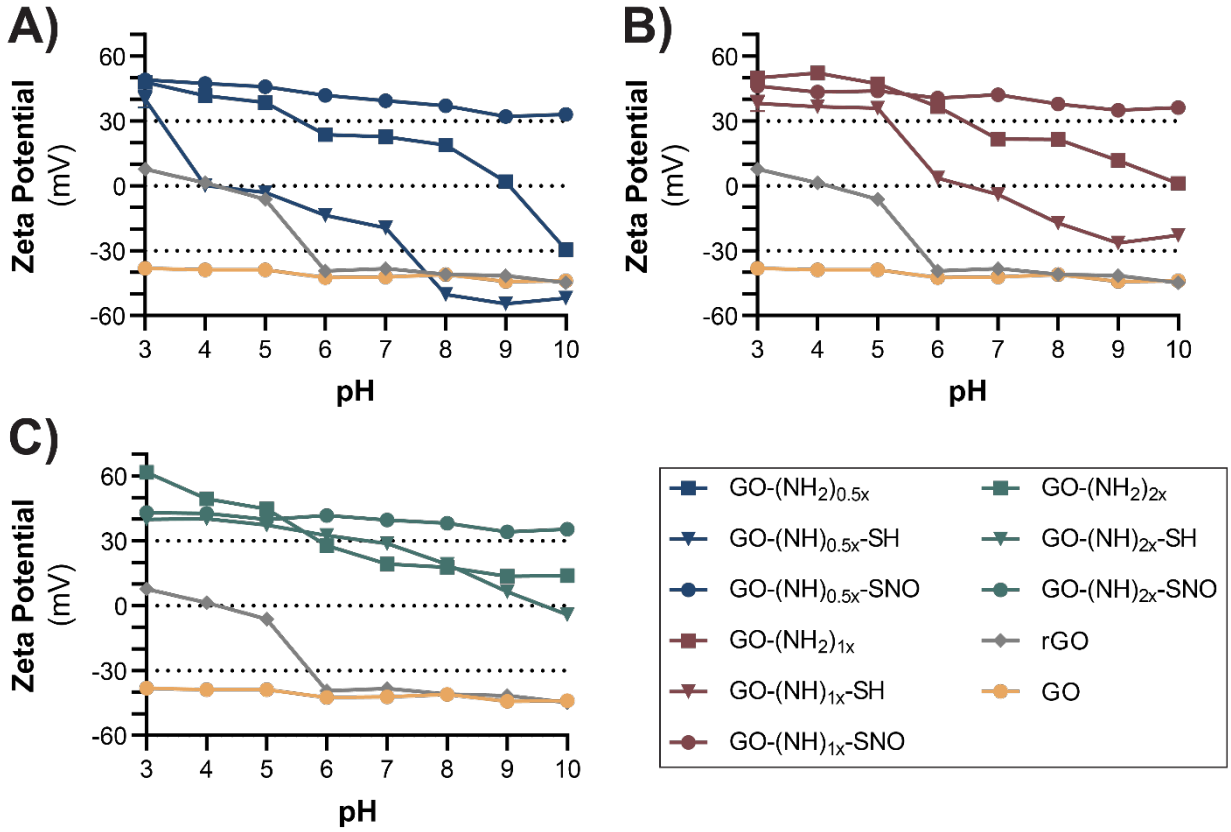

Figure 3.9 Zeta potential measurements of (A) graphene oxide controls and GO-$(NH_2)_{2x}$ derivatives, (B) GO-$(NH_2)_{1x}$ derivatives, and (C) GO-$(NH_2)_{0.5x}$ derivatives. Data are presented as the mean zeta potential (mV) ± SD.

3.4.4 Cytocompatibility Assessment Cytotoxicity evaluation of the NO-releasing GO-$(NH)_{2x}$-SNO analogue against pristine GO demonstrated comparable retention of viability at lower concentrations of analyte (≤ 500 µg/mL, **Figure 3.10A**). At the lowest tested concentrations, the GO-$(NH)_{2x}$-SNO exhibited a mild proliferative effect, likely owed to slow decomposition of the

NO donor groups leading to NO and related metabolite accumulation. This trend was consistent with previous observations of enhanced viability of fibroblast cells after treatment with NO donor compounds.[31,44] At higher concentrations, the GO-$(NH)_{2x}$-SNO analogue demonstrated greater viability compared to the GO control ($p < 0.05$, **Figure 3.10A**), being able to tradeoff some of the potentially cytotoxic components of GO (e.g., synthetic impurities such as inorganic acids, generation of ROSs, etc.) in indirect contact testing.[45] At all test concentrations, both GO-$(NH)_{2x}$-SNO and GO were able to maintain suspension after 24 h, agreeing with our prior zeta potential studies showing stability of both across pH environments. While the aminated and thiolated analogues show some flocculation and colloidal instability, both GO-$(NH)_{2x}$-SNO and GO retain general positive and negative charge across pH microenvironments, respectively (**Figure 3.9A**). Based on these findings, further antibacterial testing was proceeded with GO-$(NH)_{2x}$-SNO and GO through filter deposition and adhesion testing as well as biofilm dispersal testing.

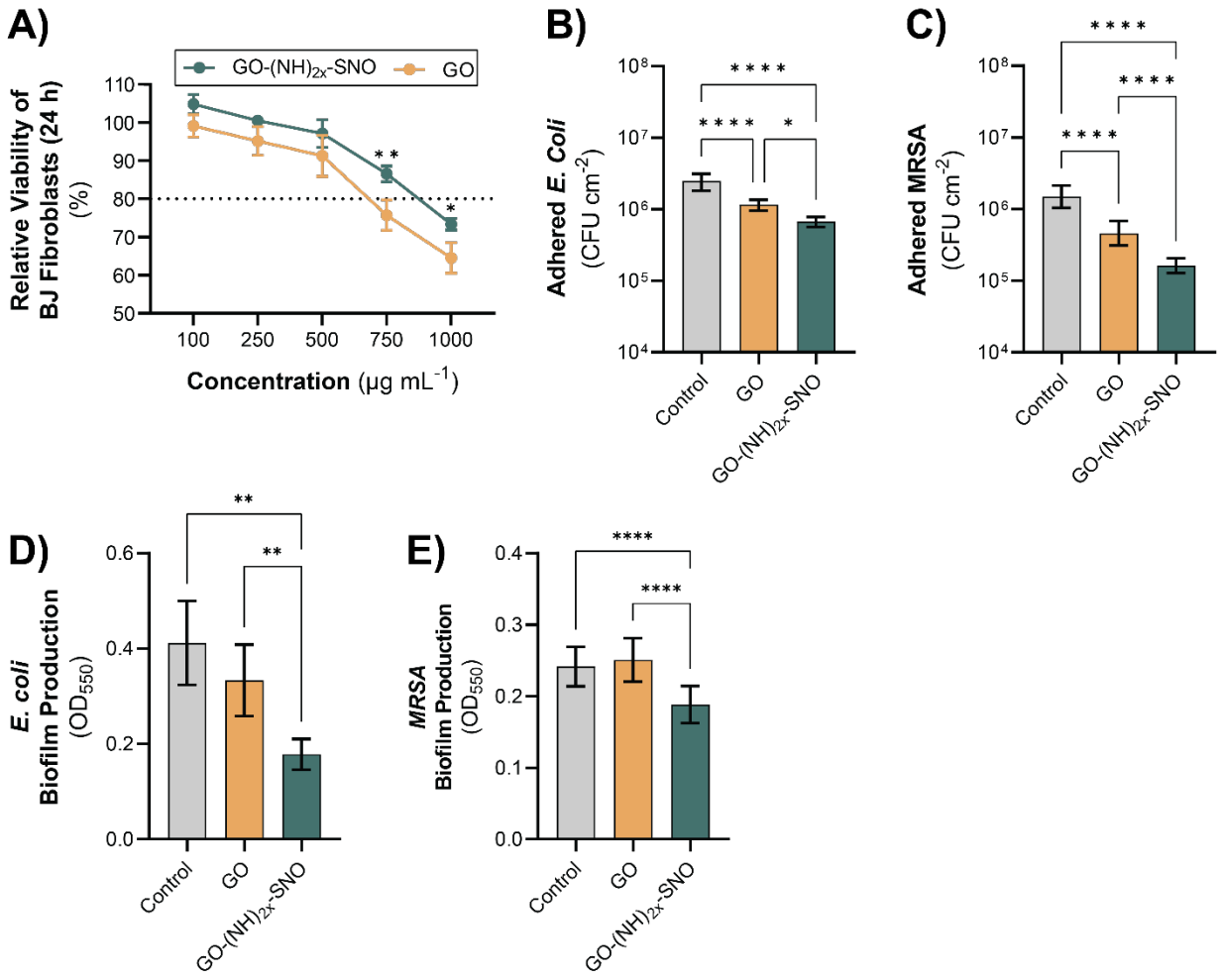

Figure 3.10 Biological studies comparing GO and GO-$(NH)_{2x}$-SNO nanosheets. (A) Indirect contact cytotoxicity screening of GO-$(NH)_{2x}$-SNO and GO against human fibroblast cells showed increased viability of cells at higher concentrations of GO-$(NH)_{2x}$-SNO compared to GO. Data shown as the mean percent viability normalized against untreated cells ± SD (N = 3). Antibacterial assessment through 4-h adhesion tests to GO-$(NH)_{2x}$-SNO and GO-treated membranes against (B) *E. coli* and (C) MRSA showed reduced viable adhered bacteria. Final data are reported as the mean viable CFU cm^{-2} ± SD. Further biofilm quantification via crystal violet staining after 24-h treatment with 0.5 mg/mL GO-$(NH)_{2x}$-SNO and GO against (D) *E. coli* and (E) MRSA showed reduced biofilm mass. Final data shown as mean absorbances (OD_{550}) ± SD. Statistical significance is expressed as * ($p < 0.05$), ** ($p < 0.01$), *** ($p < 0.001$), and **** ($p < 0.0001$).

3.4.5 Antibacterial Assessments The biological effects of GO-$(NH)_{2x}$-SNO were investigated. As this ratio of functionalization is maximal, so are the potential benefits and harms. To evaluate antibacterial effects of GO-$(NH)_{2x}$-SNO and GO, both adhesion and biofilm experiments were conducted. Following a previously published protocol,[33] GO and GO-$(NH)_{2x}$-

SNO dispersion were vacuumed filtered onto cellulose, which served as samples for bacterial adhesion assessment. Unmodified cellulose was used as a control. Upon 4 h exposure to 0.1 OD MRSA, GO showed a 0.51 ± 0.17 log reduction in adhered viable CFU compared to the control (**Figure 3.10B**). GO-$(NH)_{2x}$-SNO, however, significantly outperformed ($P < 0.0001$) GO with its 0.96 ± 0.10 log reduction. A similar trend is seen with *E. coli* adhesion (**Figure 3.10C**). Compared to the control, GO and GO-$(NH)_{2x}$-SNO reduced viable adhesion by 0.32 ± 0.07 and 0.56 ± 0.07 log, respectively. These lesser reductions may be due to the protection that the characteristic outer membrane provides Gram negative bacteria, but they are statistically significant compared to the control ($P < 0.0001$) and each other ($P < 0.05$).

While the mechanism is not completely known, GO has been noted to have anti-biofilm effects, likely due to the variety of bonds that it can form with polymers, proteins, and nucleic acids (hydrogen bonds, π-π interactions, etc.).[9] Biofilm dispersing properties were evaluated by treating 24 h biofilms with 0.5 mg/mL GO or GO-$(NH)_{2x}$-SNO for an additional 24 h. The remaining biofilms were then stained with crystal violet, dissolved in acetic acid, and quantified via plate reader. While GO's antibiofilm properties have been noted at high concentrations (e.g., 4 mg/mL[9]), it did not significantly change MRSA (**Figure 3.1.D**) or *E. coli* biofilms (**Figure 3.10E**) at 0.5 mg/mL. GO-$(NH)_{2x}$-SNO, however, did decrease biofilm mass compared to both the controls and GO. MRSA biofilms were reduced by 19.5 ± 11.0 % and *E. coli* biofilms by 48.4 ± 9.36 %.

3.5 Conclusion

The field of materials science continues to strive towards improved multifunctionality and tunability. In this work, the first combination of an RSNO and GO is reported. This novel material

is characterized via FTIR, XPS, NOA, quantitative analyses, and zeta potential measurements. It is demonstrated that the NO release profiles of GO-$(NH)_x$-SNO can be tuned by both degrees of functionalization and through the use of low-leveled electrical currents. The biological effects of GO-$(NH)_{2x}$-SNO are explored via bacterial and biocompatibility assays. GO-$(NH)_{2x}$-SNO was shown to reduce viable bacterial adhesion (0.96-log with MRSA and 0.56-log with *E. coli* compared to controls), significantly outperforming unmodified GO (0.51-log with MRSA and 0.32-log with *E. coli* compared to controls). GO-$(NH)_{2x}$-SNO was also demonstrated to have biofilm dispersing properties at low concentrations where unmodified GO does not (19.5% and 48.4% reductions for MRSA and *E. coli*, respectively, compared to controls). Moreover, GO-$(NH)_{2x}$-SNO was shown to have superior cytocompatibility compared to GO. In conclusion, GO-$(NH)_x$-SNO is a highly tunable, antibacterial, and biocompatible material that has great potential for biomedical applications.

3.6 References

1. Ferreira ADBL, Nóvoa PRO, Marques AT. Multifunctional Material Systems: A state-of-the-art review. *Composite Structures.* 2016;151:3-35.

2. Geim AK, Novoselov KS. The rise of graphene. *Nat Mater.* 2007;6(3):183-191.
3. Dideikin AT, Vul' AY. Graphene Oxide and Derivatives: The Place in Graphene Family. *Frontiers in Physics.* 2019;6.

4. Innocenzi P, Stagi L. Carbon-based antiviral nanomaterials: graphene, C-dots, and fullerenes. A perspective. *Chemical Science.* 2020;11(26):6606-6622.

5. Ye S, Shao K, Li Z, et al. Antiviral Activity of Graphene Oxide: How Sharp Edged Structure and Charge Matter. *ACS Applied Materials & Interfaces.* 2015;7(38):21571-21579.

6. Tadyszak K, Wychowaniec JK, Litowczenko J. Biomedical Applications of Graphene-Based Structures. *Nanomaterials (Basel).* 2018;8(11).

7. Arkowski J, Obremska M, Kędzierski K, Sławuta A, Wawrzyńska M. Applications for graphene and its derivatives in medical devices: Current knowledge and future applications. *Adv Clin Exp Med.* 2020;29(12):1497-1504.

8. Wu X, Tan S, Xing Y, Pu Q, Wu M, Zhao JX. Graphene oxide as an efficient antimicrobial nanomaterial for eradicating multi-drug resistant bacteria in vitro and in vivo. *Colloids Surf B Biointerfaces.* 2017;157:1-9.

9. Di Giulio M, Zappacosta R, Di Lodovico S, et al. Antimicrobial and Antibiofilm Efficacy of Graphene Oxide against Chronic Wound Microorganisms. *Antimicrobial agents and chemotherapy.* 2018;62(7):e00547-00518.

10. Jones ML, Ganopolsky JG, Labbé A, Wahl C, Prakash S. Antimicrobial properties of nitric oxide and its application in antimicrobial formulations and medical devices. *Applied Microbiology and Biotechnology.* 2010;88(2):401-407.

11. Ashcraft M, Douglass M, Garren M, et al. Nitric Oxide-Releasing Lock Solution for the Prevention of Catheter-Related Infection and Thrombosis. *ACS Applied Bio Materials.* 2022.

12. Garren MR, Ashcraft M, Qian Y, Douglass M, Brisbois EJ, Handa H. Nitric oxide and viral infection: Recent developments in antiviral therapies and platforms. *Appl Mater Today.* 2021;22:100887-100887.

13. Tuteja N, Chandra M, Tuteja R, Misra MK. Nitric Oxide as a Unique Bioactive Signaling Messenger in Physiology and Pathophysiology. *J Biomed Biotechnol.* 2004;2004(4):227-237.

14. Morbidelli L, Donnini S, Ziche M. Chapter 4 - Therapeutic Implications of the Nitric Oxide Pathway in the Angiogenesis of Tumors and Inflammatory-Related Disorders. In: Morbidelli L, Bonavida B, eds. *Therapeutic Application of Nitric Oxide in Cancer and Inflammatory Disorders.* Academic Press; 2019:65-91.

15. Thomas DD, Liu X, Kantrow SP, Lancaster JR, Jr. The biological lifetime of nitric oxide: implications for the perivascular dynamics of NO and O2. *Proceedings of the National Academy of Sciences of the United States of America.* 2001;98(1):355-360.

16. Liang H, Nacharaju P, Friedman A, Friedman JM. Nitric oxide generating/releasing materials. *Future Sci OA.* 2015;1(1).

17. Hopkins SP, Pant J, Goudie MJ, Schmiedt C, Handa H. Achieving Long-Term Biocompatible Silicone via Covalently Immobilized S-Nitroso- N-acetylpenicillamine (SNAP) That Exhibits 4 Months of Sustained Nitric Oxide Release. *ACS Appl Mater Interfaces.* 2018;10(32):27316-27325.

18. Ashcraft M, Douglass M, Chen Y, Handa H. Combination strategies for antithrombotic biomaterials: an emerging trend towards hemocompatibility. *Biomaterials Science.* 2021;9(7):2413-2423.

19. Yu H, Cui L-X, Huang N, Yang Z-L. Recent developments in nitric oxide-releasing biomaterials for biomedical applications. *Med Gas Res.* 2019;9(4):184-191.

20. Douglass M, Hopkins S, Chug MK, et al. Reduction in Foreign Body Response and Improved Antimicrobial Efficacy via Silicone-Oil-Infused Nitric-Oxide-Releasing Medical-Grade Cannulas. *ACS Applied Materials & Interfaces.* 2021;13(44):52425-52434.

21. Roberts TR, Garren MRS, Wilson SN, Handa H, Batchinsky AI. Development and In Vitro Whole Blood Hemocompatibility Screening of Endothelium-Mimetic Multifunctional Coatings. *ACS Applied Bio Materials.* 2022;5(5):2212-2223.

22. Douglass M, Ghalei S, Brisbois E, Handa H. Potent, Broad-Spectrum Antimicrobial Effects of S-Nitroso-N-acetylpenicillamine-Impregnated Nitric Oxide-Releasing Latex Urinary Catheters. *ACS Applied Bio Materials.* 2022;5(2):700-710.

23. Kim C, Diring S, Furukawa S, Kitagawa S. Light-induced nitric oxide release from physiologically stable porous coordination polymers. *Dalton Transactions.* 2015;44(34):15324-15333.

24. Douglass ME, Goudie MJ, Pant J, et al. Catalyzed Nitric Oxide Release via Cu Nanoparticles Leads to an Increase in Antimicrobial Effects and Hemocompatibility for Short-Term Extracorporeal Circulation. *ACS Applied Bio Materials.* 2019;2(6):2539-2548.

25. Tanum J, Jeong H, Heo J, Choi M, Park K, Hong J. Assembly of graphene oxide multilayer film for stable and sustained release of nitric oxide gas. *Applied Surface Science.* 2019;486:452-459.

26. Moynihan HA, Roberts SM. Preparation of Some Novel S-Nitroso Compounds as Potential Slow-Release - Agents of Nitric-Oxide in-Vivo. *J Chem Soc Perk T 1.* 1994(7):797-805.

27. Frost MC, Meyerhoff ME. Synthesis, characterization, and controlled nitric oxide release from S-nitrosothiol-derivatized fumed silica polymer filler particles. *Journal of Biomedical Materials Research Part A.* 2005;72A(4):409-419.

28. Huang J, Ding SM, Xiao WM, Peng YD, Deng SJ, Zhang N. 3-Aminopropyl-triethoxysilane Functionalized Graphene Oxide: A Highly Efficient and Recyclable Catalyst for Knoevenagel Condensation. *Catalysis Letters.* 2015;145(4):1000-1007.

29. Ferris C, Casas M, Lucero MJ, de Paz MV, Jiménez-Castellanos MR. Synthesis and characterization of a novel chitosan-N-acetyl-homocysteine thiolactone polymer using MES buffer. *Carbohydrate Polymers.* 2014;111:125-132.

30. Espeel P, Du Prez FE. One-pot multi-step reactions based on thiolactone chemistry: A powerful synthetic tool in polymer science. *European Polymer Journal.* 2015;62:247-272.

31. Ghalei S, Hopkins S, Douglass M, Garren M, Mondal A, Handa H. Nitric oxide releasing halloysite nanotubes for biomedical applications. *J Colloid Interface Sci.* 2021;590:277-289.

32. Goudie MJ, Pant J, Handa H. Liquid-infused nitric oxide-releasing (LINORel) silicone for decreased fouling, thrombosis, and infection of medical devices. *Sci Rep.* 2017;7(1):13623.

33. Perreault F, de Faria AF, Nejati S, Elimelech M. Antimicrobial Properties of Graphene Oxide Nanosheets: Why Size Matters. *ACS Nano.* 2015;9(7):7226-7236.

34. Standards ISO. ISO 10993-5: 2009 (E). Biological evaluation of medical devices—Part 5: Tests for cytotoxicity in vitro. In: International Organizational for Standardization Geneve; 2009.

35. Garren M, Maffe P, Melvin A, et al. Surface-Catalyzed Nitric Oxide Release via a Metal Organic Framework Enhances Antibacterial Surface Effects. *ACS Appl Mater Interfaces.* 2021;13(48):56931-56943.

36. Zhi X, Mao Y, Yu Z, et al. γ-Aminopropyl triethoxysilane functionalized graphene oxide for composites with high dielectric constant and low dielectric loss. *Composites Part A: Applied Science and Manufacturing.* 2015;76:194-202.

37. Frost MC, Meyerhoff ME. Controlled photoinitiated release of nitric oxide from polymer films containing S-nitroso-N-acetyl-DL-penicillamine derivatized fumed silica filler. *J Am Chem Soc.* 2004;126(5):1348-1349.

38. Grommersch BM, Pant J, Hopkins SP, Goudie MJ, Handa H. Biotemplated Synthesis and Characterization of Mesoporous Nitric Oxide-Releasing Diatomaceous Earth Silica Particles. *ACS Appl Mater Interfaces.* 2018;10(3):2291-2301.

39. Hummers WS, Offeman RE. Preparation of Graphitic Oxide. *Journal of the American Chemical Society.* 1958;80(6):1339-1339.

40. Compton OC, Jain B, Dikin DA, Abouimrane A, Amine K, Nguyen ST. Chemically Active Reduced Graphene Oxide with Tunable C/O Ratios. *ACS Nano.* 2011;5(6):4380-4391.

41. Konkena B, Vasudevan S. Understanding Aqueous Dispersibility of Graphene Oxide and Reduced Graphene Oxide through pKa Measurements. *The Journal of Physical Chemistry Letters.* 2012;3(7):867-872.

42. Gallegos-Pérez WR, Reynosa-Martínez AC, Soto-Ortiz C, et al. Effect of UV radiation on the structure of graphene oxide in water and its impact on cytotoxicity and As(III) adsorption. *Chemosphere.* 2020;249:126160.

43. Sahoo JK, Paikra SK, Baliarsingh A, et al. Surface functionalization of graphene oxide using amino silane magnetic nanocomposite for Chromium (VI) removal and bacterial treatment. *Nano Express.* 2020;1(1):010062.

44. Villalobo A. Nitric oxide and cell proliferation. *FEBS J.* 2006;273(11):2329-2344.

45. Rhazouani A, Gamrani H, El Achaby M, et al. Synthesis and Toxicity of Graphene Oxide Nanoparticles: A Literature Review of In Vitro and In Vivo Studies. *Biomed Res Int.* 2021;2021:5518999.

CHAPTER 4

Dual-Action Pegylated Nitric Oxide-releasing Materials for Antimicrobial and Nonthrombotic Dynamic Blood-Contacting Applications[3]

[2]This chapter is prepared for submission as: Ashcraft, M.*, Garren, M.*, Lautner-Csorba, O., Pinon, V., Wu, Y., Crowley, D., Bartlett, R., Brisbois, E., Handa, H. Dual-Action Pegylated NO-releasing Materials for Antimicrobial and Nonthrombotic Dynamic Blood-Contacting Applications. To be submitted to Biomaterials. (* Indicates that these authors contributed equally).

4.1 Abstract

Extracorporeal life support technologies often fail due to infection, platelet activation, and thrombus formation. Nitric oxide (NO) maintains many homeostasis functions in the native endothelium, including platelet quiescence and eradication of bacteria. Despite recent developments in NO-releasing polymer technology, there remain unmet challenges due to eventual surface fouling. In this study, a novel two-step fabrication is developed to modify silicone rubber with NO evolution at the polymer-solution interface and for surface passivation via incorporation of a synthetic NO donor and surface silanization with polyethylene glycol (NO+PEG). These simple, robust, and scalable surfaces preserve NO release kinetics while facilitating enhanced surface wettability and over 70% reduction in plasma protein adsorption compared to unmodified materials. These NO+PEG surfaces were shown to be cytocompatible, while incurring > 1.50-log reduction in adhered *Staphylococcus epidermidis* and *Escherichia coli* strains in 24-h studies. Further screening of the NO+PEG materials with porcine whole blood demonstrated a > 96% reduction in adhered platelets, with negligible hemolytic potential found. Developing the NO+PEG coatings for 4-h *in vivo* thrombogenicity models with New Zealand white hares, a greater than 79% decrease in thrombus mass formation was recorded, with greater than 95% platelet preservation during each hour of the studies. Further hematological assessment showed no significant differences in activated clotting times and activated partial thromboplastin times in the NO+PEG (1:1) group, suggesting maintenance of blood flow without significant intrinsic pathway activation. Overall, these findings show many complimentary biological properties associated with the NO+PEG surface strategy, supporting its translation to other medical device technologies.

4.2 Introduction

Extracorporeal life support (ECLS) technologies are a critical component in the treatment of organ and/or system failure. Since its debut in 1953, great strides have been made in increasing the safety and therapeutic efficacy of ECLS technologies with significant emphasis being placed on the development of materials to deter complications, such as thrombosis.[1] Even with modern improvements and practices, however, thrombotic complications are estimated to occur in 8-31% of patients undergoing ECLS therapies.[2,3]

Upon contact, plasma proteins rapidly adsorb to foreign materials, such as ECLS components. Plasma proteins initiate and largely facilitate the subsequent contact activation pathway of coagulation (also known as the intrinsic pathway) and the interconnected complement activation response of the immune system.[4] These are universal concerns for blood-contacting medical devices (BCMD); however, these undesirable responses are particularly prevalent in extracorporeal circuits (ECCs) given their substantial surface areas and dynamic flow conditions. In addition to the direct complications, the consumption of blood and immune cells in these processes can also lead to hypocoagulability post-treatment.[1]

Due to the lack of materials that do not activate the innate thrombo-inflammatory responses, the use of systemic anticoagulants is necessary to prevent clotting and subsequent BCMD failure. While instrumental to the use of ECLS, anticoagulants come with their inherent risks and complications. For example, heparin, the most commonly used anticoagulant for extracorporeal membrane oxygenation (ECMO) and hemodialysis, has been associated with heparin-induced thrombocytopenia and bone disease in addition to the risk of major bleeding that all anticoagulants have.[5] When necessary, anticoagulation can be reversed, but this comes with additional thrombotic risks.[6]

Another common complication of ECLS usage is infection. Bloodstream infections in adults undergoing ECMO have an estimated prevalence of 3 – 18%,[7] and there is a higher risk of infection with longer usage.[8] In addition to their contributions to morbidity and mortality, bloodstream infections are considered among the most expensive nosocomial complications.[9] Furthermore, thrombosis and infection are often connected as thrombi provide a surface that bacteria can easily attach to and certain bacteria can contribute to thrombi formation (e.g., coagulase-positive *Staphylococcus*).[10,11]

To attempt to eliminate the need for systemic anticoagulation and generally reduce biofouling, various hemocompatible design strategies have been investigated. Coating circuits with anticoagulants, such as heparin, provides anticoagulant effects with reduced risks compared to systemic administration of the same agents. However, the literature notes that heparin-coated devices only have short-term benefits and require the use of supplemental anticoagulation therapies.[12] Other investigations have focused on the incorporation of lubricants to prevent blood components from attaching to the surfaces.[13,14] Still more strategies attempt to mimic the endothelium's physiology, as it is the only truly hemocompatible material researchers have to model. These strategies include modifying surface chemistry (e.g., incorporating zwitterions,[15] changing wettability,[16,17] etc.) and the release of antithrombotic agents (e.g., heparin,[18] nitric oxide (NO),[19] etc.). Many of these material designs have been shown to increase hemocompatibility alone, but there is significant evidence that combining multiple strategies (as the endothelium does) can lead to complementary and/or synergistic effects.[20]

NO is an endogenous, gaseous molecule that plays a role in many biological systems. Within the immune system, NO is used as a potent antimicrobial and antiviral agent.[21] It is also produced by endothelial cells and used to help regulate vasodilation and mitigate thrombosis on

the surface of the endothelium through temporary inhibition of platelet activation.[22] As a free radical, NO has a short biological half-life (~2 s).[23] To achieve prolonged effects, NO donor molecules are often utilized in a variety of forms [24]. They have been incorporated into solutions,[25] creams,[26] gels,[27,28] polymers,[24,29] fibers,[30] and coatings for various materials.[31] *S*-nitroso-*N*-acetyl-DL-penicillamine (SNAP) is one such established NO donor molecule. In addition to its relative stability compared to many other donor molecules,[32] SNAP has the advantageous ability to be integrated into prefabricated, medical-grade polymers via solvent impregnation methods.[33] For example, SNAP swelled into various silicone rubbers (SRs) has been demonstrated to release NO at physiologically relevant levels while maintaining biocompatibility.[13,33,34]

Although NO release has been shown to reduce thrombosis via platelet inhibition,[35] it does not prevent plasma proteins from adhering to surfaces. However, previous work has shown that the combination of NO release and increased hydrophilicity has complementary anti-biofouling properties.[36] In this work, we screen and demonstrate the advantage of this combination strategy using SNAP-swelled SR with a poly(ethylene glycol) (PEG) coating. PEG is a highly hydrophilic molecule that is frequently used to increase the biocompatibility of nanoparticles among other materials.[37] This polymer has been shown to prevent interactions between plasma proteins and hydrophobic surfaces as its hydrophilicity interferes with the nonpolar bonds that would otherwise form between the two. In this sense, PEG coatings act as a hydration layer on surfaces, preventing much of the electrostatic interactions between plasma proteins and material interfaces.[38]

In this study, the novel combination of NO release and a PEG coating is thoroughly characterized and explored for ECLS applications. The NO+PEG coating is fabricated in a multi-step process involving solvent swelling of the NO donor, SNAP, O_2 plasma treatment (to activate surfaces), and covalent attachment of silanated PEG chains. The material's multifunctionality is

demonstrated via characterization methods including attenuated total reflectance-Fourier transform infrared (ATR-FTIR) spectroscopy, surface contact angle, and NO release studies, confirming each step of the fabrication. Protein adhesion studies demonstrate enhanced resistance to hydrophobic plasma protein adhesion. *In vitro* biological studies exhibit NO-PEG SR's excellent resistance to bacteria and platelet adhesion while maintaining cytocompatibility. Finally, the efficacy of the NO+PEG formulation is assessed via the construction of ECCs with this design and their evaluation in a 4-h rabbit thrombogenicity model, demonstrating reduced thrombus mass, enhanced platelet preservation, and key relationships in coagulation pathway activation. Overall, NO+PEG is shown to have excellent anti-biofouling properties with great clinical potential for improving therapeutic outcomes for ECLS patients.

4.3 Materials and Methods

4.3.1 Materials. Drabkin's reagent and Saint-Gobain Tygon™ Formula 3350 silicone tubing were purchased from VWR (Atlanta, GA). *S*-nitroso-*N*-acetyl-DL-penicillamine (SNAP) was purchased from PharmaBlock USA, Inc. (Hatfield, PA). 3-[methoxy(polyethyleneoxy)6-9]propyltrimethoxysilane (PEG-silane) was purchased from Gelest, Inc. (Morrisville, PA). Acetone, ethanol, ethylenediaminetetraacetic acid (EDTA), methanol, tetrahydrofuran (THF), and Triton-X-100 were acquired from Sigma-Aldrich (St. Louis, MO). Phosphate-buffered saline (PBS) without calcium or magnesium was purchased from Corning (Manassas, VA). All other chemical supplies were reagent-grade and used without further purification. The *Staphylococcus epidermidis* (ATCC 35984) and *Escherichia coli* (ATCC 25922) strains were grown from stocks originally acquired from American Type Culture Collection (Manassas, VA). Luria-Bertani (LB) and Mueller-Hinton (MH) broth and agar were purchased from Sigma-Aldrich (St. Louis, MO).

All other bacteria-related supplies were purchased from VWR (Atlanta, GA). BJ fibroblast (ATCC CRL-2522) cells were subcultured from cryopreserved stocks that were originally purchased from American Type Culture Collection (Manassas, VA). Human vascular endothelial cells (HUVEC) were acquired from Thermo Fisher Scientific (Waltham, MA). Fetal bovine serum (FBS), minimum essential medium (MEM), and penicillin-streptomycin (5,000 units/mL) were purchased from VWR (Atlanta, GA). EGM-2 endothelial cell growth basal media as well as EMG-2 growth supplements were purchased from Lonza (Greenwood, SC).

4.3.2 Fabrication of NO-PEG Surfaces. NO-releasing SR surfaces were prepared following previously reported methods.[33] In brief, SR samples were placed into an anhydrous THF solution with SNAP (25 mg/mL) and rocked for 24 h at room temperature with protection from light. Afterward, SR samples were removed from the solution and dried on glass Petri dishes for an additional 24 h in a fume hood with protection from light. Finally, samples were briefly rinsed in methanol, padded dry, and dried under vacuum for an additional 4 h to afford NO-releasing SR (NO control, see **Figure 4.1**). Samples were stored at -20 °C and protected from light until use.

PEGylated surfaces were prepared using a previously reported method with minor deviation.[39] Substrates were first treated with low-pressure oxygen plasma at 30 W for 15 min to facilitate hydroxyl group coverage on surfaces. Immediately afterward, treated surfaces were submerged in PEG-silane at [1:2 1:1 2:1] volumetric ratios to anhydrous acetone for 1 h. Samples were then briefly rinsed with DI water and dried under a vacuum overnight. Both PEGylated controls (PEG control) and PEGylated NO-releasing surfaces (NO+PEG) were prepared (**Figure 4.1**). Samples were stored at -20 °C and protected from light until use.

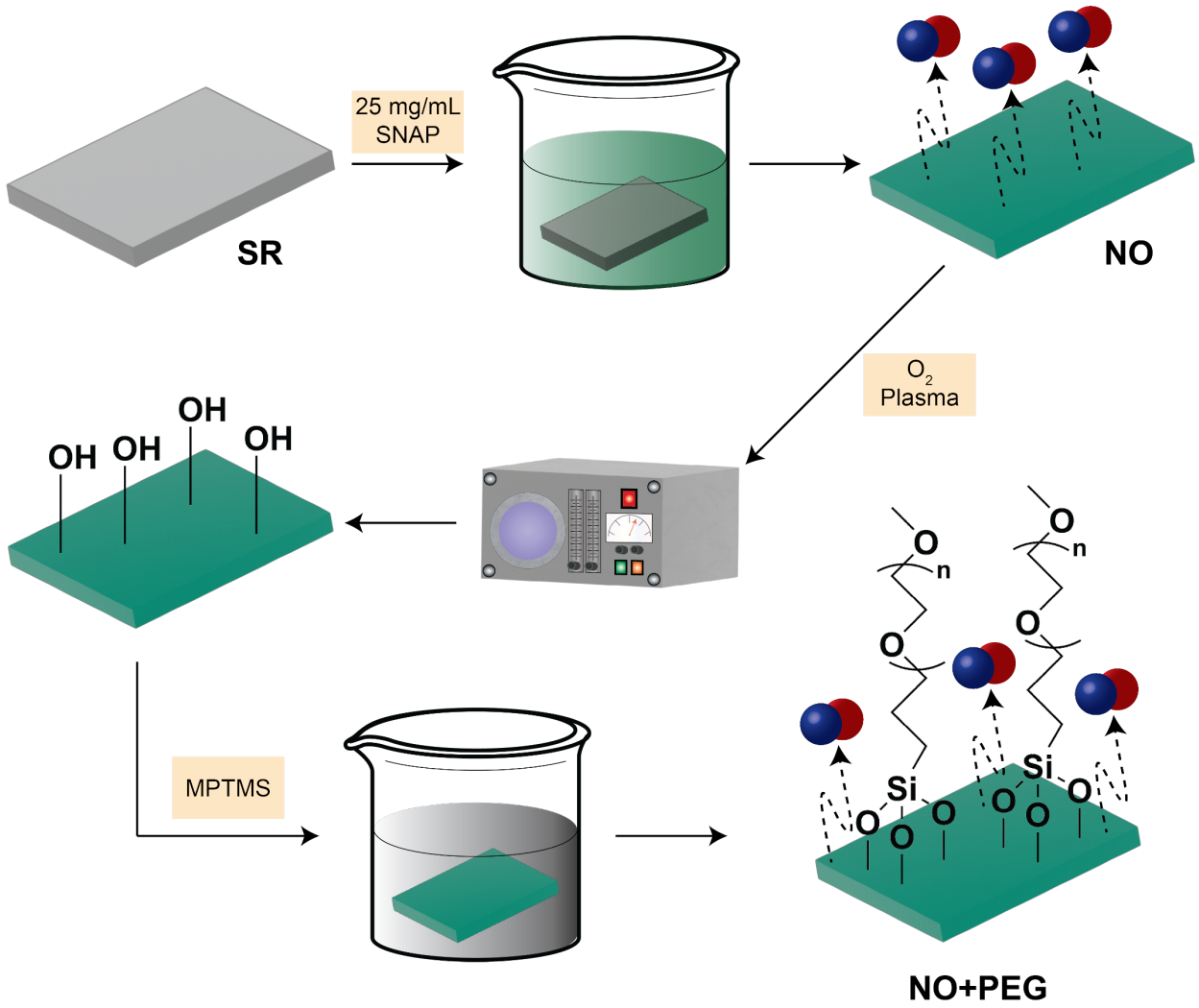

Figure 4.1 Fabrication of NO-releasing, PEGylated coatings (NO+PEG). SR is modified with the synthetic NO donor, SNAP, using a solvent impregnation technique for 24 h. Afterward, the NO-releasing materials are subjected to oxygen plasma treatment to form hydroxyl groups on the surface of the polymer. The treated tubing is then incubated in a solution of silanated PEG at different volumetric ratios to anhydrous acetone to form the NO-releasing PEGylated coating (NO+PEG).

4.3.3 Characterization of NO-PEG Surfaces.

4.3.3.1 Attenuated Total Reflectance-Fourier Transform Infrared (ATR-FTIR) Spectroscopy. ATR-FTIR scanning of surfaces was performed to confirm surface conjugation of the hydrophilic PEG groups. Infrared spectra were collected from 4000 – 650 cm^{-1} using a Perkin-Elmer Spectrum 3 Spectrometer with a PIKE Technologies VeeMAX III accessory equipped with

a flat GE 60° crystal plate. A total of 128 scans with a resolution of 4 cm^{-1} were collected for each sample.

4.3.3.2 Surface Contact Angle Measurement. Static contact angle measurements of the SR substrates were performed using an Ossila Contact Angle Goniometer on treated SR samples (~ 1 cm^2) secured on glass slides. Droplets (5 μL) of deionized water were dispensed on surfaces. Using video frame captures, the static contact angle was calculated using the sessile drop approximation. Final values are reported as the mean contact angle for each substrate type ± standard deviation (SD) (N = 3 samples from independently prepared substrates).

4.3.4 NO Release Studies. Realtime NO evolution from the SNAP-impregnated SR materials was determined using a Zysense Nitric Oxide Analyzer (NOA 280i). The NOA uses a chemiluminescence-based detection method with a purging sample vessel to continuously sweep NO from the solution via a nitrogen stream into an internal reaction chamber. Simultaneously, the NOA passes an oxygen stream into an ozone generator, and the resulting ozone is fed into the reaction chamber. Ozone and NO then react to form excited-state nitrogen dioxide, which upon relaxation emits a photon that is registered by a detector. This high sensitivity analytical method enables the correlation of NO gas at the PPB scale using an internal calibration constant (mol NO PPB^{-1} min^{-1}), enabling the determination of NO surface flux from polymeric materials (mol NO cm^{-2} min^{-1}). All samples were incubated in 1x PBS with EDTA at 37 °C during and between measurements to mimic physiologically relevant conditions. Final results are reported as the mean surface flux of NO ± SD (N = 3 runs for each time point across independently prepared samples for each substrate type).

4.3.5 SNAP Loading. SNAP loading studies were conducted over 24 h at ambient temperature (25 °C) with films incubated in 1 mL of anhydrous THF with protection from light. A standard curve of SNAP in THF at known concentrations was created via an Agilent Cary 60 UV-Vis. SR controls in THF were also tested for absorbance to account for monomer leaching from the polymer. From sample absorbance values and the standard curve, the concentration (mg/mL) and mass of SNAP leached were determined to calculate loading ratios for experimental samples. Final values are reported as the mean wt% for each substrate type ± SD (N = 5 samples from independently prepared substrates).

3.3.6 SNAP Leaching. SNAP leaching studies were conducted over 24 h under physiological conditions (1x PBS, 37 °C). Incubation of 8 mm films was conducted in 1 mL of 1x PBS with EDTA with protection from light. A standard curve was created using known concentrations of SNAP in PBS with EDTA. Leaching was measured by obtaining absorbance values of PBS incubation solutions (λ_{max} = 340 nm) via a Thermo-Fisher Genesys 10S UV-Vis at various time points (30 min, 1 h, 4 h, and 24 h). These absorbance values were converted to concentration values for SNAP leached using standard curve measurements and normalized to mg of SNAP leached relative to the total mass of SNAP loaded in the polymer samples. Final values are reported as the mean weight percent of SNAP (defined as mean mg SNAP per mg total of each substrate type × 100%) ± SD (N = 5 samples from independently prepared substrates).

3.3.7 *In Vitro* Bacteria Studies (24 h).

3.3.7.1 Preparation of Bacteria Cultures. Bacterial solutions were grown from stocks in MH broth until reaching the log phase as determined by optical density measurement (OD_{600} ~0.8 – 1.0). At this point, the solution was centrifuged to form a pellet of bacteria, the media was

replaced with PBS, and the bacteria were resuspended as a wash step. Following further centrifugation and resuspension in PBS, the bacterial solution was diluted to an OD_{600} of 0.1 for use in adhesion experiments.

3.3.7.2 Bacteria Adhesion Studies (24 h). SR substrates were sterilized via ultraviolet irradiation for 15 min on each side before bacterial exposure. Individual samples were then placed in 1 mL of 0.1 OD_{600} bacterial solutions and shaken for 24 h at 37 °C with protection from light. After incubation, the samples were rinsed with sterile PBS to remove any unadhered bacteria and homogenized in 1 mL PBS. The homogenates were diluted 10x times and plated with the assistance of an Eddy Jet W2 spiral plater (IUL, Farmingdale, NY) on MH agar. After overnight incubation at 37 °C, colony-forming units (CFUs) were counted using a SphereFlash automated colony counter (IUL, Farmingdale, NY). Data are presented as the mean CFU cm^{-2} ± SD (N = 5 per sample type). Percent bacterial reduction is calculated using **Equation 4.1**.

$$\textit{(4.1)} \quad \text{Percent Bacteria Reduction} = \frac{\text{Count}_{\text{control}}(\text{CFU cm}^{-2}) - \text{Count}_{\text{treatment}}(\text{CFU cm}^{-2})}{\text{Count}_{\text{control}}(\text{CFU cm}^{-2})} \times 100\%$$

3.3.8 *In Vitro* Cytotoxicity Studies (24 h).

3.3.8.1 Preparation of Mammalian Cell Culture. BJ cells and HUVEC were revived from cryopreservation stocks and subcultured under a 5% CO_2-humidified atmosphere at 37 °C. BJ cells were cultured in MEM media supplemented with 10% FBS and 1% penicillin-streptomycin. HUVECs were cultured in EBM-2 with the manufacturer-specified growth supplements from the EGM-2 kit. Both cell lines were subcultured for up to ten passages between experiments. When monolayers showed > 70% confluency, cells were treated with 0.25% trypsin supplemented with 5 mM EDTA for detachment. Detached cells were collected via centrifugation, counted, and plated for experiments.

3.3.8.2 Polymer Leachate Cytotoxicity Screening (24 h). Evaluation of cytocompatibility of the SR substrates followed the International Organization for Standardization (ISO) 10993-5 standards for the biological evaluation of medical devices.[40] Circular punchouts of the modified SR materials normalized for surface area (~0.865 cm^2) were UV sterilized for 15 min on both sides of the films. Each specimen was then individually soaked in 1 mL of supplemented media and incubated at 37 °C for 24 h. Concurrently, seeded 96-well plates were grown for 24 h to achieve > 70% monolayer confluency. The media on the plates was then aspirated and replaced with leachate-containing media, plated across eight replicate wells on a given plate. After an additional 24 h incubation, each plate was refreshed with clean media supplemented with 10% CCK-8 reagent. Plates were incubated for an additional 1 h and then quantified for optical density (OD, λ = 450 nm with λ_{ref} = 600 nm). Relative viabilities of cells treated with polymer leachates compared to cells treated with clean media were calculated according to **Equation 4.2**. Final data are presented as mean percent cellular viability ± SD (N = 3 treatment sets developed across independent passages).

$$\textit{(4.2)} \quad \text{Percent Cellular Viability} = \frac{(OD_{450}-OD_{650})_{\text{treatment}}}{(OD_{450}-OD_{650})_{\text{control}}} \times 100\% \tag{4.2}$$

4.3.9 *In Vitro* Blood Compatibility Screening.

4.3.9.1 Collection and Processing of Porcine Whole Blood. All procedures concerning the use of porcine whole blood (WB) and its components were approved by the Institutional Animal Care and Use Committee of the University of Georgia. Porcine WB was drawn using 3.2% sodium citrate solution at a 1:10 dilution through blind draws from a donor population. Collected blood was assessed for quality compliance (i.e., nominal platelet counts, white blood cell counts, and hemoglobin levels) and then fractionated into platelet-rich plasma (PRP) via centrifugation

(277 RCF, 12 min). The PRP was extracted and analyzed for hematological parameters, with the remaining fractions further spun down (3082 RCF, 20 min) to obtain platelet-poor plasma (PPP). All blood samples were processed and tested within 4 h of drawing.

4.3.9.2 In Vitro Platelet Adhesion Assessment. Platelet adhesion to the derivatized SR surfaces was assessed using previously reported methods with minor deviation.[41,42] PRP was diluted with PPP to obtain a final platelet count of 2×10^8 mL^{-1} with anticoagulation reversed using calcium chloride (2.5 mM). Circular punches of the modified SR materials normalized for surface area (~0.865 cm^2) were then incubated with the diluted PRP (4 mL) for 90 min at 37 °C with gentle rocking. After incubation, polymer samples were removed from the PRP and gently washed with calcium and magnesium-free PBS to remove nonadherent platelets. Adherent platelets were then lysed using 2 % v/v Triton-X-100 in PBS and quantified using the Roche® Cytotoxicity Detection Kit based on the colorimetric detection of lactate dehydrogenase (LDH) from lysed cells (λ = 492 nm with λ_{ref} = 620 nm). These readings were calculated against a standard curve of lysed platelets to determine the total number of adherent platelets and normalized to sample surface area. Final data are reported as mean platelets per cm^2 ± SD (N = 3 per treatment).

4.3.9.3 Hemolysis Screening. Hemolysis screening of the NO+PEG (1:1) coating and other modified SR samples was performed following the ISO 10993-4 standards for the biological evaluation of medical device interactions with blood and our previously reported methods.[43,44] Freshly drawn porcine WB was diluted in 1x PBS (Ca^{2+} and Mg^{2+} free) to a final hemoglobin concentration of 10.0 ± 1.0 mg/mL. Modified SR samples were placed in the diluted WB with a standardized surface area to volume ratio of 3 cm^2/mL. Reference samples included a PBS blank (7 mL diluted WB and 1 mL 1x PBS), unmodified SR negative control (3 cm^2/mL) in diluted WB, and deionized water positive control (7 mL WB and 1 mL of deionized water). Samples were

incubated at 37 °C for 3 h with manual rocking every 30 min. Afterward, the WB and extract solutions were spun down (800xg, 15 min) and the supernatants were collected for processing. The supernatants were then mixed 1:1 with Drabkin's reagent and allowed to stand for 15 min. Absorbance was then quantified (λ = 540 nm) and used to calculate percent hemolysis per **Equation 4.3**. Final data are reported as mean percent hemolysis and hemolytic indices (normalized to the mean percent hemolysis of the HDPE negative control) ± SD (N = 3 per treatment).

$$\textit{(4.3)} \quad \text{Percent Hemolysis (\%)} = \frac{\text{OD}_{\text{Sample}} - \text{OD}_{\text{Blank}}}{\text{OD}_{\text{Dil. WB}} - \text{OD}_{\text{Blank}}} \times 100\%$$

4.3.10 *In Vivo* Extracorporeal Circulation Rabbit Model.

4.3.10.1 Extracorporeal Circuit Fabrication. The ECC loops used for *in vivo* evaluation were prepared similarly to a previously reported method.[33] Briefly, silicone tubing was swelled with SNAP in THF as previously discussed above. The loops consisted of two segments of 5/8 cm inner diameter tubing (16 cm in length) on either side of one segment of 1 7/8 cm inner diameter tubing (8 cm), which served as the thrombogenicity chamber. The pieces were assembled using a silicone sealant and allowed to cure for 24 h before further modification. Unmodified silicon tubing was likewise assembled and used as controls. The constructed SNAP-SR loops were plasma treated for 15 min before being filled with 1:1 PEG silane in acetone. The ends were clamped to prevent acetone evaporation. After 1 h of incubation, the loops were thoroughly rinsed with DI water and allowed to dry. Angiocatheters (16- and 14-gauge) were coated with Carbosil® dissolved in THF (controls) or SR containing 10 wt% SNAP in THF (samples). All ECC loops were soaked in normal saline for 60 min before use.

4.3.10.2 *In Vivo* Thrombogenicity Model. In total, 10 New Zealand white rabbits (Robinson Services Inc, MI) were used in the study, and all rabbits weighed 2.2-3.0 kg. An established 4-h arteriovenous (AV) shunt model was used to evaluate the thrombogenicity of the fabricated ECC.[33,45] Briefly, the animals were pre-anesthetized with intramuscular injections of 5 mg/kg xylazine injectable (AnaSed® Lloyd Laboratories Shenandoah, Iowa) and 30 mg kg^{-1} ketamine hydrochloride (Hospira, Inc. Lake Forest, IL), and the anesthesia was maintained via isoflurane gas inhalation at a rate of 2-4%. IV fluids of Lactated Ringers were given at a rate of 10 mL kg^{-1} h^{-1} to maintain blood pressure stability. The custom-built circuit (with a thrombogenicity chamber in the middle) was placed in the animal's left carotid artery and right external jugular vein. The right carotid artery was cannulated using a 16-gauge IV angiocatheter (Jelco®, Johnson & Johnson, Cincinnati, OH) for blood sample collection as well as for blood pressure and heart rate monitoring. Body temperature was maintained at 37 °C using a water-jacketed heating blanket and was monitored with a rectal probe. Animals were not systemically anticoagulated during the experiments. The animal handling and surgical procedures were approved by the University of Michigan, University Committee on the Use and Care of Animals following university and federal regulations (UM protocol# PRO00010710).

4.3.10.3 Blood Sample Collection and Analysis. Blood samples were collected at baseline and every hour after the initiation of the blood flow in the ECC for a total of 4 h for *in vitro* measurements. Hemodynamic parameters, as well as arterial blood pH, pCO_2, pO_2, and total hemoglobin were measured using a blood-gas analyzer (ABL 825 Radiometer, Radiometer Copenhagen, DK). Platelet counts (IDEXX ProCyte Dx Westbrook, ME), plasma fibrinogen levels (Dade Behring BCS XP, Siemens Deerfield, IL), and activated clotting times (ACT, Hemochron Blood Coagulation System Model 801, International Technidyne Corp. Edison, NJ) were also

determined and monitored. Platelet function was further assessed using a Chrono-Log optical aggregometer model 490 (Havertown, PA).[45]

4.3.11 Statistical Analysis. All statistical comparisons were performed with GraphPad Prism 9 (GraphPad Software, San Diego, CA). All materials characterization and *in vitro* data are reported as the mean ± standard deviation (SD) unless explicitly stated otherwise. Comparisons between treated and control groups in these studies were made using ordinary one-way analysis of variance (ANOVA), implementing Tukey's method for correction of multiple comparisons. Values of $p < 0.05$ were deemed significant.

All *in vivo* data is reported as the mean ± standard error of the mean (SEM) for each animal group following outlier analysis (N = 4 screened rabbits per group) unless explicitly stated otherwise. All intragroup time-course-dependent *in vivo* comparisons were made using one-way ANOVA with Tukey's method for multiple comparisons. Values of $p < 0.05$ were deemed significant. All intergroup comparisons were made using two-way ANOVA. To account for multiple hypothesis testing, the false discovery rate was controlled using the two-stage step-up method of Benjamini, Krieger, and Yekutieli. A false discovery rate $q < 0.05$ was deemed significant. The corresponding *p*-values are indicated for comparisons wherein $p < 0.05$.

4.4 Results and Discussion

4.4.1 Surface Characterization. SR was impregnated with SNAP (**Figure 4.1**) following previously reported methods to develop a NO-releasing polymeric platform.[33] SNAP is a well-characterized NO donor that has previously been incorporated into polyurethanes, polyvinyl chloride, silicone rubber, and other medical-grade polymers via blending, solvent impregnation,

and covalent immobilization.[20,29] While SNAP-impregnated materials are antithrombotic and antimicrobial,[1] they lack mechanisms for preventing surface fouling that ultimately compromises blood-contacting medical devices. Surface PEGylation is a common surface passivation strategy that confers resistance to protein and bacteria surface fouling, thereby complementing the active mechanisms of NO.

4.4.2 FTIR Analysis. Deposition of silanated PEG (~0.46 – 0.59 kDa) on the NO-releasing silicone surfaces was first characterized by FTIR (**Figure 4.2**). Several characteristic peaks for the condensed silanated PEG were observed through grazing angle reflection techniques, including the formation of siloxane (-Si-O-Si-) bonds (1095 cm^{-1}) on both SR and NO surfaces. Hydrolysis of the trialkoxysilane leads to the formation of silanol groups, which facilitates condensation and subsequent monolayer or aggregate formation of the PEG coating. Further evidence of surface PEGylation was observed by hydroxyl group (-OH) stretching (3620-3160 cm^{-1}), alkylsilane (Si-C) stretching (~1280 cm^{-1}), as well as symmetric and asymmetric aliphatic (C-H) stretching (2924/2872 cm^{-1}) (**Figure 4.2**). These findings are consistent with previous reports for silane-based surface PEGylation.[46,47]

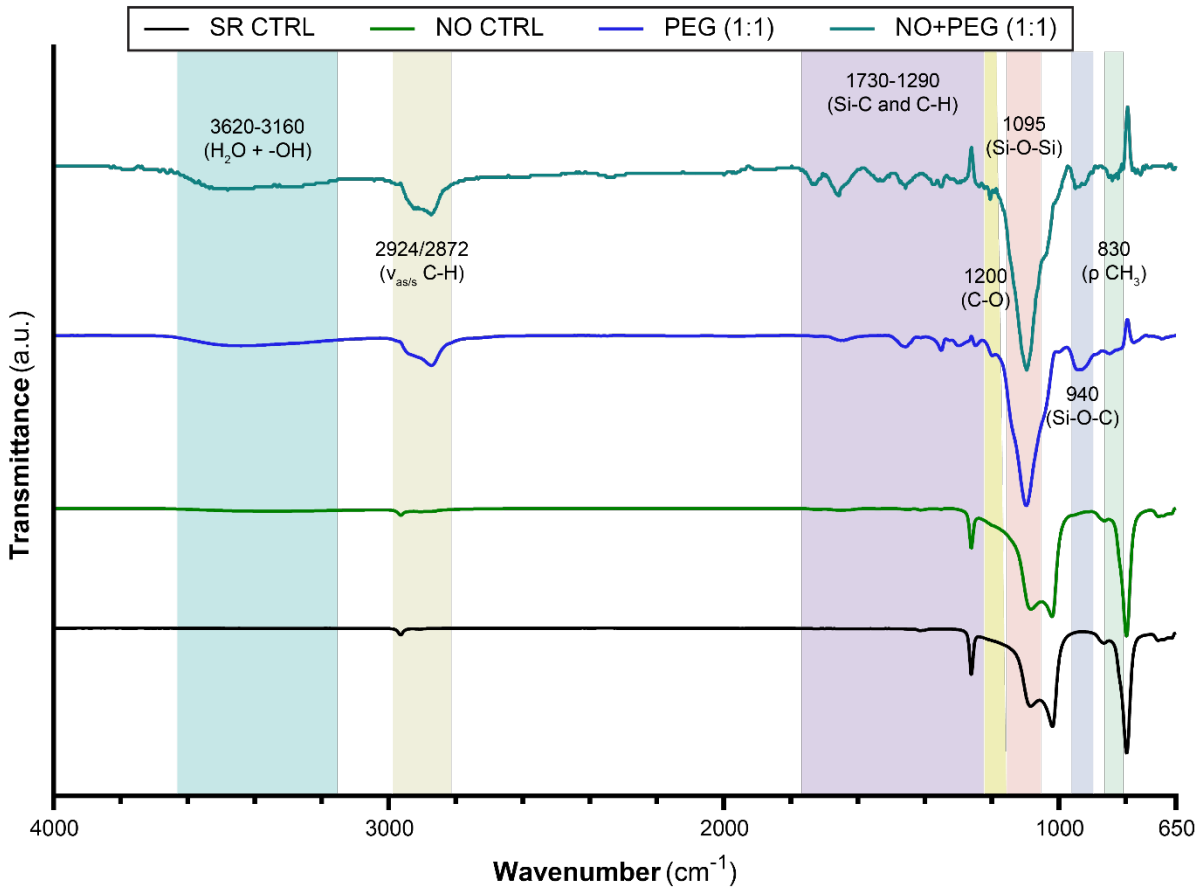

Figure 4.2 Fourier-transform infrared spectroscopy (FTIR) of PEGylated SR and NO-modified surfaces. Surface PEGylation was confirmed by the emergence of several characteristic peaks associated with condensation of the silanated PEG on the O_2 plasma-treated surfaces, including symmetric and asymmetric C-H stretching from side chains (2924/2872 cm^{-1}), Si-C stretching (1290 cm^{-1}) and the emergence of siloxane bonds (1095 cm^{-1}).

4.4.3 Surface Wettability. Static contact angle measurements were performed on the SR substrates to assess changes in surface wettability during the fabrication process. Solvent impregnation with SNAP led to no appreciable difference in surface wettability compared to untreated SR ($p > 0.05$, **Figure 4.3A**). In contrast, all PEG-treated groups showed a significant reduction in contact angle compared to both SR and NO groups ($p < 0.05$). Among the PEG-coated substrates, significant differences were observed between the PEG (1:2) and (2:1) coatings, while the integration of SNAP led to different wettability between the NO+PEG (1:1) and (2:1) coatings. SNAP is a water-soluble synthetic NO donor that has been previously shown to increase surface

retention of water, which may justify the increased wettability of the NO+PEG (2:1) coating by the facilitation of silane condensation.[48] Surface wetting is a good indicator of a material's resistance to biofouling, as the formation of water hydration layers on wetting materials facilitates the repulsion of hydrophobic plasma proteins and resistance to bacterial colonization and platelet adhesion.[49]

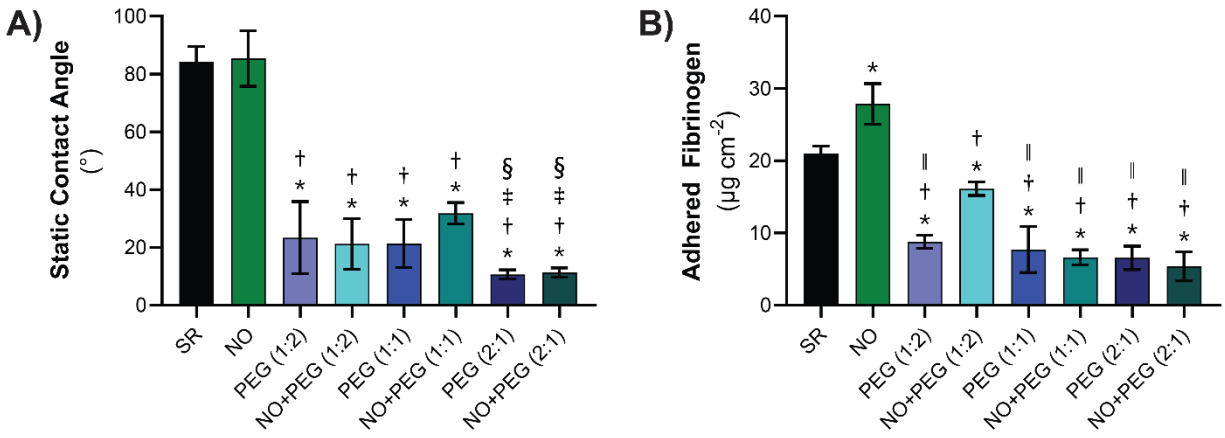

Figure 4.3 Surface wettability and antifouling performance of PEGylated, NO-releasing materials. Static contact angle measurements of the pristine surfaces (A) showed surface-dependent changes in wettability based on the volumetric ratio of silanated PEG used with respect to anhydrous acetone in the deposition process. In parallel, measurements of fibrinogen adsorption to the surfaces (B) demonstrated significant improvement in antifouling performance with a PEG ratio of 1:1 or higher. Final data are reported as the mean ± SD (N > 5, see Methods Sections). *Indicates a significant difference against the SR control group. †Indicates a significant difference against the NO control group. ‡Indicates a significant difference against the PEG (1:2) group. §Indicates a significant difference against the NO+PEG (1:1) group. ‖Indicates a significant difference against the NO+PEG (1:2) group. Statistical significance is defined as an adjusted $p < 0.05$.

4.4.4 Resistance to Protein Adhesion. Surface passivation is a well-known strategy for the prevention of surface-induced thrombosis and bacteria contamination but may not confer holistic protection for improving hemocompatibility of medical devices used under flow and in longer-term applications.[20,50] For this reason, combining PEGylated surfaces with NO release technology may help avoid an untoward effect of thrombosis and infection by facilitating a direct biocidal mechanism against bacteria and inducing localized platelet quiescence.[1,29]

Fibrinogen (Fg) is a hydrophobic plasma protein that undergoes enzymatic conversion in the presence of thrombin, leading to fibrin formation that is key to both platelet adhesion and bacterial colonization of blood-contacting medical devices.[1] Upon evaluating Fg adsorption to the PEGylated SR surfaces, a general trend towards resistance to surface fouling was observed (**Figure 4.3B**). NO-releasing control materials showed a ~32% increase in Fg adsorption compared to unmodified SR, consistent with previous reports of increased Fg binding to NO-releasing materials.[51] With the addition of the PEG coating to the NO-releasing substrates, up to a ~74 and 80% reduction in adhered Fg was observed compared to unmodified SR and NO controls, respectively (**Figure 4.3B**). Interestingly, the NO+PEG (1:2) coating exhibited inferior resistance to protein contamination compared to the NO+PEG (1:1) and (2:1) coatings, possibly because of reduced PEG concentration in the treatment solution affecting deposition efficacy. Similar reductions in Fg adhesion between the NO+PEG (1:1) and (2:1) coatings suggest that an antifouling threshold was reached with the surface, after which additional PEG did not confer extra benefit. Previously, others have shown that PEG coatings may reach saturation in both surface coverage and density, thereby limiting the added benefit of larger chain lengths, higher concentration incubation solutions, and incubation times.[46,52] Based on these findings, the PEGylated surfaces were further evaluated for the influence of the surface deposition process on NO donor retention and the overall effect on NO release kinetics.

4.4.5 Nitric Oxide Release Kinetics. The synthetic NO donor compound SNAP readily liberates NO in the presence of heat, light, or metal ions via homolytic cleavage of its *S*-nitrosothiol linkage (**Figure 4.4A**). SNAP decomposition in NO-releasing polymers follows pseudo-first-order reaction kinetics, enabling the development of sustained NO surface fluxes when exposed to

physiological conditions.[53,54] Since solvent impregnation of SNAP into SR implies that a finite reservoir of the drug is loaded, it is essential to evaluate how further processing of the SR substrates affects SNAP retention.[33,55] As shown in **Figure 4.4B**, surface PEGylation at the 1:2 ratio led to a significant ~25% drop in SNAP loading, while both the 1:1 and 2:1 ratios lead to an insignificant decline in loading. Anhydrous acetone has been previously reported to have a swelling ratio (*S*) of 1.06 into SR, compared to *S* of 1.38 for THF [56]. Therefore, it is reasonable to expect that the higher volumetric ratio of acetone in the 1:2 coating leads to a proportionately higher loss in SNAP loading. This phenomenon coupled with our prior findings on surface wettability and protein adhesion implicates that the 1:2 formulation is unacceptable for the NO-releasing application, as too many tradeoffs are made in surface properties. Concurrently, while the higher PEG ratio of 2:1 exhibited excellent material properties, the increased expense from the higher silanated PEG concentration may make it unfavorable for practical application and commercial translation. Therefore, further studies of NO release kinetics and biological evaluation reported herein consider the 1:1 PEGylation formulation.

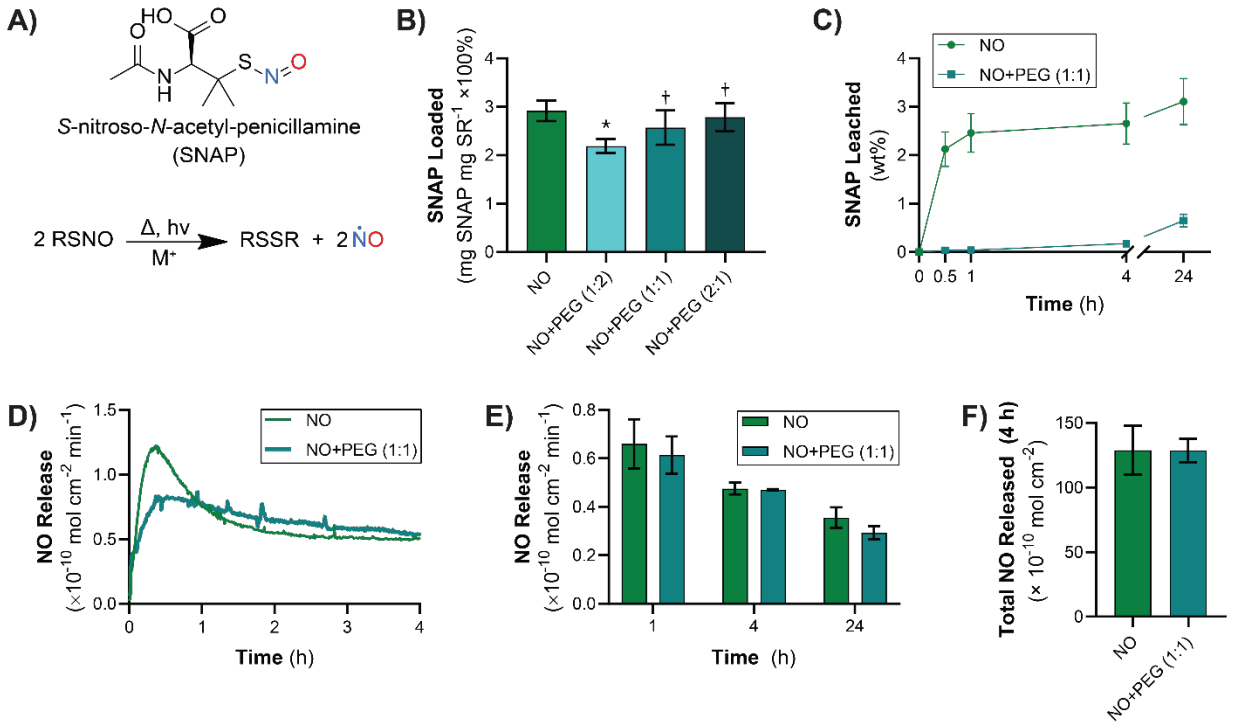

Figure 4.4 NO release studies from SR materials modified via solvent impregnation with the NO donor SNAP (A) which produces NO as a result of environmental stimuli. SR materials impregnated with SNAP and surface treated with silanated PEG showed (B) dissimilar retention of SNAP after fabrication. A study of SNAP leaching (C) from the NO+PEG (1:1) decreased diffusion of the donor from SR. Final data are reported as the mean ± SEM (N = 5 per formulation). Further study of the NO+PEG (1:1) formulation showed that the (D) instantaneous NO surface flux profiles, (E) average NO surface fluxes at several timepoints, and (F) total NO release thresholds after 4 h were similar to NO controls under physiological conditions (37 °C in 1x PBS with 100 mM EDTA). Final data are reported as the mean ± SD (N = 5 per formulation). *Indicates a significant difference against the NO control group. †Indicates a significant difference against the NO+PEG (1:2) group. Statistical significance is defined as an adjusted $p < 0.05$.

The extent of NO donor leaching from the polymer is a key consideration for the translation of the coating technology. Ideally, the NO-releasing surface will evolve NO via intrapolymeric degradation of SNAP without significant leaching of the donor into the surrounding physiological environment which could trigger secondary biocidal effects.[57] Therefore, the NO-releasing coatings were further evaluated for leaching over 24 h in physiological conditions (i.e., 1x PBS, 37 °C), showing remarkably decreased SNAP leaching from the NO+PEG (1:1) coating (**Figure 4.4C**). We reason that this is related to the emergence of both amorphous and crystalline states of

SNAP in SR as a result of SNAP being unable to reach solubility equilibrium within the polymer matrix during the impregnation step, as was previously reported for other SR-based materials.[33,58] This is a key tradeoff of the solvent impregnation process, wherein SNAP may also become degraded over time due to the presence of trace water or environmental conditions. Therefore, we reason that the decreased leaching would result from some loss of SNAP during the PEGylation step (i.e., acetone uptake and solubilization of SNAP), especially from the amorphous (dissolved) state, which has been previously associated with the elevated NO release kinetics from SR substrates when first placed under physiological conditions.[59,60]

Using a chemiluminescence-based detection method, the NO release kinetics of the developed materials were further evaluated during an initial 24-h timeframe to parallel biological screening. Representative NO surface flux profiles from both the NO and NO+PEG (1:1) surfaces demonstrate that the NO-only surfaces exhibited higher initial release rates, likely corresponding to the greater availability of dissolved SNAP in the polymer proximal to the polymer-solution interface (**Figure 4.4D**). These differences, however, were ultimately found insignificant after 1 h, with the surface flux from both NO and NO+PEG (1:1) surfaces showing no significant differences at either 4 or 24 h (**Figure 4.4E**). Similarly, the NO and NO+PEG (1:1) coatings showed no appreciable difference in the total NO released after 4 h (**Figure 4.4F**). Prior reports of SNAP-swollen silicone rubber materials have reported similar surface fluxes, with the fluxes heavily dependent on the thickness of the tubing, SNAP concentration in the swelling solution, and duration of swelling.[60,61] Based on our prior work, we reason that the NO surface flux can be further tailored by manipulation of these parameters, such as to develop higher surface fluxes or longer-term thresholds in an application-dependent context.[57,61] Careful manipulation of the NO

surface flux within the endothelial range (i.e., < 0.5 – 4.0 × 10^{-10} mol cm^{-2} min^{-1}) is essential, as higher fluxes and donor leaching have been reported to induce hemolytic responses.[62]

Although we have investigated surface flux only during the initial 24 h (corresponding to *in vitro* and *in vivo* studies described herein), prior reports of SNAP-swollen silicone rubber have demonstrated physiologically actionable NO release for over three weeks.[60] Prior work with hydrophilic NO-releasing surfaces has considered the incorporation of high water-uptake polyurethanes[49] or post-swelling processing by further surface functionalization with polyphosphorylcholine zwitterion brushes.[63,64] In both cases, polyurethanes with either polyether or polydimethylsiloxane soft segments were used to coat existing silicone-based medical devices for infection-related applications. In contrast, the approach reported herein offers several unique advantages by ready modification of existing silicone-based devices, including fewer fabrication steps, a more robust sense of scalability (e.g., solvent impregnation of preformed devices versus solvent blending and casting), and a facile surface strategy not as readily susceptible to hydrolytic degradation.[63,64] These unique properties of the NO+PEG formulation were therefore evaluated further for translatable feasibility in several *in vitro* and *in vivo* studies.

4.4.6 *In Vitro* Evaluation of Cytocompatibility. Ensuring that the PEGylated surfaces do not induce a cytotoxic effect is a critical checkpoint to pass before further evaluation in an *in vivo* model as a medical device coating. Therefore, the dual-action NO+PEG materials were tested in a 24-h indirect contact (leachate) cytotoxicity screening following ISO 10993-5 standards concerning the biological evaluation of medical devices.[40] Human-derived fibroblasts (BJ) and endothelial cells (HUVECs) were used as model cell lines. As shown in **Figure 4.5A**, leachates from the NO and PEG control surfaces introduced no significant change in BJ fibroblast viability,

while the combination NO+PEG (1:1) maintained > 90% viability. We attribute this slight decrease in viability to the distinct possibility that reactive oxygen species (ROSs) such as peroxynitrite ($ONOO^-$) and hydroxyl radicals ($^\bullet OH$) formed in the presence of NO and superoxide (O_2^-) may elicit oxidative degradation of the PEG chains at terminal hydroxyl groups, resulting in an untoward yet minor decrease in viability.[65,66] The NO+PEG (1:1) material was previously shown to have decreased SNAP leaching compared to the NO control, with comparable total NO release rates (**Figures 4.4C, 4.4D, 4.4E,** and **4.4F**). Practically, however, further modification of the terminal hydroxyl end groups has been reported to further modulate stability and biological activity, such as by zwitterion end-capping.[39]

Further evaluation of the SR substrates with HUVECs demonstrated similar findings, with the PEG (1:1) coating causing no significant difference in the cellular viability compared to the SR control (**Figure 4.5B**). On the other hand, the active NO release components of both the NO control and NO+PEG (1:1) surfaces enhanced cellular proliferation (**Figure 4.5B**), consistent with prior findings of enhanced endothelial cell proliferation in the presence of NO.[44,57] In this sense, we warrant that any cytotoxic effect from the PEG component in the presence of ROSs with the NO+PEG (1:1) coating is countered by the enhanced proliferative effect of NO with HUVECs. With clear trends of cytocompatibility during the initial 24-h period, the substrates were further analyzed for their ability to resist bacterial adherence and reduce infection risks.

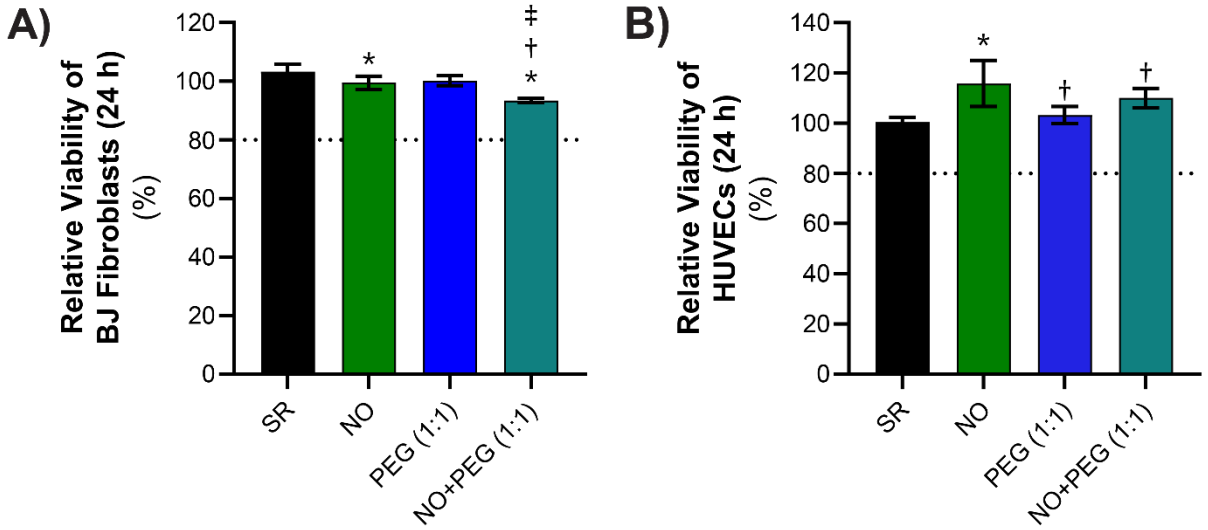

Figure 4.5 Cytocompatibility screening of the NO+PEG (1:1) surface coating against (A) human fibroblasts and (B) human vascular endothelial cells in 24-h indirect contact leachate studies. All coatings were found to retain greater than 80% cellular viability compared to the SR control. Final data are reported as the mean percent viability of cell cultures treated with leachates from each formulation ± SD (N = 9 independently tested films with cultures). *Indicates a significant difference against the SR control group. †Indicates a significant difference against the NO control group. ‡Indicates a significant difference against the NO+PEG (1:1) group. Statistical significance is defined as an adjusted $p < 0.05$.

4.4.7 *In Vitro* Evaluation of Antibacterial Performance. Demonstrating the potential for cytocompatibility, another key consideration for the construction of blood-contacting materials with antifouling properties is quantifying any antibacterial effects that may be elicited. NO-releasing materials are well established to be bactericidal with the ability to reduce the viability of adhered bacteria on the polymer surface. The addition of the PEG coating, however, prevents initial attachment, granting multifunctionality to the NO+PEG substrate. This mechanism is identical to that of the anti-fouling ability demonstrated with decreased protein adsorption (described above); the hydration layer that the PEG silane creates prevents hydrophobic and electrostatic interactions between the material's surface and bacterial cells.

These properties and PEG-NO's advantageous combination are demonstrated via 24 h adhesion experiments with *S. epidermis* and *E. coli*, as representative Gram-positive and Gram-negative bacteria, respectively. Upon exposure to *S. epidermis*, PEG or NO alone decreased viable

bacterial adhesion by 55.25% and 88.49%, respectively (**Figure 4.6A** and **Table 4.1**). However, the combination of the PEG coating and NO release reduced adhesion by 98.67%, showcasing the complementary nature of the dual active-passive mechanism of anti-biofouling action. This is further evidenced by exposure to *E. coli*. PEG and NO alone decreased viable adherence by 92.42% and 79.35%, respectively, but the combination of the two resulted in a statistically significant reduction of 97.46% ($P < 0.05$) (**Figure 4.6B** and **Table 4.2**). These results are consistent with the existing literature. Our group has repeatedly shown that Gram-positive bacteria are more susceptible to NO-releasing materials compared to Gram-negative bacteria,[67,68] as is observed here. The literature also supports the demonstrated decrease in bacterial adhesion shown on PEG-coated materials for Gram-negative bacteria compared to Gram-positive bacteria.[69] These trends may be attributed to differences in bacterial membranes and surface chemistries. Overall, the combination NO+PEG coatings exhibit complimentary antibacterial surface effects through a contact-active mechanism in conjunction with surface passivation, leading to decreased viable bacterial adhesion for both Gram-positive and Gram-negative strains (1.88 and 1.59-log reductions respectively).

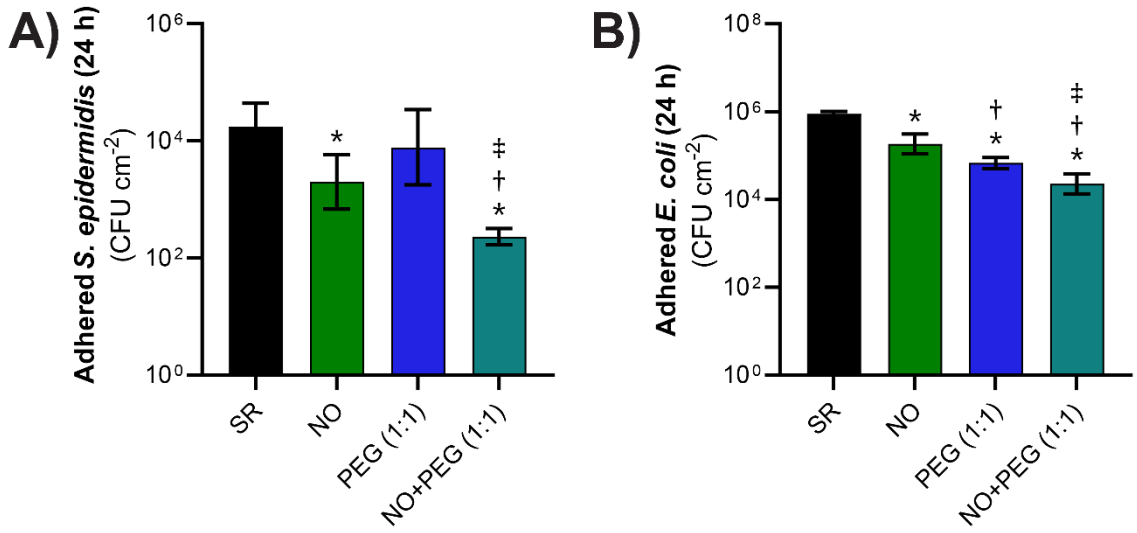

Figure 4.6 Antimicrobial studies of the NO+PEG (1:1) surface coating against clinically relevant (A) *S. epidermidis* and (B) *E. coli* demonstrated an enhanced reduction in viable, adherent bacteria

to surfaces with the combination coating strategy. The NO+PEG (1:1) coating resulted in 1.88 and 1.59-log reductions of *S. epidermidis* and *E. coli* after 24 h, respectively. Final data are reported as the mean colony-forming unit counts adjusted to surface area (CFU/cm^2) ± SD (n = 4). *Indicates a significant difference against the SR control group. †Indicates a significant difference against the NO control group. ‡Indicates a significant difference against the NO+PEG (1:1) group. Statistical significance is defined as an adjusted $p < 0.05$.

Table 4.1 Bacterial Adhesion for *S. epidermidis* at 24 h (CFU/cm^2)

	SR	NO	PEG (1:1)	NO+PEG (1:1)
AVG CFU/cm^2	1.74×10^4	2.00×10^3	7.77×10^3	2.30×10^2
% reduction compared to SR	- -	88.49%	55.25%	98.67%
p value vs SR	- -	0.0211	0.6195	< 0.0001
p value vs NO+PEG (1:1)	< 0.001	0.0213	0.0003	- -

Table 4.2 Bacteria Adhesion for *E. coli* at 24 h (CFU/cm^2)

	SR	NO	PEG (1:1)	NO+PEG (1:1)
AVG CFU/cm^2	8.94×10^5	1.84×10^5	6.77×10^4	2.27×10^4
% reduction compared to SR	- -	79.35%	92.42%	97.46
p value vs SR	- -	0.0006	< 0.0001	< 0.0001
p value vs NO+PEG (1:1)	< 0.001	< 0.0001	0.0108	- -

4.4.8 *In Vitro* Screening Evaluation of Blood Compatibility. *In vitro* hemocompatibility screening of the NO+PEG (1:1) formulation and analogs were conducted against diluted porcine PRP and WB for platelet adhesion and hemolysis. These screening studies are critical before *in vivo* testing to verify the translational feasibility of surface fouling resistance and NO release on platelet quiescence and blood compatibility. Platelet adhesion testing in fresh, diluted porcine PRP (~2 × 10^8 platelets/mL) for 90 min showed significant reductions in platelet adhesion with all test groups compared to SR controls (**Figure 4.7A**). Notably, the NO+PEG (1:1) group showed the

highest, statistically significant reduction in platelet adhesion compared to all other groups, with > 96% reduction compared to SR controls (**Figure 4.7A**). Interestingly, even without an active mechanism for platelet quiescence from NO donor infusion, the PEG (1:1) control managed to perform well, with nearly an 85% reduction in platelet adhesion relative to the SR control. These findings were consistent with our previous reports with other NO-releasing control materials and confirm the complementary effect of PEG with NO to improve resistance to platelet adhesion and activation.[13,70]

While SNAP-impregnated samples were able to confer a platelet quiescence effect as a pathway to adhesion resistance, it was necessary to further evaluate the blood compatibility of the coatings via benchmark of their tendency to cause red blood cell lysis. Following ISO 10993-5 standards for hemolysis testing, none of the NO or PEG-modified surfaces were found to induce a hemolytic response (**Figure 4.7B**). This trend is consistent with our prior findings with NO-releasing materials[44,71] and supports the general hemocompatibility of the NO+PEG surface for further evaluation of performance in a rabbit thrombogenicity model.

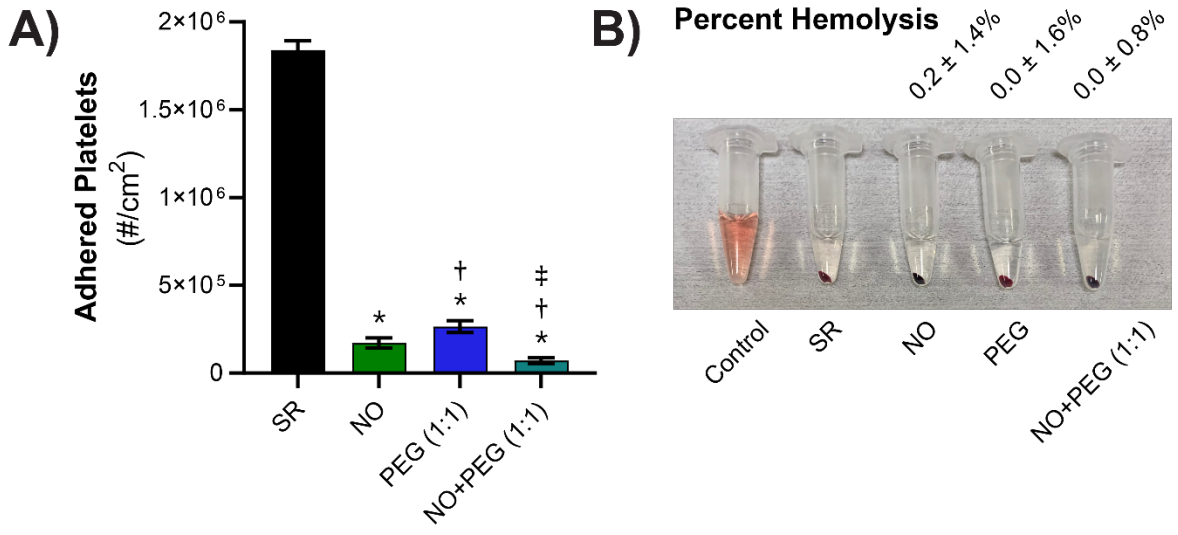

Figure 4.7 *In vitro* blood compatibility screening of NO+PEG (1:1) and related surface modifications. Studies of platelet adhesion (A) with diluted porcine PRP showed a greater than 96% reduction in platelet adhesion to surfaces relative to the SR control with (B) maintenance of blood compatibility by not inducing a hemolytic response. Final data are reported as the mean ±

SD (N = 3). *Indicates a significant difference against the SR control group. †Indicates a significant difference against the NO control group. ‡Indicates a significant difference against the PEG (1:1) control group. Statistical significance is defined as an adjusted $p < 0.05$.

4.4.9 *In Vivo* Rabbit Model of Extracorporeal Circulation. Based on promising *in vitro* data for cytocompatibility, antibacterial potential, and blood compatibility, the NO+PEG (1:1) coating was further assessed in an *in vivo* extracorporeal rabbit thrombogenicity model. The NO+PEG (1:1) coating was used in the construction of extracorporeal circuits (ECCs) which were applied to 4-h arteriovenous studies in a well-established model with New Zealand White hares.[33,45,72] Both NO+PEG (1:1) and SR control circuits were evaluated, with circuits primed for 1 h with normal saline before implantation to deter any systemic effects from burst release of NO that may be induced by initial SNAP leaching.[33,72] The NO release from the NO+PEG (1:1) circuits was measured following the 1 h saline flush and 4-h implantation, with nominal NO release levels of $> 0.52 \times 10^{-10}$ mol cm^{-2} min^{-1} throughout the study. This finding was consistent with our prior studies of the NO+PEG (1:1) coating in PBS (**Figure 4.4E**) and other NO-releasing coatings, implying maintenance of NO surface flux within endothelial levels without significant change in the overall release kinetics as a result of blood exposure.[33,67]

Gross analysis of the ECC circuits following 4 h implantation demonstrated a significant 79% reduction in thrombus mass on the thrombogenicity chambers with the NO+PEG (1:1) coating compared to SR controls (**Figure 4.8A**). This finding was further corroborated by a 134% increase in chamber patency with NO+PEG (1:1) compared to SR controls (**Figure 4.8B)** from ImageJ analysis of cross-sectional chamber occlusion. Visual inspection of the thrombogenicity chambers found the emergence of dense, mature clots in the SR controls (**Figure 4.8C**) leading to some degree of occlusion, whereas only thin blood films with some nascent clot coverage were observed with the NO+PEG (1:1) loops after 4 h (**Figure 4.8D**).

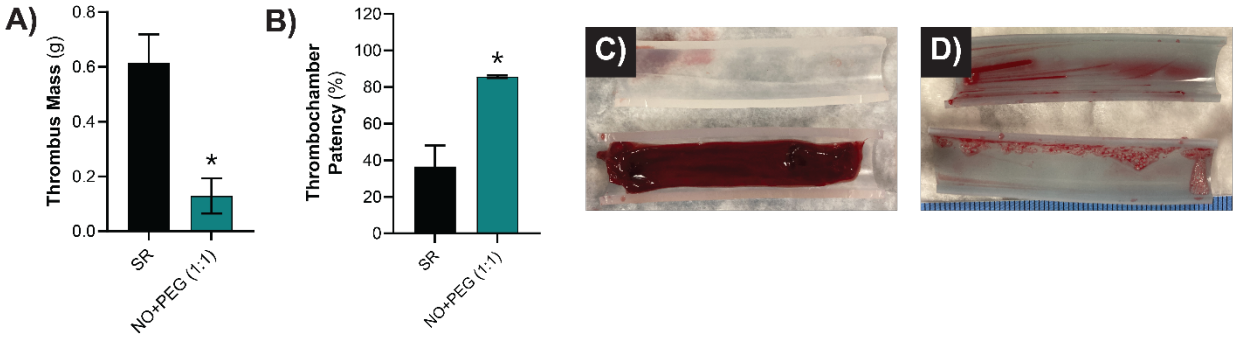

Figure 4.8 Analysis of extracorporeal circuits following termination of the study (4 h). Measurements of thrombus mass (A) and further calculations of chamber patency percentage via imaging software (B) demonstrate suppression of aggregate clot formation on the NO+PEG coating. Representative images of (C) unmodified SR circuits and (D) the NO+PEG (1:1) circuits are provided. Final data are reported as the mean ± SEM (N = 4). *Indicates a significant difference against the SR control group. Statistical significance is defined as an adjusted $p < 0.05$.

Key hemodynamic parameters were monitored throughout the 4 h experiment, including mean arterial pressure (MAP), heart rate (HR), and circuit blood flow (ECC BF) (**Table 4.3**). No key changes were observed in MAP and HR vital parameters with control circuits, while a slight drop in MAP was recorded for NO+PEG (1:1) circuits by 4 h. This less than 25% drop in MAP relative to baseline for NO+PEG (1:1) was unexpected, compared to our prior studies of NO-releasing circuits showing > 50% drop in MAP.[33] The greater preservation in MAP may be correlated with the reduced SNAP leaching of the NO+PEG circuits, as NO is known to lower pressure by enhancement of vasodilation.[73] Reduced SNAP leaching observed with the NO+PEG (1:1) coating (**Figure 4.4C**) may therefore reduce systemic effects from nonlocalized NO release, which is ideal for pinpointing the effects of the circuits proximal to the polymer-solution interface. ECC blood flow proportionately increased for the NO+PEG (1:1) group, which can be attributed to hemodilution effects from IV fluids administration as well as possible lubrication effects of PEGylated surfaces.[33,74,75]

Table 4.3 Evaluation of rabbit hemodynamic parameters as a result of the NO+PEG (1:1) and SR control ECC circuits during 4 h of blood flow. Mean arterial pressure (MAP), heart rate (HR), and extracorporeal circuit blood flow (ECC BF).

Hemodynamics						
ECC	Parameter		Time on ECC (h)			
		Baseline	1	2	3	4
SR	MAP (mmHg)	46 ± 5	35 ± 4	38 ± 3	39 ± 2	40 ± 3
	HR (beats/min)	201 ± 8	179 ± 10	191 ± 10	206 ±4	221 ± 5
	ECC BF (mL/min)	77 ± 2	72 ± 9	81 ± 9	88 ± 14	93 ± 12
NO+PEG (1:1)	MAP (mmHg)	49 ± 2	39 ± 2	40 ± 5	35 ± 3*	37 ± 1*
	HR (beats/min)	191 ± 14	195 ± 2	195 ± 3	207 ± 12	213 ± 16
	ECC BF (mL/min)	62 ± 4	83 ± 3*	84 ± 4*	80 ± 3*	83 ± 4*

Final values reported as mean ± SEM (N = 4).
*Indicates a significant difference against baseline ($p < 0.05$)

Throughout the 4 h experiment, platelet activation and functionality were monitored by assessing platelet count, white blood cell count, plasma fibrinogen levels, and pathway activation. Critically, the NO+PEG (1:1) displayed superior platelet preservation (adjusted for hemodilution and normalized to baseline) at all time points (**Figure 4.9A**). Platelet counts were maintained at near baseline levels for NO+PEG (1:1) loops after 4 h of blood flow while SR circuits exhibited a significant time-dependent loss in counts in dropping to less than < 75% of baseline. While both loop configurations appeared to exhibit a modest upward trend in WBC counts (including lymphocytes, monocytes, and granulocytes) over time with leveling off by 4 h, no significant differences were found (**Figure 4.9B**). This finding was consistent with our prior studies of NO-releasing and catalyzing coatings.[33,74] Initial plasma fibrinogen levels were 246.6 ± 14.9 and 230.0 ± 14.7 mg dL^{-1} for SR and NO+PEG (1:1), respectively, and corrected for hemodilution. During the time course of flow studies, the SR group exhibited a significant ~40% drop in plasma fibrinogen levels, whereas the NO+PEG (1:1) group exhibited a ~30% drop by 4 h (**Figure 4.9C**).

While these drops are significant within treatment groups, nominal levels are consistent with previous reports for the animal breed.[76,77] The loss in plasma fibrinogen is associated with its adsorption to foreign surfaces and further role in thrombus formation.[1] Previously, NO-releasing materials have been associated with increased fibrinogen adsorption and d-dimer formation at the blood-polymer interface as a result of hydrophobic surface interactions and NO evolution.[51,62] The previously observed reduction in fibrinogen on the NO+PEG (1:1) surfaces compared to NO controls (**Figure 4.9B**) is thereby able to act complimentary to NO release in the NO+PEG (1:1) coatings to facilitate significantly improved platelet preservation and reduction in clot formation. Previously, increased fibrinogen adsorption has been observed on NO-releasing materials proportional to the magnitude of the NO surface flux,[51] which can attract platelets and facilitate blood contact activation.[35] By reducing the amount of fibrinogen loss from circulation, NO+PEG confers an additional protective effect through surface passivation that prevents fibrinogen attachment and therefore reduced focal points for platelet adhesion. This ensures a dual-action strategy with NO for mediating platelet quiescence and mimicking endothelial homeostasis at the polymer-solution interface.

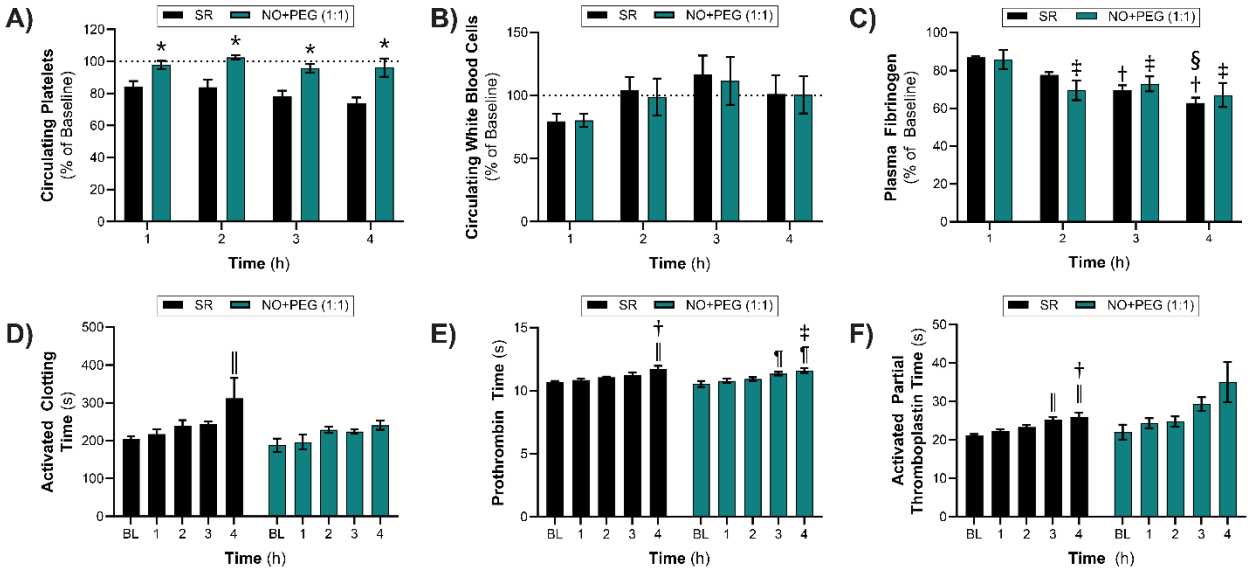

Figure 4.9 Hematological assessment of circuits was conducted every hour of the ECC flow studies. Circulating (A) platelets and (B) white blood cells (WBC), adjusted for hemodilution, and normalized against baseline showed greater platelet preservation with the NO+PEG (1:1) group with no significant difference in WBC counts. Plasma fibrinogen levels (C) showed a general decrease over time compared to baseline, likely to hemodilution effects and adsorption to circuits. Clotting assessment of WB showed a significant increase in activated clotting time (ACT) in the SR group compared to baseline (BL). Further pathway activation assessment of isolated plasma showed (C) elevated prothrombin time for both the SR and NO+PEG (1:1) groups as well as elevated activated partial thromboplastin time (aPTT) with the SR group compared to BL values, suggesting pathway dysregulation. Final data reported as mean ± SEM (N = 4 circuits per group). *Indicates a significant difference between the SR and NO+PEG (1:1) groups at the specified timepoint. †Indicates a significant difference against SR control at hour 1. ‡Indicates a significant difference against NO+PEG (1:1) at hour 1. §Indicates a significant difference against SR control at hour 2. ‖Indicates a significant difference against the SR baseline. ¶Indicates a significant difference against the NO+PEG (1:1) baseline. Statistical significance is defined as an adjusted $p < 0.05$.

Further assessment of platelet function first investigated activated clotting time (ACT) for change in hemodynamics as a result of WB stimulation with factor XII activators at each hour mark in the ECC studies. Elevated ACTs were observed for the SR group by study termination ($p < 0.05$), with a general trend towards elevation in the NO+PEG (1:1) group ($p = 0.0513$) (**Figure 4.9D**). Elevated ACT is indicative of platelet dysfunction and thrombocytopenia, but is typical of the ECC model due to hemodilution effects and concurrent plasma fibrinogen adsorption onto the circuit surfaces.[78] Further analysis of plasma at each time point showed elevated prothrombin time (PT) by study termination for both groups, indicative of extrinsic and common pathway activation (**Figure 4.9E**). This finding is typical of the ECC surgery, which has the potential to cause injury to the vessel wall and disrupt blood homeostasis, resulting in some inherent platelet activation and other conformational changes.[1,29]

Testing for activated partial thromboplastin time (aPTT) showed elevation in the SR group but no statistically significant increase in the NO+PEG (1:1) group (**Figure 4.9F**), implying intrinsic pathway activation in the SR control group. This finding idealizes the role of the NO+PEG

(1:1) coating in minimizing blood interaction with the circuit surfaces, thereby reducing the stimuli that induce contact activation of the intrinsic pathway and activation of circulating platelets. However, the general trend towards significance in elevated ACT for the NO+PEG (1:1) (p = 0.0513) while being unable to fully account for any hemodilution and Fg adsorption effects makes it unclear the extent to which the NO+PEG (1:1) coating inhibits contact (intrinsic) and common pathway activation. NO is an antiplatelet agent known to regulate function through the activation of guanylyl cyclase receptors and prevention of platelet morphological changes via spatial confinement.[79-81] Concurrently, PEG coatings are known not to inhibit coagulation processes in native blood but can reduce the extent of activation.[82] Taken together, the *in vivo* findings suggest that delayed thrombus formation on the NO+PEG (1:1) coatings is related to the downregulation of surface contact activation via the promotion of fewer interactions with the circuit walls as well as the facilitation of platelet quiescence via localized NO elution.

4.5 Conclusion

In summary, we have investigated the surface properties and translational feasibility of a combination NO-releasing and PEGylated surface strategy to confer enhanced resistance to infection and thrombosis to SR substrates that is suitable for dynamic blood flow applications in extracorporeal life support technologies. In this work, the synthetic NO donor SNAP was impregnated into prefabricated silicone rubber tubing and surface treated with a silanated PEG to confer potent antifouling, antimicrobial, and antiplatelet capabilities. This novel combination strategy exhibited low water contact angles while retaining NO release kinetics viable for physiological action. This contributed to over a 74% reduction in Fg adsorption and up to a 1.88-log reduction in adherent bacteria while maintaining the cytocompatibility of the base silicone

material. Blood compatibility screening of the coatings demonstrated a greater than 96% reduction in platelet adhesion with negligible hemolytic potential. Further evaluation in a 4-h ECC rabbit model of thrombogenicity demonstrated a 79% reduction in thrombus mass on the thrombogenicity chambers, a 134% increase in patency with the combination coating, and further highlighted the coating's ability for superior platelet preservation, maintenance of plasma fibrinogen levels, and reduced perturbations of the coagulation cascade. Results of this study suggest the potential of improving both infection resistance and hemocompatibility of existing medical devices via a simple two-step fabrication technique without incurring difficult synthetic procedures.

4.6 References

1. Roberts TR, Garren MRS, Handa H, Batchinsky AI. Toward an artificial endothelium: Development of blood-compatible surfaces for extracorporeal life support. *J Trauma Acute Care Surg.* 2020;89(2S Suppl 2):S59-s68.

2. Dalton HJ, Garcia-Filion P, Holubkov R, et al. Association of bleeding and thrombosis with outcome in extracorporeal life support. *Pediatr Crit Care Med.* 2015;16(2):167-174.

3. Cartwright B, Bruce HM, Kershaw G, et al. Hemostasis, coagulation and thrombin in venoarterial and venovenous extracorporeal membrane oxygenation: the HECTIC study. *Scientific Reports.* 2021;11(1):7975.

4. Brash JL, Horbett TA, Latour RA, Tengvall P. The blood compatibility challenge. Part 2: Protein adsorption phenomena governing blood reactivity. *Acta Biomater.* 2019;94:11-24.

5. Kato C, Oakes M, Kim M, et al. Anticoagulation strategies in extracorporeal circulatory devices in adult populations. *European Journal of Haematology.* 2021;106(1):19-31.

6. Thomas S, Makris M. The reversal of anticoagulation in clinical practice *Clin Med (Lond).* 2018;18(4):314-319.

7. Kim HS, Park S, Ko HH, Ha SO, Lee SH, Kim YK. Different characteristics of bloodstream infection during venoarterial and venovenous extracorporeal membrane oxygenation in adult patients. *Scientific Reports.* 2021;11(1):9498.

8. Wang J-R, Huang J-Y, Hu W, Cai X-Y, Hu W-H, Zhu Y. Bloodstream infections in patients undergoing extracorporeal membrane oxygenation. *Pak J Med Sci.* 2020;36(6):1171-1176.

9. Anand P, Kranker K, Chen AY. Estimating the hospital costs of inpatient harms. *Health Serv Res.* 2019;54(1):86-96.

10. Crosby HA, Kwiecinski J, Horswill AR. Staphylococcus aureus Aggregation and Coagulation Mechanisms, and Their Function in Host-Pathogen Interactions. *Adv Appl Microbiol.* 2016;96:1-41.

11. Nakazawa N. Infectious and thrombotic complications of central venous catheters. *Semin Oncol Nurs.* 2010;26(2):121-131.

12. Silvetti S, Koster A, Pappalardo F. Do we need heparin coating for extracorporeal membrane oxygenation? New concepts and controversial positions about coating surfaces of extracorporeal circuits. *Artif Organs.* 2015;39(2):176-179.

13. Goudie MJ, Pant J, Handa H. Liquid-infused nitric oxide-releasing (LINORel) silicone for decreased fouling, thrombosis, and infection of medical devices. *Sci Rep.* 2017;7(1):13623.

14. Li J, Ueda E, Paulssen D, Levkin PA. Slippery Lubricant-Infused Surfaces: Properties and Emerging Applications. *Advanced Functional Materials.* 2019;29(4):1802317.

15. Liu X, Yuan L, Li D, et al. Blood compatible materials: state of the art. *J Mater Chem B.* 2014;2(35):5718-5738.

16. Avramescu RE, Ghica MV, Dinu-Pirvu C, Prisada R, Popa L. Superhydrophobic Natural and Artificial Surfaces-A Structural Approach. *Materials (Basel).* 2018;11(5).

17. Vogler EA, Siedlecki CA. Contact activation of blood-plasma coagulation. *Biomaterials.* 2009;30(10):1857-1869.

18. Maitz MF, Zitzmann J, Hanke J, et al. Adaptive release of heparin from anticoagulant hydrogels triggered by different blood coagulation factors. *Biomaterials.* 2017;135:53-61.

19. Yu H, Cui L-X, Huang N, Yang Z-L. Recent developments in nitric oxide-releasing biomaterials for biomedical applications. *Med Gas Res.* 2019;9(4):184-191.

20. Ashcraft M, Douglass M, Chen Y, Handa H. Combination strategies for antithrombotic biomaterials: an emerging trend towards hemocompatibility. *Biomater Sci.* 2021;9(7):2413-2423.

21. Garren MR, Ashcraft M, Qian Y, Douglass M, Brisbois EJ, Handa H. Nitric oxide and viral infection: Recent developments in antiviral therapies and platforms. *Appl Mater Today.* 2021;22:100887-100887.

22. Tousoulis D, Kampoli AM, Tentolouris C, Papageorgiou N, Stefanadis C. The role of nitric oxide on endothelial function. *Curr Vasc Pharmacol.* 2012;10(1):4-18.

23. Thomas DD, Liu X, Kantrow SP, Lancaster JR, Jr. The biological lifetime of nitric oxide: implications for the perivascular dynamics of NO and O2. *Proceedings of the National Academy of Sciences of the United States of America.* 2001;98(1):355-360.

24. Rong F, Tang Y, Wang T, et al. Nitric Oxide-Releasing Polymeric Materials for Antimicrobial Applications: A Review. *Antioxidants (Basel).* 2019;8(11).

25. Ashcraft M, Douglass M, Garren M, et al. Nitric Oxide-Releasing Lock Solution for the Prevention of Catheter-Related Infection and Thrombosis. *ACS Applied Bio Materials.* 2022.

26. Saidkhani V, Asadizaker M, Khodayar MJ, Latifi SM. The effect of nitric oxide releasing cream on healing pressure ulcers. *Iran J Nurs Midwifery Res.* 2016;21(3):322-330.

27. Shurbaji S, El-Sherbiny IM, Alser M, et al. Nitric Oxide Releasing Hydrogel Nanoparticles Decreases Epithelial Cell Injuries Associated With Airway Reopening. *Frontiers in Bioengineering and Biotechnology.* 2021;8.

28. Estes Bright LM, Garren MRS, Ashcraft M, et al. Dual Action Nitric Oxide and Fluoride Ion-Releasing Hydrogels for Combating Dental Caries. *ACS Applied Materials & Interfaces.* 2022.

29. Wo Y, Brisbois EJ, Bartlett RH, Meyerhoff ME. Recent advances in thromboresistant and antimicrobial polymers for biomedical applications: just say yes to nitric oxide (NO). *Biomater Sci.* 2016;4(8):1161-1183.

30. Douglass M, Hopkins S, Pandey R, Singha P, Norman M, Handa H. S-Nitrosoglutathione-Based Nitric Oxide-Releasing Nanofibers Exhibit Dual Antimicrobial and Antithrombotic Activity for Biomedical Applications. *Macromolecular Bioscience.* 2021;n/a(n/a):2000248.

31. Sadrearhami Z, Shafiee FN, Ho KKK, et al. Antibiofilm Nitric Oxide-Releasing Polydopamine Coatings. *ACS Applied Materials & Interfaces.* 2019;11(7):7320-7329.

32. Wo Y, Li Z, Brisbois EJ, et al. Origin of Long-Term Storage Stability and Nitric Oxide Release Behavior of CarboSil Polymer Doped with S-Nitroso-N-acetyl-d-penicillamine. *ACS Applied Materials & Interfaces.* 2015;7(40):22218-22227.

33. Brisbois EJ, Major TC, Goudie MJ, Bartlett RH, Meyerhoff ME, Handa H. Improved hemocompatibility of silicone rubber extracorporeal tubing via solvent swelling-impregnation of S-nitroso-N-acetylpenicillamine (SNAP) and evaluation in rabbit thrombogenicity model. *Acta Biomater.* 2016;37:111-119.

34. Douglass M, Hopkins S, Chug MK, et al. Reduction in Foreign Body Response and Improved Antimicrobial Efficacy via Silicone-Oil-Infused Nitric-Oxide-Releasing Medical-Grade Cannulas. *ACS Applied Materials & Interfaces.* 2021;13(44):52425-52434.

35. Douglass M, Garren M, Devine R, Mondal A, Handa H. Bio-inspired Hemocompatible Surface Modifications for Biomedical Applications. *Progress in Materials Science.* 2022:100997.

36. Singha P, Pant J, Goudie MJ, Workman CD, Handa H. Enhanced antibacterial efficacy of nitric oxide releasing thermoplastic polyurethanes with antifouling hydrophilic topcoats. *Biomaterials Science.* 2017;5(7):1246-1255.

37. Mishra D, Hubenak JR, Mathur AB. Nanoparticle systems as tools to improve drug delivery and therapeutic efficacy. *J Biomed Mater Res A.* 2013;101(12):3646-3660.

38. Lowe S, O'Brien-Simpson NM, Connal LA. Antibiofouling polymer interfaces: poly(ethylene glycol) and other promising candidates. *Polymer Chemistry.* 2015;6(2):198-212.

39. Plegue TJ, Kovach KM, Thompson AJ, Potkay JA. Stability of Polyethylene Glycol and Zwitterionic Surface Modifications in PDMS Microfluidic Flow Chambers. *Langmuir.* 2018;34(1):492-502.

40. Standards ISO. ISO 10993-5: 2009 (E). Biological evaluation of medical devices—Part 5: Tests for cytotoxicity in vitro. In: International Organizational for Standardization Geneve; 2009.

41. Ozkan E, Mondal A, Singha P, et al. Fabrication of Bacteria- and Blood-Repellent Superhydrophobic Polyurethane Sponge Materials. *ACS Applied Materials & Interfaces.* 2020;12(46):51160-51173.

42. Ozkan E, Mondal A, Douglass M, et al. Bioinspired ultra-low fouling coatings on medical devices to prevent device-associated infections and thrombosis. *J Colloid Interf Sci.* 2022;608:1015-1024.

43. Standards ISO. ISO 10993-4: 2017 Biological evaluation of medical devices—Part 4: Selection of tests for interactions with blood. In: International Organizational for Standardization Geneve; 2017.

44. Ashcraft M, Douglass M, Garren M, et al. Nitric Oxide-Releasing Lock Solution for the Prevention of Catheter-Related Infection and Thrombosis. *ACS Appl Bio Mater.* 2022.

45. Major TC, Brant DO, Reynolds MM, et al. The attenuation of platelet and monocyte activation in a rabbit model of extracorporeal circulation by a nitric oxide releasing polymer. *Biomaterials.* 2010;31(10):2736-2745.

46. Zhu XY, Jun Y, Staarup DR, et al. Grafting of High-Density Poly(Ethylene Glycol) Monolayers on Si(111). *Langmuir.* 2001;17(25):7798-7803.

47. Das M, Bandyopadhyay D, Singh RP, Harde H, Kumar S, Jain S. Orthogonal biofunctionalization of magnetic nanoparticles via "clickable" poly(ethylene glycol) silanes: a "universal ligand" strategy to design stealth and target-specific nanocarriers. *Journal of Materials Chemistry.* 2012;22(47):24652-24667.

48. Goudie MJ, Singha P, Hopkins SP, Brisbois EJ, Handa H. Active Release of an Antimicrobial and Antiplatelet Agent from a Nonfouling Surface Modification. *ACS Appl Mater Interfaces.* 2019;11(4):4523-4530.

49. Singha P, Pant J, Goudie MJ, Workman CD, Handa H. Enhanced antibacterial efficacy of nitric oxide releasing thermoplastic polyurethanes with antifouling hydrophilic topcoats. *Biomater Sci.* 2017;5(7):1246-1255.

50. Reviakine I, Jung F, Braune S, et al. Stirred, shaken, or stagnant: What goes on at the blood-biomaterial interface. *Blood Rev.* 2017;31(1):11-21.

51. Lantvit SM, Barrett BJ, Reynolds MM. Nitric oxide releasing material adsorbs more fibrinogen. *J Biomed Mater Res A.* 2013;101(11):3201-3210.

52. Jo S, Park K. Surface modification using silanated poly(ethylene glycol)s. *Biomaterials.* 2000;21(6):605-616.

53. Field L, Dilts RV, Ravichandran R, Lenhert PG, Carnahan GE. An unusually stable thionitrite from N-acetyl-D,L-penicillamine; X-ray crystal and molecular structure of 2-(acetylamino)-2-carboxy-1,1-dimethylethyl thionitrite. *Journal of the Chemical Society, Chemical Communications.* 1978(6):249-250.

54. Wo Y, Li Z, Colletta A, et al. Study of Crystal Formation and Nitric Oxide (NO) Release Mechanism from S-Nitroso-N-acetylpenicillamine (SNAP)-Doped CarboSil Polymer Composites for Potential Antimicrobial Applications. *Compos B Eng.* 2017;121:23-33.

55. Colletta A, Wu J, Wo Y, et al. S-Nitroso-N-acetylpenicillamine (SNAP) Impregnated Silicone Foley Catheters: A Potential Biomaterial/Device To Prevent Catheter-Associated Urinary Tract Infections. *Acs Biomater Sci Eng.* 2015;1(6):416-424.

56. Lee JN, Park C, Whitesides GM. Solvent compatibility of poly(dimethylsiloxane)-based microfluidic devices. *Anal Chem.* 2003;75(23):6544-6554.

57. Garren M, Maffe P, Melvin A, et al. Surface-Catalyzed Nitric Oxide Release via a Metal Organic Framework Enhances Antibacterial Surface Effects. *ACS Appl Mater Interfaces.* 2021;13(48):56931-56943.

58. Wo Y, Brisbois EJ, Wu J, et al. Reduction of Thrombosis and Bacterial Infection via Controlled Nitric Oxide (NO) Release from S-Nitroso-N-acetylpenicillamine (SNAP) Impregnated CarboSil Intravascular Catheters. *Acs Biomater Sci Eng.* 2017;3(3):349-359.

59. Mondal A, Singha P, Douglass M, et al. A Synergistic New Approach Toward Enhanced Antibacterial Efficacy via Antimicrobial Peptide Immobilization on a Nitric Oxide-Releasing Surface. *ACS Appl Mater Interfaces.* 2021;13(37):43892-43903.

60. Douglass M, Hopkins S, Chug MK, et al. Reduction in Foreign Body Response and Improved Antimicrobial Efficacy via Silicone-Oil-Infused Nitric-Oxide-Releasing Medical-Grade Cannulas. *ACS Appl Mater Interfaces.* 2021;13(44):52425-52434.

61. Homeyer KH, Goudie MJ, Singha P, Handa H. Liquid-Infused Nitric-Oxide-Releasing Silicone Foley Urinary Catheters for Prevention of Catheter-Associated Urinary Tract Infections. *Acs Biomater Sci Eng.* 2019;5(4):2021-2029.

62. Roberts TR, Garren MRS, Wilson SN, Handa H, Batchinsky AI. Development and In Vitro Whole Blood Hemocompatibility Screening of Endothelium-Mimetic Multifunctional Coatings. *ACS Appl Bio Mater.* 2022.

63. Liu Q, Singha P, Handa H, Locklin J. Covalent Grafting of Antifouling Phosphorylcholine-Based Copolymers with Antimicrobial Nitric Oxide Releasing Polymers to Enhance Infection-Resistant Properties of Medical Device Coatings. *Langmuir.* 2017;33(45):13105-13113.

64. Singha P, Goudie M, Liu Q, et al. Multi-Pronged Approach to Combat Catheter-Associated Infections and Thrombosis by Combining Nitric Oxide and a Polyzwitterion: A 7-day In Vivo Study in a Rabbit Model. *ACS Appl Mater Interfaces.* 2020.

65. Kawai F, Kimura T, Fukaya M, et al. Bacterial oxidation of polyethylene glycol. *Appl Environ Microbiol.* 1978;35(4):679-684.

66. Ulbricht J, Jordan R, Luxenhofer R. On the biodegradability of polyethylene glycol, polypeptoids and poly(2-oxazoline)s. *Biomaterials.* 2014;35(17):4848-4861.

67. Douglass ME, Goudie MJ, Pant J, et al. Catalyzed Nitric Oxide Release via Cu Nanoparticles Leads to an Increase in Antimicrobial Effects and Hemocompatibility for Short-Term Extracorporeal Circulation. *ACS Applied Bio Materials.* 2019;2(6):2539-2548.

68. Garren M, Maffe P, Melvin A, et al. Surface-Catalyzed Nitric Oxide Release via a Metal Organic Framework Enhances Antibacterial Surface Effects. *ACS Applied Materials & Interfaces.* 2021;13(48):56931-56943.

69. Park KD, Kim YS, Han DK, et al. Bacterial adhesion on PEG modified polyurethane surfaces. *Biomaterials.* 1998;19(7):851-859.

70. Mondal A, Devine R, Estes L, et al. Highly hydrophobic polytetrafluoroethylene particle immobilization via polydopamine anchor layer on nitric oxide releasing polymer for biomedical applications. *J Colloid Interf Sci.* 2021;585:716-728.

71. Devine R, Douglass M, Ashcraft M, Tayag N, Handa H. Development of Novel Amphotericin B-Immobilized Nitric Oxide-Releasing Platform for the Prevention of Broad-Spectrum Infections and Thrombosis. *ACS Applied Materials & Interfaces.* 2021;13(17):19613-19624.

72. Brisbois EJ, Handa H, Major TC, Bartlett RH, Meyerhoff ME. Long-term nitric oxide release and elevated temperature stability with S-nitroso-N-acetylpenicillamine (SNAP)-doped Elast-eon E2As polymer. *Biomaterials.* 2013;34(28):6957-6966.

73. Haynes WG, Noon JP, Walker BR, Webb DJ. Inhibition of nitric oxide synthesis increases blood pressure in healthy humans. *Journal of Hypertension.* 1993;11(12).

74. Major TC, Brant DO, Burney CP, et al. The hemocompatibility of a nitric oxide generating polymer that catalyzes S-nitrosothiol decomposition in an extracorporeal circulation model. *Biomaterials.* 2011;32(26):5957-5969.

75. Kobayashi M, Koide T, Hyon SH. Tribological characteristics of polyethylene glycol (PEG) as a lubricant for wear resistance of ultra-high-molecular-weight polyethylene (UHMWPE) in artificial knee join. *J Mech Behav Biomed Mater.* 2014;38:33-38.

76. Petrova Y, Petrov V, Georgieva T, Ceciliani F. Blood fibrinogen concent-rations in New Zealand White rabbits during the first year of life. *Bulgarian Journal of Veterinary Medicine.* 2018;21(3):286-291.

77. Hewitt CD, Innes DJ, Savory J, Wills MR. Normal biochemical and hematological values in New Zealand white rabbits. *Clinical Chemistry.* 1989;35(8):1777-1779.

78. Major TC, Handa H, Annich GM, Bartlett RH. Development and hemocompatibility testing of nitric oxide releasing polymers using a rabbit model of thrombogenicity. *J Biomater Appl.* 2014;29(4):479-501.

79. Butt E, Abel K, Krieger M, et al. cAMP- and cGMP-dependent protein kinase phosphorylation sites of the focal adhesion vasodilator-stimulated phosphoprotein (VASP) in vitro and in intact human platelets. *J Biol Chem.* 1994;269(20):14509-14517.

80. Eigenthaler M, Nolte C, Halbrugge M, Walter U. Concentration and regulation of cyclic nucleotides, cyclic-nucleotide-dependent protein kinases and one of their major substrates in human platelets. Estimating the rate of cAMP-regulated and cGMP-regulated protein phosphorylation in intact cells. *Eur J Biochem.* 1992;205(2):471-481.

81. Nolte C, Eigenthaler M, Horstrup K, Honig-Liedl P, Walter U. Synergistic phosphorylation of the focal adhesion-associated vasodilator-stimulated phosphoprotein in intact human platelets in response to cGMP- and cAMP-elevating platelet inhibitors. *Biochem Pharmacol.* 1994;48(8):1569-1575.

82. Hansson KM, Tosatti S, Isaksson J, et al. Whole blood coagulation on protein adsorption-resistant PEG and peptide functionalised PEG-coated titanium surfaces. *Biomaterials.* 2005;26(8):861-872.

CHAPTER 5:

CONCLUSIONS AND FUTURE DIRECTIONS

5.1 Conclusions

Infectious and thrombotic complications with medical device usage spurs investigation into novel preventative therapies. This dissertation has focused on exploring the use of RSNOs in different forms for potential biomedical applications. RSNOs are employed to provide prolonged NO release and, therefore, prolonged antibacterial and antithrombotic actions. Their demonstrated versatility in form and also multifunctionality support their advantageous incorporation into therapies and materials. The described studies evaluate RSNOs in solution as a lock solution for venous catheters, covalently attached to graphene oxide as a material for coatings, and impregnated into medical grade tubing for extracorporeal circuits.

In Chapter 2, GSNO dissolved in saline is investigated as a catheter lock solution. Venous catheters are often associated with bloodstream infections and clotting. Lock solutions containing either antimicrobials or antithrombotic agents are inserted into catheters between uses to attempt to prevent these complications. Although subjected to hydrolysis,[1] GSNO at varying concentrations was demonstrated to release NO for at least 48 hours, the maximum recommended dwell time for a catheter lock solution.[2] Its antibacterial effects were demonstrate in three assays – time kill, viable adhesion, and biofilm dispersal assays. In these setting, it was established that the NO-releasing lock solution (NOreLS) is fast acting, broad spectrum, and effective at treating established infections. Moreover, it outperformed clinical antibiotic lock solutions when treating

infected tubing. NOreLS's ability to deter clotting was assessed via exposure to whole blood. Open tubing with lock solution was incubated to resemble the tip of a locked catheter. NOreLS decreased clot formation in a dose-dependent trend and performed better than a clinical heparin lock solution. Finally, it was established that NOreLS is biocompatible at concentrations relevant to catheter leaking via cytotoxicity assessments with HUVEC and hemolysis measurements. Overall, this study supports the potential of RSNOs to be easily incorporated into clinical settings for infection and thrombosis mitigation. This work was published in *ACS Applied Bio Materials*.[3]

In Chapter 3, a precursor of the RSNO SNAP is covalently attached to graphene oxide (GO). GO is a material of interest for biomedical applications because of its inherent antimicrobial and unique conductivity properties.[4] The multi-step synthesis of NO-releasing GO is characterized via quantitative analyses, FTIR, XPS, and NO release measurements. By changing the molar ratios of aminosilane used in the synthesis, it is demonstrated that the degree of GO functionalization can be controlled. This is evident in the varying NO release profiles that differing ratios resulted in as well as quantification. Moreover, it is demonstrated that NO release profiles can be altered by applying low levels of electrical current. In proof-of-concept bacterial studies, NO-releasing GO repeatedly outperformed unmodified GO against MRSA and *E. coli*. Specifically, it better prevented viable adhesion and effectively dispersed biofilms at a low concentration at which unmodified GO was not effective. Moreover, NO-releasing GO demonstrated improved cytocompatibility compared to unmodified GO. Thus, NO-releasing GO is an exciting material that may be used in a variety of biomedical settings, such as coatings for devices. Its high tunability suggests that it can be altered for various applications as needed. This work has been prepared for submission for publication.

In Chapter 4, SNAP is impregnated into silicon rubber (SR) via an established solvent swelling method. For the first time, the combination of NO release and a polyethylene glycol (PEG) coating is evaluated. PEG is a well-known hydrophilic polymer that can create a hydration layer when immobilized to a surface. As discussed in Chapter 1, hydrophilicity is a deterrent for bacteria adhesion and plasma protein adsorption and, thus, highly desirable. PEG-coated NO-releasing SR was characterized via FTIR, leaching studies, and contact angle measurements. *In vitro* protein adsorption and the aforementioned contact angle studies demonstrated an optimal ratio of PEG to acetone for achieving the PEG coating after oxygen plasma treatment. *In vitro* bacterial and platelet adhesion studies verified that NO release and PEG act complimentary compared to the solo material designs. With such encouraging preliminary results, the combination was applied to extracorporeal circuits (ECC) for investigation in an *in vivo* rabbit model. The NO+PEG ECC loops drastically decreased thrombus formation and better maintained patency compared to the control loops. Its superior performance was further verified by platelet preservation and plasma fibrinogen levels, confirming that both mechanisms of action of NO+PEG are beneficial and complimentary. This work has been prepared for submission for publication and supported an R01 submission.

Overall, this dissertation demonstrates that RSNOs have clinical potential in many different forms. Although perceived as potentially unstable in solution due to hydrolysis, it has been demonstrated that a GSNO-based locked solution releases NO for at least 48 h, which implies its clinical relevancy. Its improved antimicrobial and antithrombotic performances compared to clinically used lock solutions and its demonstrated biocompatibility support its potential for translation. Covalently attached to GO, RSNOs also showed remarkable potential as a highly tunable coating. NO release profiles were demonstrated to be altered by degree of functionalization

and low-level electrical currents. Moreover, the NO-releasing GO showed excellent antimicrobial effects at low concentrations, outperforming unmodified GO. The versatility of RSNOs was further shown as SNAP was impregnated into SR and coated with PEG. This novel combination of material designs showed outstanding antifouling and antithrombotic effects in both *in vitro* and *in vivo* studies. The various forms that RSNOs may take while maintaining both antimicrobial and antithrombotic properties in addition to biocompatibility shows remarkable flexibility. As they are, they have excellent potential for translation into short-term applications and may eventually be appropriate for long-term applications as well (discussed in **Section 5.2**).

5.2 Future Directions

In this dissertation, RSNO is varying forms were explored for potential short-term therapies and medical device materials to combat infection and thrombosis. NO-releasing materials and technology also have great potential for longer-term therapies, but achieving steady, prolonged NO release is a noted challenge. Various strategies to overcome this obstacle are being pursued, including the use of metal ion catalysts[5] and the superior stability of covalently attached NO donor molecules,[6] providing the unprecedented four months of NO release seen by covalent SNAP PDMS. Both strategies have great potential for various applications.

Chapter 2 demonstrates the antibacterial and antithrombotic effects of a GSNO-based lock solution for venous catheters. Using a catalyst, such as Cu nanoparticles, within the lumen of a catheter could facilitate higher NO release from the same concentration of lock solution. Thus, better antibacterial and antithrombotic activity may be achieved with no elevated biocompatibility concerns.

Similarly, catalyzing more NO release from the NO+PEG ECC loops in Chapter 4 could have advantages. The NO-releasing SR was shown to have prolonged NO release (> 24 h), but after 4 h the release fell below the endothelial range (i.e., $< 0.5 – 4.0 \times 10^{-10}$ mol cm^{-2} min^{-1}).[7] With elevated release rates produced by catalysis, the benefits could conceivably be seen in an *in vivo* model longer than that of the 4 h model used. As 4 h is a common endpoint for ECC rabbit models,[5,8] this longer investigation could provide the field valuable insights.

The strategy of covalent attachment providing stabilization of NO donor molecules was in mind when designing NO-releasing GO. While it was shown to be an effective means of formulation and allow for tunability in NO content, its longevity was not fully explored as it will greatly depend on the incorporation of it in a coating or material. This will also largely determine the NO release profile seen with low levels of electrical currents. The considerations that will affect these two properties are the use of functional handles and the carbon to oxygen ratio of the NO-releasing GO. The material that it is also incorporated into will also determine NO release profiles through its NO permeability and potential conductivity. Thus, Chapter 3 presents a proof-of-concept material that could be further explored in many different directions and settings.

The concept of highly tunable NO release as presented in Chapter 3 is a potential area of interest for further exploration. One of the noted shortcomings of NO-releasing materials is that they have a finite reservoir of NO within them. When it is depleted, it no longer has its antimicrobial and antithrombotic actions attributed towards that materials modification. It would be a great advantage to control when that NO is released, i.e., to release it when needed. For example, if a patient is beginning to show early signs of infection after medical device implantation, it would be invaluable to be able to stimulate NO release from the device in order to provide localized antimicrobial effects on demand.

In summary, this dissertation has shown the versatility of RSNOs in solution, covalently attached to a potential coating material, and within medical grade SR. This work has demonstrated their potential for various medical applications, highlighting the antimicrobial and antithrombotic properties of NO-releasing materials. While focused on short-termed applications, there is great potential for the work within this dissertation to be adapted for longer-termed applications with the use of catalysts promoting NO release and the exploration of covalently attached NO donor molecules in various settings.

5.3 References

1. Broniowska KA, Diers AR, Hogg N. S-nitrosoglutathione. *Biochim Biophys Acta.* 2013;1830(5):3173-3181.

2. Zhang J, Wang B, Wang J, Yang Q. Ethanol locks for the prevention of catheter-related infection in patients with central venous catheter: A systematic review and meta-analysis of randomized controlled trials. *PLoS One.* 2019;14(9):e0222408.

3. Ashcraft M, Douglass M, Garren M, et al. Nitric Oxide-Releasing Lock Solution for the Prevention of Catheter-Related Infection and Thrombosis. *ACS Applied Bio Materials.* 2022.

4. Geim AK, Novoselov KS. The rise of graphene. *Nat Mater.* 2007;6(3):183-191.

5. Douglass ME, Goudie MJ, Pant J, et al. Catalyzed Nitric Oxide Release via Cu Nanoparticles Leads to an Increase in Antimicrobial Effects and Hemocompatibility for Short-Term Extracorporeal Circulation. *ACS Applied Bio Materials.* 2019;2(6):2539-2548.

6. Hopkins SP, Pant J, Goudie MJ, Schmiedt C, Handa H. Achieving Long-Term Biocompatible Silicone via Covalently Immobilized S-Nitroso- N-acetylpenicillamine (SNAP) That Exhibits 4 Months of Sustained Nitric Oxide Release. *ACS Appl Mater Interfaces.* 2018;10(32):27316-27325.

7. Vaughn MW, Kuo L, Liao JC. Estimation of nitric oxide production and reaction rates in tissue by use of a mathematical model. *Am J Physiol.* 1998;274(6):H2163-2176.

8. Brisbois EJ, Major TC, Goudie MJ, Bartlett RH, Meyerhoff ME, Handa H. Improved hemocompatibility of silicone rubber extracorporeal tubing via solvent swelling-

impregnation of S-nitroso-N-acetylpenicillamine (SNAP) and evaluation in rabbit thrombogenicity model. *Acta Biomater.* 2016;37:111-119.